

LINEARIZED AND DISTRIBUTED METHODS FOR POWER FLOW ANALYSIS AND
CONTROL IN SMART GRIDS AND MICROGRIDS

By

Niannian Cai

A DISSERTATION

Submitted to
Michigan State University
in partial fulfillment of the requirements
for the degree of

Electrical Engineering - Doctor of Philosophy

2014

ABSTRACT

LINEARIZED AND DISTRIBUTED METHODS FOR POWER FLOW ANALYSIS AND CONTROL IN SMART GRIDS AND MICROGRIDS

By

Niannian Cai

Optimization and control is a core part of Energy Management System (EMS), which receives the data from supervisory control and data acquisition (SCADA) system, analyzes the data centrally and provides decision actions to the system operators. Unlike conventional power system, smart grid and microgrid are more complex, dynamic and flexible, which requires a high level of computational intelligence, speed and flexibility. This dissertation presents a linearized model to analyze the optimization problem of smart grid, which can provide speed advantage as well as enough accuracy. In the meantime, a distributed multi-agent based control system is proposed in this dissertation for a flexible control of microgrids.

With the development of smart grid, power electronic control devices, such as Flexible AC Transmission Systems (FACTS), are introduced into power system. They can help system operators adjust real and reactive power flows, provide voltage support or regulate voltage. The way to determine the optimal size and location to install FACTS devices is a nonlinear optimization problem. Various nonlinear techniques have been proposed and developed to solve this optimization model, such as descent methods, Newton's methods, gradient projection methods, interior methods and so on. These nonlinear methods, to some extent, can provide accurate optimal solutions; however, they are usually computationally expensive when dealing with large power systems with tens of thousands of buses. And this computational speed sometimes cannot satisfy system operators' requirements. Therefore, many industrial applications have utilized a DC optimal power flow model which assumes a flat voltage magnitude over the system. This model can achieve the results very fast, but it sacrifices accuracy and reactive power information.

To reach a better trade-off between accuracy and speed, in the first half of this dissertation, it proposed a linearized power flow model for studying benefit of FACTS devices. This linear model

can achieve better accuracy than DC power flow model and maintain reactive power information while the computational speed is not sacrificed.

In the meantime, the increasing penetration of renewable energy and its potential accommodation paradigm, microgrids, restrict traditional central control structure in terms of cost, flexibility and reliability. Distributed control is able to address these challenges in three aspects: more economic efficiency by utilizing low-cost devices; more flexibility in terms of time-varying and adaptive configurations or functions; and more robustness by continuing working in the presence of single-point failure.

For the power balance control, this dissertation first proposed a distributed multi-agent system without considering network losses and voltage regulation. In this proposed system, the information flows in parallel and results are obtained in a non-iterative way; therefore, this method achieves superior performance in terms of speed without any convergence issues. In the case where power losses are considerable and voltage regulation is expected, this dissertation proposed a distributed multi-agent control for power balance based on Guess method. The proposed power flow algorithm fully makes use of communication time, and updates state information synchronously among agents. Therefore it can also provide speed advantage over asynchronous methods.

For economic dispatch, this dissertation first proposed a distributed algorithm for microgrids without considering network constraints. This proposed economic dispatch is merit for fast convergence and is applicable for on-line control. In order to consider the network constraints, this dissertation presented a distributed multi-agent system which can consider the network constraints with full or partial observation of system state information. The proof of convergence is also presented in the dissertation.

Dedicated to:
My parents, Youxiang Cai and Junyun Yin
My wife Hui Fang,
And my brother Weiwei Cai

ACKNOWLEDGMENTS

First of all, I would like to express my sincerely thank to my advisor Dr. Joydeep Mitra. I would like to thank him not only for his enlightening guidance and continuous support for my graduate studies, but also for all other non-academic merits that he teaches me in my daily life. He is one of the nicest people that I have seen, and always stands besides me to give me advise whenever I need. He is also very generous to tolerate and correct my countless funny mistakes. Without his support, I can not make continuous process for my graduate study and finish my dissertation.

I am also very grateful to my committee members, Dr. Fang Z. Peng, Dr. Bingsen Wang, and Dr. Jongeun Choi for their inspiring classes, valuable suggestions, and serving as my committee members.

Many thanks go to my officemates and colleagues in ERISE lab, for their valuable discussions, kindly help and priceless friendship, Ms. Nga Nguyen, Dr. Xufeng Xu, Mr. Mohammed Benidris, Mr. Salem Elsaiahs, Mr. Samer Sulaeman, Ms. Yuting Tian, Mr. Valdama Johnson, Mr. Khaleel O. Khadedah and Dr. Oluwafemi Ipinnimo.

I also would like to thank all my colleagues and friends in PELab, Dr. Shao Zhang, Dr. Shuitao Yang and Mr. Yang Liu, for your collaboration in the transformer-less UPFC project. Your valuable discussions and suggestions help me deeper understand the working principles of transformer-less UPFC. I also would like to thank Dr. Xi Lu, Dr. Qin Lei, Mr. Sisheng Liang, Mr. Xianhao Yu, Dr. Shuai Jiang and all others friends in the PELab for their valuable discussions and helps in both study and life.

I would like to express my special appreciation to my colleague, Mr. Yantao Song. Thank you for your patient discussions and valuable suggestions about power electronic circuit and control. I also want to thank you for your spiritual support and encouragement during my graduate study.

Last but not the least, I would like to thank my parents, my wife and my brother for their unconditional care, support and understanding. The thanks that I would like to express for them is beyond description.

TABLE OF CONTENTS

LIST OF TABLES	x
LIST OF FIGURES	xiii
Part I Introduction	1
Chapter 1 Introduction	2
1.1 The Need for New Optimization Techniques in Smart Grid	2
1.1.1 The Concept of Smart Grid	2
1.1.2 Optimization Techniques in Traditional Grid	3
1.1.3 The Need for New Optimization Techniques in Smart Grid	4
1.2 The Need for New Control Techniques in Microgrid	5
1.2.1 The Concept of Microgrid	5
1.2.2 Control Techniques in Traditional Grid	6
1.2.3 The Need for New Control Techniques in Microgrids	7
1.3 Scope of the Dissertation	8
Part II Linearized Methods for the Optimization in Smart Grids	10
Chapter 2 Linearized Methods for UPFC Benefit Study	11
2.1 Linearized AC Power Flow Model (Lossless Model)	12
2.2 Linearization of Transmission Line Constraint	16
2.3 Power Flow Model of UPFC	19
2.4 Linearized Power Flow Model of UPFC	23
2.5 Model of UPFC Benefit Study	26
2.5.1 Maximize Revenue for Constant Loading Conditions	26
2.5.2 Maximize Revenue for Time-Varying Loading Conditions	29
2.6 Simulation Result	32
2.6.1 Maximize Revenue for Constant Loading Conditions	32
2.6.2 Maximize Revenue for Time-Varying Loading Conditions	36
2.7 Summary	41
Chapter 3 Optimal UPFC Placement and Parameter Selection to Minimize Generation Costs	43
3.1 Introduction	43
3.2 Methodology	44
3.2.1 Problem Analysis	44
3.2.2 Sensitivity Analysis and Branch Numbering	45
3.2.3 Configuration of the Algorithm	48

3.2.3.1	Fitness Function	48
3.2.3.2	Number of Genes	50
3.2.3.3	Crossover	50
3.2.3.4	Mutation	51
3.2.3.5	Selection	51
3.3	Case Study	51
3.4	Conclusion	53
 Part III Distributed Methods for the Control in Microgrid		55
 Chapter 4 Distributed Power Balance Control		56
4.1	Introduction	56
4.2	Parallel Method: Minimal Spanning Tree	59
4.2.1	Stage 1: Discovery of Minimal Spanning Tree	59
4.2.2	Stage 2: Information Feedback Process	60
4.2.3	Stage 3: Generation and Load Dispatch	61
4.3	Multi-Agent System Implementation and Simulation	62
4.4	Summary	65
 Chapter 5 Distributed Power Balance Control Considering Voltage Regulation and Losses		66
5.1	Introduction	66
5.2	Net Power Acquisition by Gauss Method	67
5.2.1	Distributed Construction of Y_{bus}	67
5.2.2	Agent Based Power Flow	68
5.2.3	Net Power Acquisition	70
5.3	Multi-Agent Implementation Algorithm	73
5.4	Load and Generation Dispatch	74
5.5	Simulation Result	75
5.5.1	Five-Bus System	76
5.5.1.1	Multi-agent Based Construction of Y_{bus}	76
5.5.1.2	Multi-Agent Based Power Flow Calculation	77
5.5.1.3	Netpower Acquisition	78
5.5.2	14-Bus System, 30-Bus System and 57-Bus System	79
5.5.2.1	14-Bus System	80
5.5.2.2	30-Bus System	80
5.5.2.3	57-Bus System	80
5.6	Summary	81
 Chapter 6 Distributed Economic Dispatch		82
6.1	Introduction	82
6.2	Economic Dispatch Model	83
6.3	Proof of Convergence	86
6.4	Simulation Results	92

6.5	Summary	96
Chapter 7 Distributed Economic Dispatch Considering Network Constraints		97
7.1	Introduction	97
7.2	Problem Formulation	98
7.3	Proof of Convergence	99
7.4	Simulation Results	101
7.4.1	Linearized Economic Dispatch Considering Network Constraints	101
7.4.2	Nonlinear Economic Dispatch Considering Network Constraints	105
7.5	Summary	108
Chapter 8 Multi-Agent Implementation and Multi-Level Control Architecture		110
8.1	Multi-Level Control Structure	110
8.2	Multi-Agent Implementation	111
8.3	Simulation Platform of Lower Level	113
8.3.1	Master Power Electronic Interfaces	113
8.3.2	Slave Power Electronic Interfaces	115
8.4	Multi-Level Control Architecture	117
8.5	Summary	123
Part IV Conclusions		125
Chapter 9 Contributions and Future Work		126
9.1	Contributions	126
9.2	Future Work	127
BIBLIOGRAPHY		129

LIST OF TABLES

Table 2.1	Number of Variables	28
Table 2.2	Number of Constraints	29
Table 2.3	Number of Variables	31
Table 2.4	Number of Constraints	32
Table 2.5	Number of Variables	33
Table 2.6	Number of Constraints	33
Table 2.7	Simulation Result for Constant Loading Conditions	34
Table 2.8	Simulation Result For Constant Loading Conditions with Deficient Reactive Power Generation	35
Table 2.9	Load Categories	38
Table 2.10	Number of Variables	39
Table 2.11	Number of Constraints	39
Table 2.12	Simulation Result of Case 1	40
Table 2.13	Simulation Result of Case 2	41
Table 3.1	Simulation Optimal Placement and Parameter Selection of UPFC	52
Table 3.2	Simulation Results of Subsequent Investment in the Case of 5-Year Utilization of UPFC	52
Table 4.1	Parent Child Relationship Diagram	60
Table 4.2	Simulation Results for Power Balance Control	64
Table 5.1	Bus Input Data for Five-Bus System	76
Table 5.2	Line Input Data for Five-Bus System	76
Table 5.3	Local Y_i Vectors	77
Table 5.4	Results for the First Five Iteration	79

Table 5.5	Comparisons Between Power Balance Control Algorithms	81
Table 6.1	Generation Data for the Microgrid	92
Table 7.1	Observed Area for Each Bus	102
Table 7.2	Result Summary	105
Table 7.3	Observed Area for Each Bus for IEEE 9-Bus System	107
Table 7.4	Result Summary	108
Table 8.1	Generation Data	118
Table 8.2	Data for PE Interfaces and Local Controllers	119
Table 8.3	Load Profile	119

LIST OF FIGURES

Figure 2.1 Configuration of UPFC.	11
Figure 2.2 A two node simple system.	16
Figure 2.3 Transmission line constraint diagram.	18
Figure 2.4 (a) Approximation of circular boundary. (b) Linear constraints for transmission line	18
Figure 2.5 Equivalent Circuit of UPFC	20
Figure 2.6 Equivalent power injection model of UPFC	21
Figure 2.7 Vector diagram of UPFC	21
Figure 2.8 Equivalent model of UPFC	23
Figure 2.9 Feasible region of V_{sp} and V_{sq}	24
Figure 2.10 Linearization of V_{sp} and V_{sq}	25
Figure 2.11 UPFC investment versus capacity	36
Figure 2.12 UPFC benefit versus capacity	37
Figure 2.13 Production savings over equipment cost	37
Figure 3.1 (a) Bad solution space; (b) bad solution space; (c) good solution space	46
Figure 3.2 Flow chart of numbering branches	49
Figure 3.3 Configuration of the algorithm	49
Figure 3.4 Crossover strategy	51
Figure 3.5 Mutation strategy	51
Figure 3.6 Average value of the population for the genetic algorithm with optimal branch numbering and not optimal branch numbering.	53
Figure 4.1 Multi-agent system structure.	58

Figure 4.2	(a) Token transmission route. (b) Minimal spanning tree constructed. (c) Information flow path for Stage 2.	60
Figure 4.3	Simulation of multiple threads on a single-thread platform.	63
Figure 4.4	Two MAS structures: (a) completely parallel resulting in tightest coupling; (b) completely sequential resulting in loosest coupling.	65
Figure 5.1	Information flow path for multi-agent system	75
Figure 5.2	Tested five-bus system	76
Figure 6.1	Cost curve for agent m and agent n	88
Figure 6.2	Flow chart for economic dispatch	91
Figure 6.3	Neighborhood relationship diagram	93
Figure 6.4	Generation dispatch result for five-agent system	93
Figure 6.5	Marginal cost for five-agent system	94
Figure 6.6	Generation cost for five-agent system	94
Figure 6.7	Simulation results for economic dispatch	95
Figure 7.1	Neighborhood relationship for IEEE 14 bus system	101
Figure 7.2	Generation cost curve for the first scenario of case 1	102
Figure 7.3	Generation cost curve for the second scenario of case 1	103
Figure 7.4	Generation cost curve for the first scenario of case 2	103
Figure 7.5	Generation cost curve for the second scenario of case 2	104
Figure 7.6	Generation cost curve for the first scenario of case 1 for AC models	106
Figure 7.7	Generation cost curve for the second scenario of case 1 for AC models	106
Figure 7.8	Generation cost curve for the first scenario of case 2 for AC models	107
Figure 7.9	Generation cost curve for the second scenario of case 2 for AC models	108
Figure 8.1	Proposed hierarchical control architecture.	111
Figure 8.2	Configuration of PE interface.	114

Figure 8.3	Control block for voltage-source power electronic interface.	114
Figure 8.4	Control block for current-source power electronic interface.	116
Figure 8.5	Microgrid configuration under study.	118
Figure 8.6	Traces of messages for token transfer.	119
Figure 8.7	Traces of messages for Information Feedback Process.	120
Figure 8.8	Traces of messages for Generation or Load Dispatch.	121
Figure 8.9	(a) Convergence of marginal cost. (b) Dispatched values for the DGs.	121
Figure 8.10	(a) Convergence of marginal cost. (b) Dispatched values for the DGs.	122
Figure 8.11	(a) Convergence of marginal cost. (b) Dispatched values for the DGs.	122
Figure 8.12	(a) Real power output of DGs. (b) Reactive power output of DGs. (c) Real power consumed by Load. (d) Reactive power consumed by Load.	123
Figure 8.13	(a) Output current transitions of DGs at 0.5s. (b) Output current transitions of DGs at 1.0s.	123

Part I

Introduction

Chapter 1

Introduction

Optimization and control is a core part of Energy Management System (EMS), which receives the data from supervisory control and data acquisition (SCADA) system, analyzes the data centrally and provides decision actions to the system operators. However, with development of smart grid, power electronic control devices, such as Flexible AC Transmission Systems (FACTS), are introducing into power system. Traditional DC optimization or AC optimization techniques turn out no longer to satisfy accuracy or speed requirements. In the meantime, the increasing penetration of renewable energy and its potential accommodation paradigm, microgrids, restrict traditional central control structure in terms of cost, flexibility and reliability. This dissertation utilizes linearization and distributed techniques to develop innovative optimization and control methods for smart grid and microgrid.

1.1 The Need for New Optimization Techniques in Smart Grid

1.1.1 The Concept of Smart Grid

According to [1], “a smart grid is a modernized electrical grid that uses information and communications technology to gather and act on information, such as information about the behaviors of suppliers and consumers, in an automated fashion to improve the efficiency, reliability, economics,

and sustainability of the production and distribution of electricity”.

A smart grid is realized by implementing wide applications of a class of technology and devices, such as two-way communication technology, computer-based remote control, computer-based automation, wide area measurement systems, Phasor Measurement Units (PMU) and Flexible AC Transmission Systems (FACTS) devices, to bring electric delivery systems into modernization. According to EPRI [24], the roles of smart grid include engaging consumers, enhancing efficiency, ensuring reliability and enabling renewable energy and electric transportation.

1.1.2 Optimization Techniques in Traditional Grid

Optimal power flow (OPF) problem, which came into focus dating back from 1960s, covers a group of network related optimization problems in the field of power system planning, operation or control. Examples of these problems can be: minimization of transmission loss, maximization of market profit, minimization of number of altered control variables, minimization of transmission line congestion, or minimization of pollution emission and operation cost *et al.* Mathematically, it requires to solve a static constrained nonlinear optimization problem with one or more objective functions and a set of equality and inequality constraints shown in equations (1.1)–(1.3). $F(\mathbf{x}, \mathbf{u})$ is the objective function, which can be generation cost, load curtailment or transmission line congestion. $g(\mathbf{x}, \mathbf{u})$ and $h(\mathbf{x}, \mathbf{u})$ are equality and inequality constraints for the network states and control variables. Its solution offers the optimal control variables that best satisfy objectives and respect prespecified constraints. Numerous methods have been proposed to deal with OPF problem. These methods, based on their intrinsic characteristics, can be classified into two categories: linear programming (LP) based methods and non-linear programming (NLP) based methods.

$$\text{Minimize:} \quad F(\mathbf{x}, \mathbf{u}) \quad (1.1)$$

$$\text{Subject to:} \quad g(\mathbf{x}, \mathbf{u}) = \mathbf{0} \quad (1.2)$$

$$h(\mathbf{x}, \mathbf{u}) \leq \mathbf{0} \quad (1.3)$$

LP based methods are credited for their fast and reliable attributes, however, the requirement for linearized model and accuracy consideration sometimes restrict their applications. A common LP based method involves solving the OPF problem by DC power flow model [2–4]. In this method, reactive power network equations are dropped; while all the voltage magnitudes are assumed to be 1.0 per unit in the network. This method is popularly adopted in many commercial softwares because of its speed and reliability. It can be used to calculate MW flows on transmission lines, but it does not indicate any information about voltage magnitudes or MVar flows. Another common LP based method solves full power flow model at an operating point and then linearizes the OPF problem at that point. This method also benefits from high speed and reliability. However, it works when the optimal point is near the operating point and it requires pre-acquisition of system operating point; while a lot of systems do not have this information. Refs. [5–7] provide a successive LP based method for OPF problem. This method solves the non-linear network model by using repetitive linear programmings to approach the optimal solution. It requires high computational capability.

NLP based methods are favorable for high accuracy, but this merit is achieved by sacrificing computational time and vast memory. Most NLP based methods existing to address OPF problem include descent methods, Newton’s methods [8, 9], sequential quadratic programming [10, 11], gradient projection methods [12, 13], augmented lagrangian methods [14, 15], interior point methods [16–18] and heuristic methods [19–21] *et al.* Any method mentioned above is only superior to others for a certain format of nonlinear optimization problems. No single method is best at solving all kinds of optimization problems.

1.1.3 The Need for New Optimization Techniques in Smart Grid

In smart grid, FACTS devices will be widely used to achieve flexible electricity transportation. Traditional DC optimization models can not satisfy the optimization problem involving FACTS devices because they do not provide reactive power and bus voltage magnitude information. For some FACTS devices, such as STATCOM and UPFC, reactive power support and voltage regu-

lation is one of their dominant functions. Furthermore, DC optimization models sacrifice enough accuracy in order to achieve high speed. Full AC optimization models can provide accurate and full state information, however, the computation burden in terms of speed and complexity, sometimes, is forbidden. Besides, the AC models of a power system are usually highly nonlinear with thousands of state and control variables; therefore, no AC optimization techniques can guarantee to always achieve global optimum.

Suffering from the deficiencies of DC and AC optimization models, the development of smart grid highly requires an optimization model that can achieve a better trade-off between speed and accuracy. The new optimization model should be linear so that it can be solved by fast and reliable LP method. It should also include complete state information with enough accuracy, so that it can be used to analyze optimization problems involving reactive power and voltage control. This comprehensive exam presents a generic framework for optimal power flow problems with FACTS devices by using linearization methods to linearize power flow equations, transmission line constraints and FACTS devices. The proposed optimization model can be solved in one shot by LP method; therefore, it has speed and reliability advantage as DC models. Additionally, this model can provide voltage magnitude and reactive power flow information for the network, which traditional DC models can not offer. Furthermore, it also accomplishes more accurate results than DC models with substantially less computational work than full AC power flow.

1.2 The Need for New Control Techniques in Microgrid

1.2.1 The Concept of Microgrid

A microgrid is a small-scale smart grid. It is a low voltage utility system formed by a cluster of interconnected local small generations, including renewable (such as wind, PV, etc.) and conventional (micro-turbine, fuel cells, diesel generator) sources, intermediate energy storages and loads [22]. As an electrical entity that facilitates high penetration of distributed generators, the microgrid can be recognized and developed as a primary building block of smart grid.

A common expectation of a microgrid is that it should be capable of islanded (off-grid) operation. However, in this mode, several factors affect the ability of microgrids to achieve and maintain stable operation. First, the unavailability of power support from the grid requires a global power balance controller which is able to coordinate power generation and consumption in microgrids and maintain system voltage and frequency. Further, if distributed generators (DGs) in a microgrid are required to be “plug and play”, no pre-determined economic dispatch would satisfy the requirement of the microgrid; thus, an on-line economic dispatch controller is anticipated to reduce generation cost. Moreover, with substantial penetration of DGs, the controller of microgrid is required to be flexible and adaptive; because it is difficult to estimate the number and the places of DGs that are going to be connected. One of connecting nodes may supply power at one time but absorb power at another time.

1.2.2 Control Techniques in Traditional Grid

Conventionally, power system monitoring, control and decision making are realized in a central control structure. A control center utilizes a centralized supervisory control and data acquisition (SCADA) system to remotely monitor the operation of the system spread over a large geographical area, and an Energy Management System (EMS) to analyze the data, conduct necessary power flow and optimal power flow computations and provide control actions to the operators.

This centralized control system plays a vital role in traditional power system, whose configuration is comparatively permanent and does not have high penetration of renewable energy and DGs. However, as the movement of smart grid, especially the microgrid, increasing penetration of renewable energy and DGs is introduced into the system, which requires more flexible and scalable control architecture. The central control architecture also suffers from high cost and low reliability. Because the centralized control center requires a costly super computing and data-storing center, which can memorize astronomical amount of data obtained by the meters spread over the system, analyze them in real time and compute for a possible control action. It is also vulnerable to single-point failure. If the control center fails, the whole power system is under risk of collapse.

1.2.3 The Need for New Control Techniques in Microgrids

The configurations and operating modes of microgrids are allowed to dynamically change. DGs may exhaust their fuel and shed; renewable energy may cut in or out with variable wind or solar energy; storage units may continue switching between discharging and charging modes; different load resources may connect or disconnect. With the participation of plug-in hybrid/electric vehicles, the extent of dynamic feature will increase considerably.

In the context of microgrids, conventional centralized structure restricts its application in terms of cost, flexibility, and reliability. Distributed control is able to address these challenges in a flexible and secure way by providing three merits: economic efficiency by integrating various applications, utilizing lower-cost devices, and saving from the maintenance of the SCADA and EMS system; flexibility in terms of time-varying and adaptive configurations or functions; and robustness by continue working in the presence of single-point failure [23].

Multi-agent system (MAS) emerges as a potential solution that facilitates distributed control for microgrids. An agent is an autonomous entity that can perceive and react to its environment and communicate with others to achieve its local goal. MAS is a system consisting of two or more agents. These agents collaborate and compete with each other to optimize its local goal, and therefore overall to achieve a global goal. An agent has three characteristics: reactivity (reactive to its environment), pro-activeness (exhibit goal-directed behavior), and social ability (communicate with each other) [46]. Agents in microgrid are expected to implement tasks as sensory, communication and actuation [45].

Previously, MAS-based methods have been widely applied to various power system problems, including microgrid control. Refs. [46, 47] have provided an excellent overview of such applications. Ref. [48] decomposed the optimal power flow problem and solved for the smaller subsystems in parallel by using MAS. In [49, 50], by making use of autonomous and decentralized characteristics, MAS was introduced to solve electricity market problem. Refs. [39, 41, 51, 52] proposed various methods to utilize MAS technique for power balance control and operation. Other MAS applications include power system monitoring [53–55], protection [56], restoration [57–60] and

stability enhancement [61–63].

The distributed control techniques proposed in this dissertation are designed based on a decentralized multi-agent platform for the control and operation of microgrids. In this decentralized architecture, all agents are hierarchically identical. There is no central or master agent, therefore, it enhances the controller’s reliability and flexibility.

1.3 Scope of the Dissertation

This dissertation is organized as follows:

Chapter 2 utilizes linearization techniques to derive linearized optimization models for optimal power flow problems with FACTS devices. It includes linearization of power flow equations, linearization of transmission line constraints, and linearization of FACTS devices. It also presents linearized models for revenue maximization problems of installing UPFC in both constant and time-varying loading conditions.

Chapter 3 presents an efficient combined algorithm using genetic algorithm and linearized optimal power flow framework for the optimal location and parameter selection of UPFC. An optimal branch numbering strategy is also proposed in this chapter to accelerate the convergence speed of the algorithm. Simulation results showing the benefits of installing UPFC versus investments, as well as diminishing returns of the subsequent investments are also presented in this chapter.

Chapter 4 proposes a distributed method for power balance control of microgrids without considering network losses and voltage regulation. The information flows in parallel and results are obtained in non-iterative way; therefore, the algorithm can achieve superior performance in terms of speed without any convergence issues.

Chapter 5 presents a distributed algorithm for power balance control of microgrids considering network losses and voltage regulation based on Gauss method. The distributed power flow algorithm fully makes use of communication time, and updates state information synchronously among agents, which offers potential speed advantage.

Chapter 6 proposes a distributed economic dispatch algorithm for microgrids without considering network constraints. The Proof of convergence and proof of global optimization are presented in this chapter. Simulation results show that the proposed algorithm is applicable for on-line economic dispatch.

Chapter 7 proposes a distributed algorithm for economic dispatch considering network constraints. Convergence of the algorithm is presented to ensure its stability. Simulation results show that if the system states are globally observed, the proposed algorithm can achieve global optimization; if the system states are partially observed, the proposed algorithm can minimize total generation cost, but it may be trapped by local optimum.

Chapter 8 presents the implementation of multi-agent system using Java Agent DEvelopment (JADE) platform. It proposes a multi-level control architecture for the safe and economic operation of microgrids. The upper MAS power balance layer accomplish exact power balance in three sweeps, regardless of system size. The lower MAS based economic dispatch layer is able to conduct economic dispatch on-line. Local control layer complies with the instructions from MAS and implement control locally.

Chapter 9 discusses the conclusions and future work.

Part II

Linearized Methods for the Optimization in Smart Grids

Chapter 2

Linearized Methods for UPFC Benefit

Study

Unified Power Flow Controller (UPFC) is one of the most widely used Flexible Alternating Current Transmission Systems (FACTS) devices that can control real and reactive power flow through a transmission line and regulate bus voltage simultaneously and independently. It promotes the grid “smarter” by enabling flexible electric transportation. Utilization of UPFC can increase the transfer capability of existing transmission lines and potentially reduce the demand for new transmission facilities. From 2001 to 2008, Edison Electric Institute (EEI) invested nearly \$57.5 billion in the upgrade of its member company transmission infrastructure [26]. Future transmission expansion can be deferred by developing UPFCs.

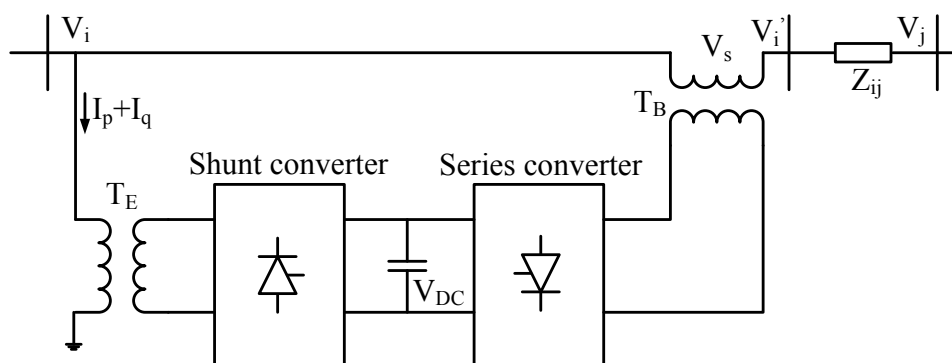


Figure 2.1: Configuration of UPFC.

Figure 2.1 shows the configuration of UPFC. It is consisted of two back-to-back converters. The series converter can generate a series voltage V_s in the range $0 \leq V_s \leq V_{smax}$ with phase angle φ_s in the range $0 \leq \varphi_s \leq 2\pi$; therefore the terminal voltage V_i' can be controlled for the regulation of real and reactive power flow through the transmission line. The shunt converter absorbs a real power current to compensate for the real power consumption of series converter in order to maintain DC capacitor voltage, and injects a reactive power current to regulate bus voltage V_i and provide reactive power support. Overall, UPFC has two main functions: real and reactive power control of a transmission line, and bus voltage or shunt reactive power control.

Traditional UPFC benefit study either uses DC model or full AC model. DC model can compute the benefit and determines the optimum size of series converter; however, It does not provide any reactive power and voltage magnitude information for the system; while reactive power flow control and bus voltage regulation is an important function that UPFC can realize. It was therefore considered important to extend the OPF framework to accommodate reactive power injections and flows. On the other hand, series converter and parallel converter of UPFC are two independent parts. How to determine the optimal capacity of each part for a given power system is also a key problem for UPFC economic study. DC power flow study is capable of helping us determine the optimal capacity of the series converter, but it cannot help us to decide the shunt size. Full AC power flow optimization is a traditional solution to deal with both real and reactive power, but its nonlinear characteristics and complexity requires a long time to find the optimal solution. Due to this consideration, this dissertation proposed an innovative linearized ac power flow, which is able to cope with both real and reactive power, but it also benefits from linear character and simple implementation.

2.1 Linearized AC Power Flow Model (Lossless Model)

It is well known that the basic power flow equations for real and reactive power are presented as:

$$P_k = V_k \sum_{m \in S} V_m (G_{km} \cos \delta_{km} + B_{km} \sin \delta_{km}) \quad (2.1)$$

$$Q_k = V_k \sum_{m \in S} V_m (G_{km} \sin \delta_{km} - B_{km} \cos \delta_{km}) \quad (2.2)$$

where P_k and Q_k are real and reactive power injected into node k ; V_k and V_m are voltage magnitude at node k and node m ; S is the set of all the buses in the system. δ_{km} is the voltage angle difference between node k and node m ; G_{km} and B_{km} are the real and reactive part of (k,m) element of bus admittance matrix (Y_{km}).

In the steady state, power system is usually operated around the operating point; therefore bus voltage magnitude is always around 1.0 p.u.

$$V_k = 1.0 + \Delta V_k \quad (2.3)$$

If we ignore the small portion ΔV_k , the magnitude of the voltage at bus k can be approximated by 1.0 p.u. However, it is important to note that this is only an approximation that enables the linearization; it is not an assumption that the voltage magnitude equals 1.0 p.u.

$$P_k \approx \sum_{m \in S} V_m (G_{km} \cos \delta_{km} + B_{km} \sin \delta_{km}) \quad (2.4)$$

$$Q_k \approx \sum_{m \in S} V_m (G_{km} \sin \delta_{km} - B_{km} \cos \delta_{km}) \quad (2.5)$$

If the phase angles between two adjacent buses are small enough, it is valid to make the approximation that $\sin \delta_{km} = \delta_{km}$, $\cos \delta_{km} = 1$. Then the equations above can be expressed as:

$$P_k \approx \sum_{m \in S} (V_m G_{km} + V_m B_{km} \delta_{km}) \quad (2.6)$$

$$Q_k \approx \sum_{m \in S} (V_m G_{km} \delta_{km} - V_m B_{km}) \quad (2.7)$$

Again,

$$V_m = 1.0 + \Delta V_m \quad (2.8)$$

Take (2.8) into (2.6) and (2.7).

$$P_k \approx \sum_{m \in S} (V_m G_{km} + B_{km} \delta_{km} + \Delta V_m B_{km} \delta_{km}) \quad (2.9)$$

$$Q_k \approx \sum_{m \in S} (G_{km} \delta_{km} + \Delta V_m G_{km} \delta_{km} - V_m B_{km}) \quad (2.10)$$

Note that both ΔV_m and δ_{km} are small numbers around zero. Therefore, it is reasonable to eliminate the terms that contain a product of ΔV_m and δ_{km} . Hence:

$$P_k \approx \sum_{m \in S} (V_m G_{km} + B_{km} \delta_{km}) \quad (2.11)$$

$$Q_k \approx \sum_{m \in S} (G_{km} \delta_{km} - V_m B_{km}) \quad (2.12)$$

Let us focus on equation (2.11) first, it can be further written as:

$$P_k = \sum_{m \in S} V_m G_{km} + \sum_{m \in S} B_{km} \delta_k - \sum_{m \in S} B_{km} \delta_m \quad (2.13)$$

Since

$$B_{km} = \begin{cases} \sum_{n \neq k} b_{kn} + b_{kk} & \text{for } m = k \\ -b_{km} & \text{for } m \neq k \end{cases}$$

where b_{kk} is the total shunt susceptance at bus k . b_{km} is the susceptance of branch connecting

node k and node m . Hence,

$$\begin{aligned} \sum_{m \in S} B_{km} \delta_k &= [-b_{k1} - \dots + (\sum_{m \neq k} b_{km} + b_{kk}) - \dots - b_{kN}] \delta_k \\ &= b_{kk} \delta_k \end{aligned} \quad (2.14)$$

Finally, linearized real power equation can be obtained by rearranging equation (2.13):

$$P_k = \sum_{m \in S} V_m G_{km} - \sum_{m \neq k} B_{km} \delta_m - (B_{kk} - b_{kk}) \delta_k \quad (2.15)$$

In the same manner, the linearized reactive power can be expressed as:

$$Q_k = - \sum_{m \neq k} G_{km} \delta_m - (G_{kk} - g_{kk}) \delta_k - \sum_{m \in S} V_m B_{km} \quad (2.16)$$

In matrix form, the linearized AC power flow can be described as:

$$\begin{bmatrix} P \\ Q \end{bmatrix} = \begin{bmatrix} -B' & G \\ -G' & -B \end{bmatrix} \begin{bmatrix} \delta \\ V \end{bmatrix} \quad (2.17)$$

where

$$B' = \begin{bmatrix} (B_{11} - b_{11}) & B_{12} & \dots & B_{1N} \\ B_{21} & (B_{22} - b_{22}) & \dots & B_{2N} \\ \dots & \dots & \dots & \dots \\ B_{N1} & B_{N2} & \dots & (B_{NN} - b_{NN}) \end{bmatrix}$$

$$G = \begin{bmatrix} G_{11} & G_{12} & \dots & G_{1N} \\ G_{21} & G_{22} & \dots & G_{2N} \\ \dots & \dots & \dots & \dots \\ G_{N1} & G_{N2} & \dots & G_{NN} \end{bmatrix}$$

$$G' = \begin{bmatrix} (G_{11} - g_{11}) & G_{12} & \dots & G_{1N} \\ G_{21} & (G_{22} - g_{22}) & \dots & G_{2N} \\ \dots & \dots & \dots & \dots \\ G_{N1} & G_{N2} & \dots & (G_{NN} - g_{NN}) \end{bmatrix}$$

$$B = \begin{bmatrix} B_{11} & B_{12} & \dots & B_{1N} \\ B_{21} & B_{22} & \dots & B_{2N} \\ \dots & \dots & \dots & \dots \\ B_{N1} & B_{N2} & \dots & B_{NN} \end{bmatrix}$$

2.2 Linearization of Transmission Line Constraint

In traditional DC optimal power flow calculation, reactive power flow is always not considered. Power flow constraints of transmission lines are simply assumed to be real power flow constraints, which can be stated as equation (2.18). This simplification will introduce considerable error in the optimal power flow calculation, since reactive power flow sometimes takes up a non-neglectable portion in the power flow of transmission line.

$$|P_{ij}| \leq |S_{ij}^{max}| \quad (2.18)$$

In the linearized power flow proposed in section 2.1, it is accessible to obtain voltage magnitude and reactive power state information. Consequently, it provides a prerequisite to linearize transmission line constraint considering reactive power. First consider a simple system shown in Fig. 2.2.

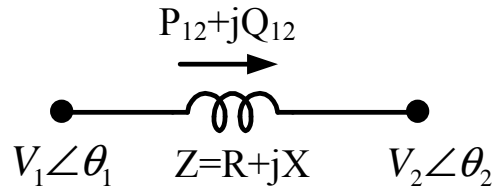


Figure 2.2: A two node simple system.

Power flow in this transmission line can be calculated as:

$$P_{12} = \frac{R}{Z^2}(V_1^2 - V_1V_2 \cos \delta_{12}) + \frac{X}{Z^2}V_1V_2 \sin \delta_{12} \quad (2.19)$$

$$Q_{12} = \frac{X}{Z^2}(V_1^2 - V_1V_2 \cos \delta_{12}) - \frac{R}{Z^2}V_1V_2 \sin \delta_{12} \quad (2.20)$$

Practically, the difference between δ_1 and δ_2 is not significant, it is reasonable to make the approximation that $\sin \delta_{12} \approx \delta_{12}$, $\cos \delta_{12} \approx 1$. Considering in the transmission system, $R \ll X$. Therefore, it is also acceptable to approximate that $R \approx 0$, $X \approx Z$. When the system is operated near operating point, then we have $V_1 \approx 1.0$ p.u., $V_2 \approx 1.0$ p.u.. Consequently, equations (2.19) and (2.20) can be simplified as:

$$P_{12} = \frac{\delta_1 - \delta_2}{X} \quad (2.21)$$

$$Q_{12} = \frac{V_1 - V_2}{X} \quad (2.22)$$

Originally, expression of transmission line power flow constraint is:

$$|S_{12}| = \sqrt{P_{12}^2 + Q_{12}^2} \leq |S_{12}^{max}| \quad (2.23)$$

Equation (2.23) indicates that eligible real and reactive power flow without violating transmission line constraint is bounded by a circle, whose radius is S_{12}^{max} . The circle shown in Fig. 2.3 depicts the boundary restricting real and reactive power flow of transmission line. Obviously the constraint is not linear.

To linearize the constraint, a piecewise approximation of the boundary can be utilized. In Fig. 2.4 (a), a total number of twelve straight lines are adopted to approach the circular boundary. However, considering constraints of bus voltage magnitude, six of the constraints in which reactive power value is larger than real power flow value can be neglected.

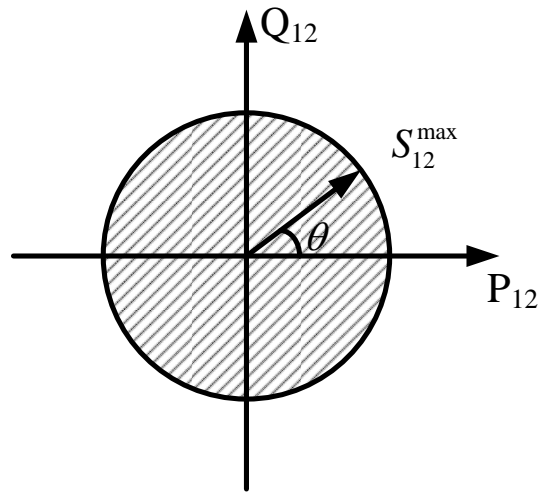


Figure 2.3: Transmission line constraint diagram.

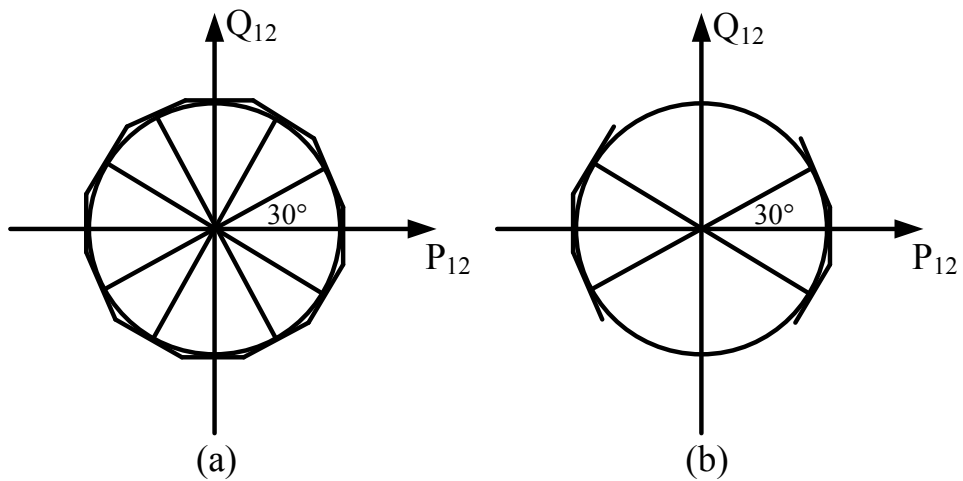


Figure 2.4: (a) Approximation of circular boundary. (b) Linear constraints for transmission line

Then the number of linear constraints for a transmission line is reduced to six as shown in Fig. 2.4 (b). Notice that the two constraints perpendicular to P axis are the old constraints for traditional DC power flow, mathematically stated as:

$$-S_{12}^{max} \leq P_{12} \leq S_{12}^{max} \quad (2.24)$$

The other four constraints perpendicular to diameters with angles 30° or -30° shown in Fig. 2.4 (b) can be geometrically formulated as:

$$-1.15S_{12}^{max} \leq P_{12} - 0.58Q_{12} \leq 1.15S_{12}^{max} \quad (2.25)$$

$$-1.15S_{12}^{max} \leq P_{12} + 0.58Q_{12} \leq 1.15S_{12}^{max} \quad (2.26)$$

Equations (2.24–2.26) are integrated together to construct linear constraints of transmission lines for linearized optimal power flow. In this paper, 6 linearized constraints are used. However, generally, the number of constraints can be other number depending on the individual situations. If high accuracy is expected, a larger number of constraints can be utilized to approach the circle constraint. If less computation is preferred, fewer number of constraints can be used. The degree of the diameters which is perpendicular to the constraints is also a variable that can be changed based on preference.

2.3 Power Flow Model of UPFC

UPFC steady state equivalent circuit is shown in Figure 2.5 [25]. The shunt converter is installed on the bus side so that it can provide/absorb reactive power into/from the grid and participate in the voltage regulation if necessary. The other converter is installed in series with the transmission line to provide a series voltage \mathbf{V}_s , so that voltage \mathbf{V}'_i and the power flow passing through this transmission line can be regulated. \mathbf{I}_q is the reactive power portion of the current of the shunt

converter. It is always perpendicular to voltage vector \mathbf{V}_i , expressed in equation (2.27). I_p is the real power portion of the shunt current. Its function is to absorb or inject real power from/into grid, so as to keep capacitor voltage V_{dc} constant, expressed in equation (2.28). It is in parallel with vector \mathbf{V}_i , described in (2.29). There are three independent control variables for UPFC, series voltage magnitude V_s , series voltage phase φ_s and magnitude of shunt reactive current I_q . They satisfy $0 \leq V_s \leq V_{smax}$, $0 \leq \varphi_s \leq 2\pi$, $0 \leq I_q \leq I_{qmax}$. V_{smax} and I_{qmax} are two variables that determine UPFC capacity.

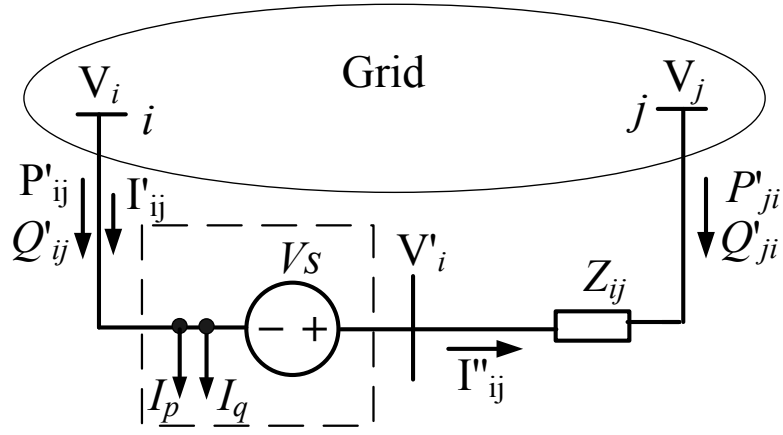


Figure 2.5: Equivalent Circuit of UPFC

$$\mathbf{I}_q \perp \mathbf{V}_i \quad (2.27)$$

$$\mathbf{I}_p = \frac{\text{Re}[\mathbf{V}_s \mathbf{I}'_{ij*}]}{\mathbf{V}_i} \quad (2.28)$$

$$\mathbf{I}_p // \mathbf{V}_i \quad (2.29)$$

The series converter and shunt converter of UPFC can be modeled as a voltage source and a current source respectively [25]. It is easy to see that the optimal generation and power flow values inside the Grid in Fig. 2.6 will be equivalent to those inside the Grid in Fig. 2.5, as long as the power flowing out of bus i and the power flowing into bus j are the same in Fig. 2.5 and Fig. 2.6.

Therefore, the UPFC model in Fig. 2.6 is equivalent to the power injection model of Fig. 2.5 when the power injection values are equal to the values shown in Fig. 2.6.

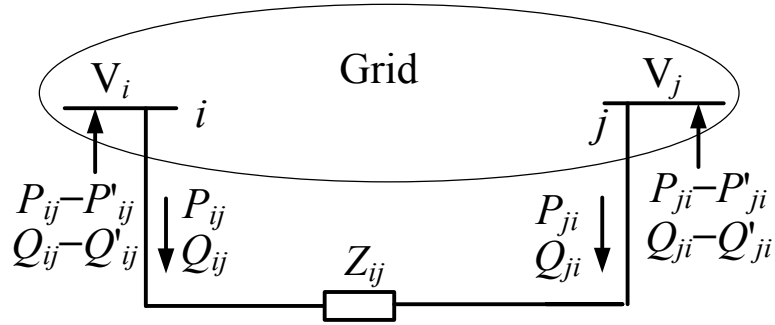


Figure 2.6: Equivalent power injection model of UPFC

The vector diagram for UPFC is shown in Figure 2.7.

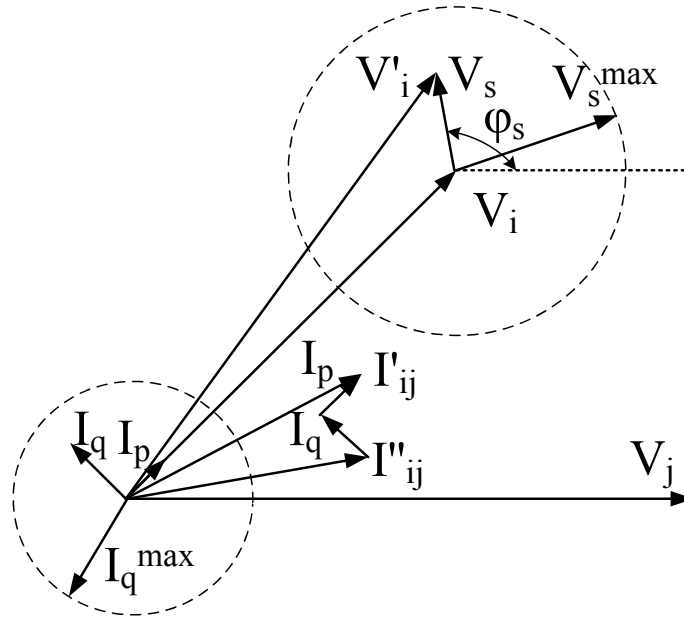


Figure 2.7: Vector diagram of UPFC

Power flow from bus i to bus j can be computed as:

$$\mathbf{S}_{ij} = P_{ij} + jQ_{ij} = \mathbf{V}_i(j\mathbf{V}_i B/2 + \mathbf{I}_q + \mathbf{I}_p + \mathbf{I}''_{ij})^* \quad (2.30)$$

Power flow from bus j to bus i can be computed as:

$$\mathbf{S}_{ji} = P_{ji} + jQ_{ji} = \mathbf{V}_j(j\mathbf{V}_j B/2 - I''_{ij})^* \quad (2.31)$$

Therefore, real and reactive power flow through the transmission line after installing UPFC can be formulated as:

$$P_{ij} = (V_i^2 + V_s^2)G_{ij} + 2V_iV_sG_{ij} \cos(\varphi_s - \delta_{ij}) - V_jV_s(G_{ij} \cos \varphi_s + B_{ij} \sin \varphi_s) - V_iV_j(G_{ij} \cos \delta_{ij} + B_{ij} \sin \delta_{ij}) \quad (2.32)$$

$$Q_{ij} = -V_iI_q - V_i^2(B_{ij} + B/2) - V_iV_s[G_{ij} \sin(\varphi_s - \delta_{ij}) + B_{ij} \cos(\varphi_s - \delta_{ij})] - V_iV_j(G_{ij} \sin \delta_{ij} - B_{ij} \cos \delta_{ij}) \quad (2.33)$$

$$P_{ji} = V_j^2G_{ij} - V_jV_s(G_{ij} \cos \varphi_s - B_{ij} \sin \varphi_s) - V_iV_j(G_{ij} \cos \delta_{ij} - B_{ij} \sin \delta_{ij}) \quad (2.34)$$

$$Q_{ji} = -V_j^2(G_{ij} + B/2) - V_jV_s(G_{ij} \sin \varphi_s - B_{ij} \cos \varphi_s) + V_iV_j(G_{ij} \sin \delta_{ij} + B_{ij} \cos \delta_{ij}) \quad (2.35)$$

The injected power at two buses can be computed by:

$$\mathbf{S}_i = \mathbf{V}_i(-\mathbf{I}_p - \mathbf{I}_q - \mathbf{V}_s/\mathbf{Z}_{ij})^* \quad (2.36)$$

$$\mathbf{S}_j = \mathbf{V}_j(\mathbf{V}_s/\mathbf{Z}_{ij})^* \quad (2.37)$$

Hence, the equivalent injected active and reactive power are:

$$P_i = -V_s^2 G_{ij} - 2V_i V_s G_{ij} \cos(\varphi_s - \delta_{ij}) + V_j V_s (G_{ij} \cos \varphi_s + B_{ij} \sin \varphi_s) \quad (2.38)$$

$$Q_i = V_i I_q + V_i V_s [G_{ij} \sin(\varphi_s - \delta_{ij}) + B_{ij} \cos(\varphi_s - \delta_{ij})] \quad (2.39)$$

$$P_j = V_j V_s (G_{ij} \cos \varphi_s - B_{ij} \sin \varphi_s) \quad (2.40)$$

$$Q_j = -V_j V_s (G_{ij} \sin \varphi_s + B_{ij} \cos \varphi_s) \quad (2.41)$$

The effect of UPFC is equivalent to two injected sources at bus i and bus j respectively, shown in Figure 2.8.

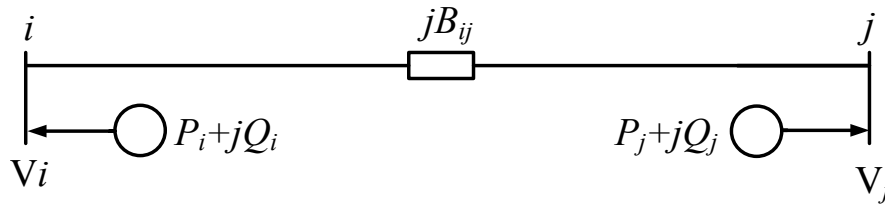


Figure 2.8: Equivalent model of UPFC

2.4 Linearized Power Flow Model of UPFC

For the transmission system, $|G_{ij}|$ is a very small number. It is widely acceptable to approximate $G_{ij} \approx 0$. The angle difference between two adjacent buses is also very small. Hence, $\varphi_s - \delta_{ij} \approx \varphi_s$, $\sin \delta_{ij} \approx \delta_{ij}$ and $\cos \delta_{ij} \approx 1$. If the system is operated around operating point. Then $V_i \approx 1.0$, $V_j \approx 1.0$.

Then the equation (2.38-2.41) can be approximated as:

$$P_i = V_s B_{ij} \sin \varphi_s \quad (2.42)$$

$$Q_i = I_q + V_s B_{ij} \cos \varphi_s \quad (2.43)$$

$$P_j = -V_s B_{ij} \sin \varphi_s \quad (2.44)$$

$$Q_j = -V_s B_{ij} \cos \varphi_s \quad (2.45)$$

Let $V_s \sin \varphi_s = V_{sp}$, $V_s \cos \varphi_s = V_{sq}$. V_{sp} , V_{sq} satisfy $V_{sp}^2 + V_{sq}^2 = V_s^2 \leq V_{smax}^2$. Hence, V_{sp} , V_{sq} can only lie in the cycle with radius V_{smax} , shown in Figure 2.9.

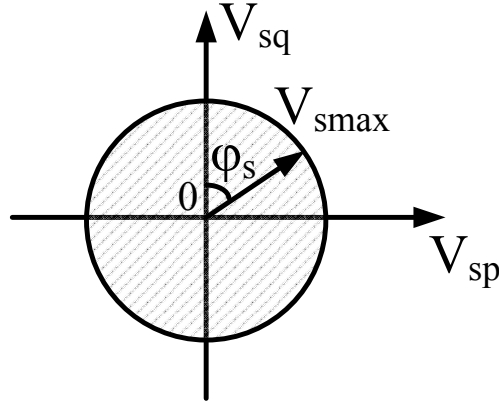


Figure 2.9: Feasible region of V_{sp} and V_{sq}

The cycle constraint on V_{sp} , V_{sq} can be linearized by six linear constraints, shown in Figure 2.10.

Mathematically, the constraints for V_{sp} , V_{sq} can be described as:

$$-V_{smax} \leq V_{sq} \leq V_{smax} \quad (2.46)$$

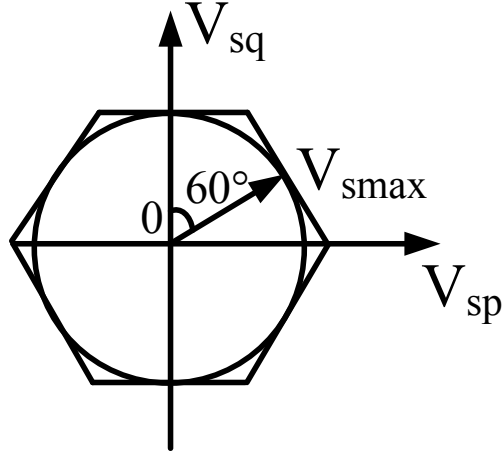


Figure 2.10: Linearization of V_{sp} and V_{sq}

$$-2V_{smax} \leq V_{sq} + \sqrt{3}V_{sp} \leq 2V_{smax} \quad (2.47)$$

$$-2V_{smax} \leq V_{sq} - \sqrt{3}V_{sp} \leq 2V_{smax} \quad (2.48)$$

Therefore, the linearized equivalent injected power of UPFC are:

$$P_i = B_{ij}V_{sp} \quad (2.49)$$

$$Q_i = I_q + B_{ij}V_{sq} \quad (2.50)$$

$$P_j = -B_{ij}V_{sp} \quad (2.51)$$

$$Q_j = -B_{ij}V_{sq} \quad (2.52)$$

where I_q is restricted by $0 \leq I_q \leq I_{qmax}$, V_{sp} and V_{sq} are constrained by equations (2.46-2.48)

2.5 Model of UPFC Benefit Study

2.5.1 Maximize Revenue for Constant Loading Conditions

The objective function of this model is to find an optimal size of UPFC that is capable to minimize generation cost for the studied load scenario. Numerous work has been done on the linearization of generator cost. This comprehensive exam will not cover this topic. Assume that the generator cost has been linearized and expressed as:

$$F_i = c_i P_i + d_i \quad (2.53)$$

where c_i and d_i are constants for generator i ; P_i is the real power value generated by generator i .

Therefore, the model of problem regarding minimization of generation cost by installing UPFC is described as:

$$\text{Objective:} \quad \text{Min:} \quad \sum_{j=1}^{N_G} (c_j P_{Gj} + d_j)t + c_{upfc} S_{upfc} \quad (2.54)$$

Subject to:

$$P_i = \sum_{m=1}^N V_m G_{im} - \sum_{m \neq i} B_{im} \delta_m - (B_{ii} - b_{ii}) \delta_i \quad \{i \in \phi_b, i \neq s, r\} \quad (2.55)$$

$$Q_i = -\sum_{m \neq i} G_{im} \delta_m - (G_{ii} - g_{ii}) \delta_i - \sum_{m=1}^N V_m B_{im} \quad \{i \in \phi_b, i \neq s, r\} \quad (2.56)$$

$$P_s + B_{sr} V_{sp} = \sum_{m=1}^N V_m G_{sm} - \sum_{m \neq s} B_{sm} \delta_m - (B_{ss} - b_{ss}) \delta_s \quad (2.57)$$

$$P_r - B_{sr} V_{sp} = \sum_{m=1}^N V_m G_{rm} - \sum_{m \neq r} B_{rm} \delta_m - (B_{rr} - b_{rr}) \delta_r \quad (2.58)$$

$$Q_s + I_q + B_{sr} V_{sq} = -\sum_{m \neq s} G_{sm} \delta_m - (G_{ss} - g_{ss}) \delta_s - \sum_{m=1}^N V_m B_{sm} \quad (2.59)$$

$$Q_r - B_{sr} V_{sq} = -\sum_{m \neq r} G_{rm} \delta_m - (G_{rr} - g_{rr}) \delta_r - \sum_{m=1}^N V_m B_{rm} \quad (2.60)$$

$$P_j^{min} \leq P_j \leq P_j^{max} \quad \{j \in \phi_G\} \quad (2.61)$$

$$Q_j^{min} \leq Q_j \leq Q_j^{max} \quad \{j \in \phi_G\} \quad (2.62)$$

$$V_m^{min} \leq V_m \leq V_m^{max} \quad \{m \in \phi_b\} \quad (2.63)$$

$$-\pi \leq \delta_m \leq \pi \quad \{m \in \phi_b\} \quad (2.64)$$

$$-S_{ij}^{max} \leq P_{ij} \leq S_{ij}^{max} \quad \{i, j \in \phi_b\} \quad (2.65)$$

$$-1.15 S_{ij}^{max} \leq P_{ij} - 0.58 Q_{ij} \leq S_{ij}^{max} \quad \{i, j \in \phi_b\} \quad (2.66)$$

$$-1.15 S_{ij}^{max} \leq P_{ij} + 0.58 Q_{ij} \leq S_{ij}^{max} \quad \{i, j \in \phi_b\} \quad (2.67)$$

$$-V_{smax} \leq V_{sq} \leq V_{smax} \quad (2.68)$$

$$-2V_{smax} \leq V_{sq} + \sqrt{3}V_{sp} \leq 2V_{smax} \quad (2.69)$$

$$-2V_{smax} \leq V_{sq} - \sqrt{3}V_{sp} \leq 2V_{smax} \quad (2.70)$$

$$-I_{qmax} \leq I_q \leq I_{qmax} \quad (2.71)$$

where,

$$P_{ij} = \frac{\delta_i - \delta_j}{Z_{ij}} \quad \{i, j \in \phi_b\}$$

$$Q_{ij} = -\frac{V_i B_{ij}}{2} + \frac{V_i - V_j}{Z_{ij}} \quad \{i, j \in \phi_b\}$$

And, N_G is the number of generators; N is the number of buses in the system; ϕ_b is the set of buses in the system; ϕ_G is the set of generators in the system; c_j and d_j are cost coefficients for generator j ; P_{Gj} is the real power generation from the generator unit j ; t is the time duration of the constant load scenario; c_{upfc} is the cost of UPFC in the time period t ; S_{upfc} is the installation capacity of UPFC capacity; V_m is the voltage magnitude at bus m ; δ_i is the voltage angle at bus i ; s is the number of the bus where UPFC shunt converter is installed; r is the number of the bus that is connected to the other end of transmission line, where UPFC series converter is installed; P_i and Q_i are the real and reactive power generation from generator at bus i ; B_{sr} is the bus admittance of transmission line connecting bus s and r ; V_{sp} is $V_s \sin \varphi_s$; V_{sq}^k is $V_s \cos \varphi_s$; V_{smax} is maximum voltage magnitude that series converter can provide; I_q is reactive current provided by shunt converter; I_{qmax} is the maximum reactive current that shunt converter can provide.

S_{upfc} can be calculate by equation (2.72). The first part describes the capacity of series converter and the second part describes the capacity of shunt converter. I_{sr}^{max} is the current capacity of transmission line where UPFC is installed.

$$S_{upfc} = V_{smax} I_{sr}^{max} + I_{qmax} \quad (2.72)$$

The details of number of variables and constraints involved in this problem are shown in Table 2.1 and Table 2.2 respectively.

Table 2.1: Number of Variables

Variable	δ_m	V_m	P_j	Q_j	V_{sq}	V_{sp}	V_{smax}	I_q	I_{qmax}
No.	N	N	N_G	N_G	1	1	1	1	1

Table 2.2: Number of Constraints

Constraint type	Constraints	No. of constraints
Equality constraint	P_i	N
	Q_i	N
Inequality constraint	P_{Gj}	$2N_G$
	Q_{Gj}	$2N_G$
	V_m	$2N$
	δ_m^k	$2N$
	P_{ij}, Q_{ij}	$6N_T$
	V_{sp}, V_{sq}	6
	I_q	2

This optimization model requires to $(N_G \times 2 + N \times 2 + 5)$ variables and $(6 \times N + 4 \times N_G + 6 \times N_T + 8)$ constraints. N_T is the number of transmission lines.

2.5.2 Maximize Revenue for Time-Varying Loading Conditions

The objective function of problems of this category is to maximize the gain obtained by installing UPFC minus the investment of UPFC. It is equivalent to the problem that minimizes the generation cost plus the investment of UPFC. The problem can be mathematically formulated as follows:

$$\text{Objective: Min: } \sum_{k=1}^{N_l} \sum_{j=1}^{N_G} (c_j P_{Gj}^k + d_j) t^k + c_{upfc} S_{upfc} \quad (2.73)$$

Subject to:

$$P_i^k = \sum_{m=1}^N V_m^k G_{im} - \sum_{m \neq i} B_{im} \delta_m^k - (B_{ii} - b_{ii}) \delta_i^k \quad \{i \in \phi_b, i \neq s, r\} \quad (2.74)$$

$$Q_i^k = -\sum_{m \neq i} G_{im} \delta_m^k - (G_{ii} - g_{ii}) \delta_i^k - \sum_{m=1}^N V_m^k B_{im} \quad \{i \in \phi_b, i \neq s, r\} \quad (2.75)$$

$$P_s^k + B_{sr} V_{sp}^k = \sum_{m=1}^N V_m^k G_{sm} - \sum_{m \neq s} B_{sm} \delta_m^k - (B_{ss} - b_{ss}) \delta_s^k \quad (2.76)$$

$$P_r^k - B_{sr} V_{sp}^k = \sum_{m=1}^N V_m^k G_{rm} - \sum_{m \neq r} B_{rm} \delta_m^k - (B_{rr} - b_{rr}) \delta_r^k \quad (2.77)$$

$$Q_s^k + I_q^k + B_{sr} V_{sq}^k = -\sum_{m \neq s} G_{sm} \delta_m^k - (G_{ss} - g_{ss}) \delta_s^k - \sum_{m=1}^N V_m^k B_{sm} \quad (2.78)$$

$$Q_r^k - B_{sr} V_{sq}^k = -\sum_{m \neq r} G_{rm} \delta_m^k - (G_{rr} - g_{rr}) \delta_r^k - \sum_{m=1}^N V_m^k B_{rm} \quad (2.79)$$

$$P_j^{min} \leq P_j^k \leq P_j^{max} \quad \{j \in \phi_G\} \quad (2.80)$$

$$Q_j^{min} \leq Q_j^k \leq Q_j^{max} \quad \{j \in \phi_G\} \quad (2.81)$$

$$V_m^{min} \leq V_m^k \leq V_m^{max} \quad \{m \in \phi_b\} \quad (2.82)$$

$$-\pi \leq \delta_m^k \leq \pi \quad \{m \in \phi_b\} \quad (2.83)$$

$$-S_{ij}^{max} \leq P_{ij}^k \leq S_{ij}^{max} \quad \{i, j \in \phi_b\} \quad (2.84)$$

$$-1.15 S_{ij}^{max} \leq P_{ij}^k - 0.58 Q_{ij}^k \leq S_{ij}^{max} \quad \{i, j \in \phi_b\} \quad (2.85)$$

$$-1.15 S_{ij}^{max} \leq P_{ij}^k + 0.58 Q_{ij}^k \leq S_{ij}^{max} \quad \{i, j \in \phi_b\} \quad (2.86)$$

$$-V_{smax}^k \leq V_{sq}^k \leq V_{smax}^k \quad (2.87)$$

$$-2V_{smax}^k \leq V_{sq}^k + \sqrt{3}V_{sp}^k \leq 2V_{smax}^k \quad (2.88)$$

$$-2V_{smax}^k \leq V_{sq}^k - \sqrt{3}V_{sp}^k \leq 2V_{smax}^k \quad (2.89)$$

$$0 \leq V_{smax}^k \leq V_{smax} \quad (2.90)$$

$$-I_{qmax} \leq I_q^k \leq I_{qmax} \quad (2.91)$$

where,

$$P_{ij}^k = \frac{\delta_i^k - \delta_j^k}{Z_{ij}} \quad \{i, j \in \phi_b\}$$

$$Q_{ij}^k = -\frac{V_i^k B_{ij}}{2} + \frac{V_i^k - V_j^k}{Z_{ij}} \quad \{i, j \in \phi_b\}$$

$$S_{upfc} = V_{smax} I_{sr}^{max} + I_{qmax}$$

And, N_l is the number of load scenario under study; N_G is the number of generators; N is the number of buses in the system; ϕ_b is the set of buses in the system; ϕ_G is the set of generators in the system; c_j and d_j are cost coefficients for generator j ; P_{Gj}^k is the real power generation from the generator unit j in load scenario k ; c_{upfc} is the price rate of UPFC in terms of \$/p.u.; S_{upfc} is the UPFC capacity; t^k is the time duration of load scenario k ; V_m^k is the voltage magnitude at bus m in load scenario k ; δ_i^k is the voltage angle at bus i in load scenario k ; s is the number of the bus where UPFC shunt converter is installed; r is the number of the bus that is connected to the other end of transmission line, where UPFC series converter is installed; P_i^k and Q_i^k are the real and reactive power generation from generator at bus i in load scenario k ; B_{sr} is the bus admittance of transmission line connecting bus s and r ; V_{sp}^k is $V_s \sin \varphi_s$ in scenario k ; V_{sq}^k is $V_s \cos \varphi_s$ in scenario k ; I_q^k is I_q in load scenario k ; V_{smax}^k is V_{smax} in load scenario k . V_{smax} is the maximum magnitude of series voltage that installed UPFC can provide; I_{qmax} is the maximum current magnitude of reactive power that UPFC shunt converter can provide; I_{sr}^{max} is the current capacity of transmission line where UPFC is installed.

The details of number of variables and constraints involved in this problem are shown in Table 2.3 and Table 2.4 respectively.

Table 2.3: Number of Variables

Variable	δ_m^k	V_m^k	P_j^k	Q_j^k	V_{sq}^k	V_{sp}^k	I_q^k	V_{smax}	I_{qmax}
No.	$N \times N_l$	$N \times N_l$	$N_G \times N_l$	$N_G \times N_l$	N_l	N_l	N_l	1	1

Table 2.4: Number of Constraints

Constraint type	Constraints	No. of constraints
Equality constraint	P_i^k	$N_l \times N$
	Q_i^k	$N_l \times N$
Inequality constraint	P_{Gj}^k	$N_l \times 2N_G$
	Q_{Gj}^k	$N_l \times 2N_G$
	V_m^k	$N_l \times 2N$
	δ_m^k	$N_l \times 2N$
	P_{ij}^k, Q_{ij}^k	$N_l \times 6N_T$
	V_{sp}^k, V_{sq}^k	$6N_l$
	V_{smax}^k	$2N_l$
	I_{qmax}^k	$2N_l$

The problem of this category is more complex to solve than the one described in Section 2.5.1, because all the system states in different load scenarios are coupled by V_{smax} and I_{qmax} . It is required to solve this linear optimization problem with $N_l \times (2N_G + 2N + 3) + 2$ states and $N_l \times (6N + 4N_G + 6N_T + 10)$ constraints in one shot. N_T is the number of transmission lines in the system. The limitation is that the size of memory required to store data is growing quadratically with the number of load scenarios.

2.6 Simulation Result

2.6.1 Maximize Revenue for Constant Loading Conditions

The simulation of maximizing revenue for constant load scenario is conducted on IEEE 24-bus reliability test system (IEEE-RTS) [27], which is a small-scale power system with 24 buses, 32 generators and 38 transmission lines. It was found that in the original IEEE-RTS system, the transmission system is strong compared to the generation system, and consequently little transmission congestion is encountered. Hence it was suggested [29] that the system be modified by multiplying the generation by a factor of 2 and the loads by a factor of 1.8 while keeping the transmission

capacities the same. This resulting modified RTS, sometimes referred to as MRTS, is used in this work. RTS system has 32 generators. Depending on the cost curves and locations of the generators, they are categorized into 14 groups.

The number of variables and constraints involved in this simulation are listed in Table 2.5 and 2.6. There are totally 81 variables and 436 constraints.

Table 2.5: Number of Variables

Variable	δ_m	V_m	P_j	Q_j	V_{sq}	V_{sp}	I_q	V_{smax}	I_{qmax}
No.	24	24	14	14	1	1	1	1	1

Table 2.6: Number of Constraints

Constraint type	Constraints	No. of constraints
Equality constraint	P_i	24
	Q_i	24
Inequality constraint	P_{Gj}	28
	Q_{Gj}	28
	V_m	48
	δ_m	48
	P_{ij}, Q_{ij}	228
	V_{sp}, V_{sq}	6
	I_q	2

If considering the maximum loading condition of IEEE-RTS, whose total amount of load is $2850 \times 1.8 = 5130$ MW, the simulation results are summarized in Table 2.7 for 2-month, 1-year, 3-year, 5-year and 10-year utilization of UPFC respectively. It is shown for different locations, the size of optimal UPFC and the potential revenue after installing UPFC are completely different. Therefore, it can be very beneficial to conduct benefit study before installing UPFC. The results also show that if the longevity of UPFC can be increased, the revenue is increased considerably. The column ‘‘Max Savings’’ shows the savings that if no transmission constraints exist, the amount of generation cost that can be reduced. If the UPFC is installed in branch 16–19 and the utilization of the UPFC is five years, total generation saving is \$105.6 million dollars, which is about 12.76%

of the maximum savings that can be achieved in the case of no transmission line constraints.

Table 2.7: Simulation Result for Constant Loading Conditions

No. of year	Max Savings		15–16	16–19
2 months	\$27.58 Million	Series Capacity (p.u.)	0.0644	0.2996
		Shunt Capacity (p.u.)	0	0
		Investment (Million)	\$0.2578	\$1.1982
		Revenue (Million)	\$0.05	\$2.34
1 year	\$165.51 Million	Series Capacity (p.u.)	0.067	0.3317
		Shunt Capacity (p.u.)	0	0
		Investment (Million)	\$0.2679	\$1.3269
		Revenue (Million)	\$1.61	\$20.05
3 years	\$496.5 Million	Series Capacity (p.u.)	0.0674	0.3329
		Shunt Capacity (p.u.)	0	0
		Investment (Million)	\$0.2695	\$1.3317
		Revenue (Million)	\$5.3	\$62.8
5 years	\$827.5 Million	Series Capacity (p.u.)	0.0674	0.3329
		Shunt Capacity (p.u.)	0	0
		Investment (Million)	\$0.2695	\$1.3317
		Revenue (Million)	\$9.1	\$105.6
10 years	\$1655.1 Million	Series Capacity (p.u.)	0.0674	0.3329
		Shunt Capacity (p.u.)	0	0
		Investment (Million)	\$0.2695	\$1.3317
		Revenue (Million)	\$18.5	\$212.5

In case 2, the reactive power load is multiplied by a factor of 3.2 instead of 1.8 to stress the reactive power regulation on the system. The 155 MW generator connected to bus 15 and 155 MW generator connected to bus 16 are also restricted from participating in the voltage regulation. Simulation results are shown in Table 2.8. From the table, it can be seen that for short-time utilization of UPFC, it is not economical to install shunt converter. The reason is because in this study, the objective function is to reduce generation cost taking into account of the investment of UPFC; while shunt converter is mainly responsible for voltage regulation, which has very limited influence on reducing generation cost. However, when the time of utilization grows, the value produced by each VA of shunt converter increases, then it becomes economical to install shunt converter.

Fig. 2.11 displays the relationship between the capacity of UPFC and the investment. The

Table 2.8: Simulation Result For Constant Loading Conditions with Deficient Reactive Power Generation

No. of year	Max Savings		15–16	16–19
2 months	\$27.89 Million	Series Capacity (p.u.)	0.0678	0.2936
		Shunt Capacity (p.u.)	0	0
		Investment (Million)	\$0.2712	\$1.1743
		Revenue (Million)	\$0.09	\$2.36
1 year	\$167.43 Million	Series Capacity (p.u.)	0.1983	0.2936
		Shunt Capacity (p.u.)	0	0
		Investment (Million)	0.7930	\$1.1743
		Revenue (Million)	2.6	\$20.1
3 years	\$502.1 Million	Series Capacity (p.u.)	0.1983	0.2944
		Shunt Capacity (p.u.)	0	0.222
		Investment (Million)	\$0.7930	\$2.0656
		Revenue (Million)	\$9.1	\$62.6
5 years	\$836.8 Million	Series Capacity (p.u.)	0.1983	0.2944
		Shunt Capacity (p.u.)	0	0.222
		Investment (Million)	\$0.7930	\$2.0656
		Revenue (Million)	\$15.8	\$105.8
10 years	\$1673.8 Million	Series Capacity (p.u.)	0.1983	0.3732
		Shunt Capacity (p.u.)	0	1.2003
		Investment (Million)	\$0.7930	\$6.2941
		Revenue (Million)	\$32.2	\$216.5

investment is increased when the installed capacity of the UPFC increases. Fig. 2.12 displays the relationship between the capacity of UPFC and the benefit obtained by the UPFC when the utilization of UPFC is five years and it is installed in branch 16–19. It can be seen that the benefit is achieved maximum at a specific capacity. Installing more or less capacity of UPFC than the optimal capacity will decrease the benefit; therefore, it is very meaningful to conduct benefit study to obtain the optimal capacity of UPFC required to install. Fig. 2.13 presents the production costs saved by UPFC and the payments for the equipment financed for 10 years at 5% interest. The figure shows that after 10 years, the production cost can be saved about 200 million dollars when installing UPFC at branch 16–19.

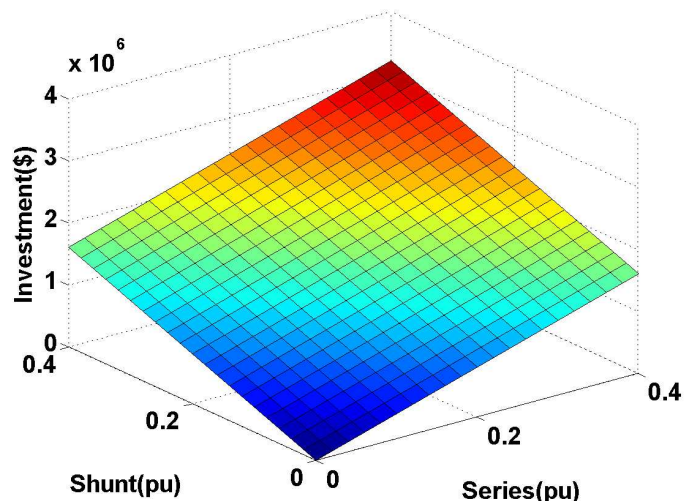


Figure 2.11: UPFC investment versus capacity

2.6.2 Maximize Revenue for Time-Varying Loading Conditions

The simulation of maximizing revenue is also conducted on IEEE 24-bus reliability test system (IEEE-RTS) [27]. It has load data of 364 days. This simulation produces load data of the 365th day the same as the load of the first day. Since they are neighbors in the calendar, their load profile may share similarity. Therefore, there are totally 8760 load points in term of hours for a year. The number of coefficients for the inequality constraints can be calculated by the number of inequality constraints multiplying the number of states. If all 8760 load points are considered, the number

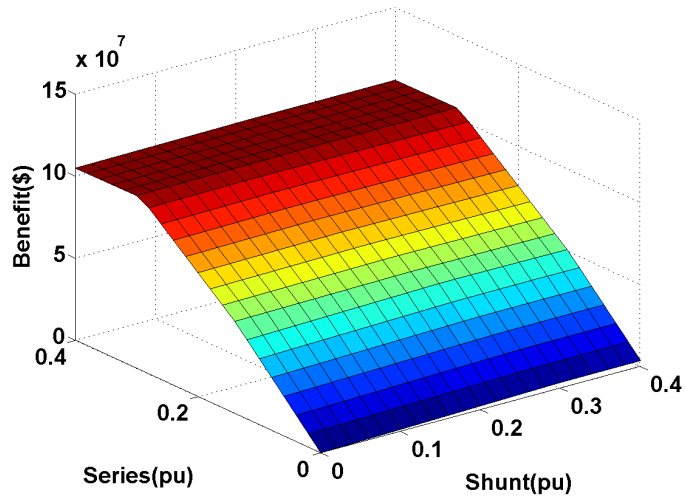


Figure 2.12: UPFC benefit versus capacity

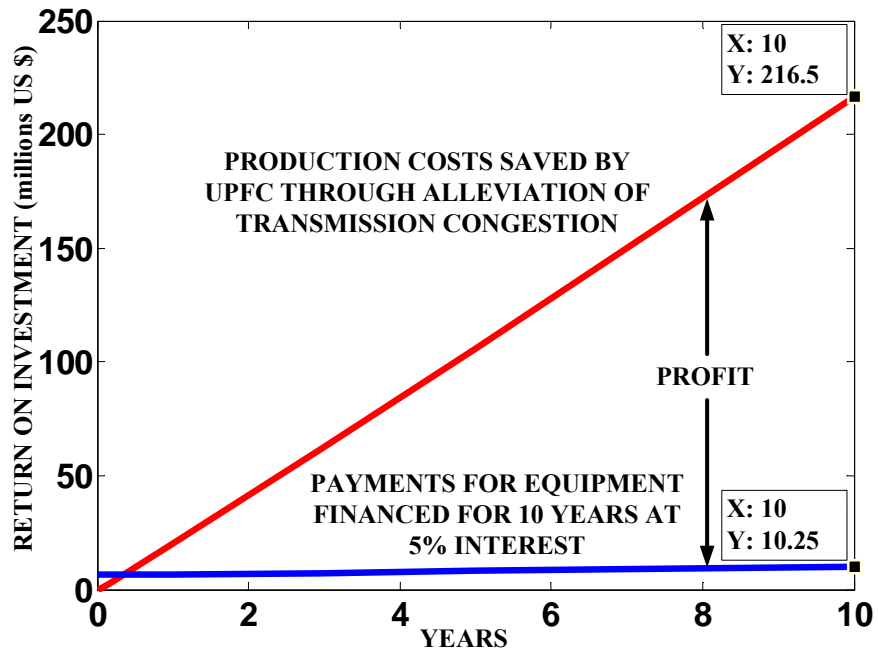


Figure 2.13: Production savings over equipment cost

of data required to store for the coefficients of inequality constraints is about 2.35×10^{12} . If the type of data is double and the simulation platform is 32-bit, then the size of memory required is about 8763 GB, which is tremendously huge. In order to reduce the memory required for the calculation, this simulation makes approximations by categorizing these 8760 load points into 6 levels and computes the weight for each load level. For example, if load demand is between 0.9 p.u. – 1.0 p.u., it belongs to category 0.9 – 1.0. Table 2.9 shows the result of the load categories. “Average” column lists the average of load demands belonging to each category. “No. of Points” column lists the number of points in each category. “Weight” column is calculated by the number of points for each category dividing total number of points. After the categorization, there are six load scenarios. The objective function in this simulation can be described as:

Table 2.9: Load Categories

Category	Average	No. of Points	Weight
0.9 – 1.0	0.9275	115	0.0131
0.8 – 0.9	0.8388	972	0.1110
0.7 – 0.8	0.7497	1456	0.1662
0.6 – 0.7	0.6484	2029	0.2316
0.5 – 0.6	0.5467	1888	0.2155
0 – 0.5	0.4443	2300	0.2626

$$F = \sum_{k=1}^6 \sum_{j=1}^{14} (c_j P_{Gj}^k + d_j) \times \omega_k \times N_{year} \times 8760 + c_{upfc} S_{upfc} \quad (2.92)$$

where ω_k is the weight for each scenario listed in Table 2.9; N_{year} is the number of years that UPFC can work. Ref. [28] summarizes cost functions for traditional FACTS devices, where c_{upfc} can be obtained. However, in this simulation $c_{upfc} = \$0.04/VA$, since the transformer-less UPFC built in Michigan State University achieves this target.

The number of variables and constraints involved in this simulation are listed in Tables 2.10 and 2.11 respectively. There are totally 476 variables and 2628 constraints.

In case 1, simulations are conducted for 1-year, 3-year, 5-year, 10-year and 20-year utilization

Table 2.10: Number of Variables

Variable	δ_m^k	V_m^k	P_j^k	Q_j^k	V_{sq}^k	V_{sp}^k	I_q^k	V_{smax}	I_{qmax}
No.	144	144	84	84	6	6	6	1	1

Table 2.11: Number of Constraints

Constraint type	Constraints	No. of constraints
Equality constraint	P_i^k	144
	Q_j^k	144
Inequality constraint	P_{Gj}^k	168
	Q_{Gj}^k	168
	V_m^k	288
	δ_m^k	288
	P_{ij}^k, Q_{ij}^k	1368
	V_{sp}^k, V_{sq}^k	36
	V_{smax}^k	12
	I_{qmax}^k	12

of UPFC respectively. Simulation results are shown in Table 2.12. From the results, it can be seen that as the time of utilization increases, the optimal capacity of UPFC will increase. It is quite reasonable, because as the time of utilization increases, the value produced by each VA is increased, which increases optimal value of the capacity of UPFC. However, there will be an upper bound on the optimal value, because any capacity value larger than this upper bound will not provide more controllability for the grid from UPFC. Note that no matter how many years the UPFC can be utilized, the shunt converter is always zero. The reason is because shunt converter is mainly responsible for reactive power and voltage regulation. In this case, the reactive power from the generators is sufficient enough to satisfy reactive load demand and regulate bus voltage. It does not need any shunt converter to participate in the reactive power regulation.

Table 2.12: Simulation Result of Case 1

No. of year	Gen. cost		17–22	16–19
1 year	\$496.05 Million	Series Capacity (p.u.)	0	0.2935
		Shunt Capacity (p.u.)	0	0
		Investment (Million)	\$0	\$1.1732
		Revenue (Million)	\$0	\$0.2000
3 years	\$1488.1 Million	Series Capacity (p.u.)	0.43	0.357
		Shunt Capacity (p.u.)	0	0
		Investment (Million)	\$1.7194	\$1.4279
		Revenue (Million)	\$0.1	\$3.3
5 years	\$2480.2 Million	Series Capacity (p.u.)	0.798	0.3595
		Shunt Capacity (p.u.)	0	0
		Investment (Million)	\$3.1929	\$1.4389
		Revenue (Million)	\$2.4	\$6.4
10 years	\$4960.5 Million	Series Capacity (p.u.)	0.8075	0.3595
		Shunt Capacity (p.u.)	0	0
		Investment (Million)	\$3.2293	\$1.4389
		Revenue (Million)	\$8.0	\$14.4
20 years	\$9921.0 Million	Series Capacity (p.u.)	0.9095	0.364
		Shunt Capacity (p.u.)	0	0
		Investment (Million)	\$3.6371	\$1.4554
		Revenue (Million)	\$19.4	\$30.2

In case 2, the reactive power load is multiplied by a factor of 3.5 instead of 1.8 to stress the reactive power regulation on the system. The 155 MW generator connected to bus 15 and 155

MW generator connected to bus 16 are also restricted from participating in the voltage regulation. Simulation results are shown in Table 2.13.

Table 2.13: Simulation Result of Case 2

No. of year	Gen. cost		15–16	16–19
1 year	\$497.9 Million	Series Capacity (p.u.)	0.273	0.2835
		Shunt Capacity (p.u.)	0	0
		Investment (Million)	1.093	\$1.1343
		Revenue (Million)	1.78	\$1.37
3 years	\$1493.7 Million	Series Capacity (p.u.)	0.277	0.358
		Shunt Capacity (p.u.)	0	0
		Investment (Million)	\$1.1080	\$1.4310
		Revenue (Million)	\$7.5	\$6.9
5 years	\$2489.5 Million	Series Capacity (p.u.)	0.2835	0.358
		Shunt Capacity (p.u.)	0.4212	0
		Investment (Million)	\$2.8183	\$1.4310
		Revenue (Million)	\$13.8	\$12.4
10 years	\$4979.0 Million	Series Capacity (p.u.)	0.318	0.3595
		Shunt Capacity (p.u.)	0.7092	0.5009
		Investment (Million)	\$4.1081	\$3.4425
		Revenue (Million)	\$31.5	\$27.2
20 years	\$9958.0 Million	Series Capacity (p.u.)	0.3095	0.3635
		Shunt Capacity (p.u.)	0.8699	0.9636
		Investment (Million)	\$4.7168	\$5.3092
		Revenue (Million)	\$67.1	\$58.9

2.7 Summary

This chapter utilizes linearization techniques and develops a fast and reliable model for UPFC benefit study. The contributions are listed as follows:

1. Developed a linearized model of UPFC taking both series and shunt converters into account.
2. Developed a complete linearized model and algorithm for UPFC benefit study, including model of maximizing revenue for constant loading condition and model of maximizing revenue for time-varying loading conditions. This model is benefit for fast, accurate and reli-

able characteristics. Because of this linear character, this algorithm is guaranteed to find the global optimal solution, which none of AC models and algorithms can guarantee.

3. The linearized algorithm developed in this chapter is a general one, which is not limited for UPFC benefit study, but can also be extended to other FACTS devices.

Future work for this chapter includes:

1. Develop an algorithm that examines all the load scenarios within acceptable size of memory. This will cover two possible solutions, 1) combining nonlinear techniques and the algorithm developed in this chapter to reduce the size of memory. 2) decoupling coefficients matrix of equality and inequality constraints to divide the memory size into small pieces and examines these pieces one by one.
2. Simulate nonlinear model and DC model for comparisons in terms of calculation time and accuracy.
3. Extend the developed algorithm to other FACTS devices.

Chapter 3

Optimal UPFC Placement and Parameter Selection to Minimize Generation Costs

3.1 Introduction

Chapter 2 presented a linearized methodology for UPFC benefit study in a pre-specific location. It showed that by deploying UPFC in certain locations, the congestion of transmission lines can be greatly alleviated and the economic profit is quite considerable because of the reduced generation cost. However, in practice, sometimes the location of the UPFC may not be given. Since the investment of UPFC requires a large capital cost and not every branch would provide benefit by installing UPFC, it is quite necessary to conduct research to determine the optimal location of placing UPFC.

The influences of installing UPFC have area characteristics. In some areas where the power transmissions are highly congested, the generation cost can be greatly improved by installing UPFC. However, in some other areas where transmission systems are not congested, installing UPFC may not provide any benefit. Previously, many researchers have realized the importance of finding an optimal place to install UPFC so that the benefit can be maximized [30–33]. A simple way to determine the optimal place of installing UPFC is to install it in every branch of the studied

power system model and calculate the benefit after installing UPFC. The branch which offers the largest benefit after installing UPFC is the optimal place. This method could be very computational expensive if the studied system is large with thousands or tens of thousands of branches.

If locations are coded as integer numbers, optimal placement and parameters selection problem of UPFC becomes a mixed-integer optimization problem. Because of the discrete characteristics of integers, traditional gradient based optimization approach usually fails in solving integer problems. Besides, differs from other mixed-integer optimization problems, the integers in this problem are names. They do not have any mathematical meanings. They can not be compared depending on their values. Therefore, the most popular integer optimization method, branch and bound, fails. Refs. [30–32] use various intelligent methods, such as genetic algorithm or particle swarms, to search for the optimal locations. These methods can find the optimal results; however, the efficiencies of these methods are not satisfying when dealing with large systems. This chapter studies the sensitivity of original power system without installing UPFC and proposes a methodology to rename/renumber the branches so that the efficiencies of intelligent methods can be greatly improved.

3.2 Methodology

3.2.1 Problem Analysis

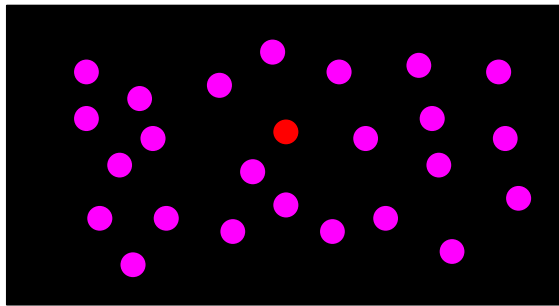
The way of numbering branches is quite critical for the efficiency of intelligent methods, such as genetic algorithm. The reasons can be explained as follows: the solutions of genetic algorithm are expressed as chromosomes and these chromosomes are composed of genes. The principle of genetic algorithm is that after the selection, chromosomes with good genes are kept while those with bad genes are abandoned. The evolution of chromosomes will lead to the best chromosome in the end, which is the optimal solution. By looking deeply into this process, there are two important and interesting points which should be paid attention on: 1. The evolutionary of chromosomes is usually slow and step by step. It always goes from worse chromosomes to better ones and then

more better ones. After many generations of evolution, it can finally reach the best one. The probability of evolution from worse chromosomes directly to the best one is quite low. 2. Better chromosomes and the best chromosomes always share some common genes. Therefore, when these genes are found and kept, the chromosomes are evolving to the best one.

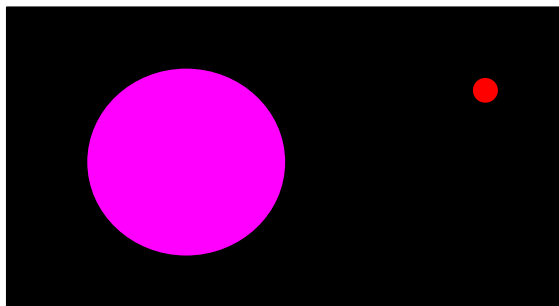
In the placement of UPFC problem, the number of branches are names. They do not have any mathematical meaning. If they are not carefully numbered, it is very high likely that the best solution is surrounded by bad solutions. In this case, the evolution to the best solution is very low efficiency. Fig. 3.1 below gives three examples of coding scenarios. Black area is the total solution space; Magenta area is the collection of good solutions with smaller fitness function values; Red dot is the optimal solution with the smallest fitness function value. In Fig. 3.1(a), locations are coded randomly. Good solutions and the optimal solution are spread out randomly in the solution space. In this case, the good solutions and optimal solution do not share any common genes. The population will be very difficult to converge to the optimal solution. Hence, it is very inefficiency for the GA to find the optimal solution. In Fig. 3.1(b), the optimal solution is coded outside the region of good solutions. It is very likely that the final population will converge to a sub-optimal solution in the magenta area while missing the optimal solution. Fig. 3.1(c) is a good coding strategy. Initially, the population is evenly distributed over the solution space; but after a certain generations, the population will find the good solutions and converge to the magenta good solution area and finally find the optimal one inside the magenta area. Therefore, it can be deduced that if good solutions are mapped together and share a few common genes, they are more easily to be found.

3.2.2 Sensitivity Analysis and Branch Numbering

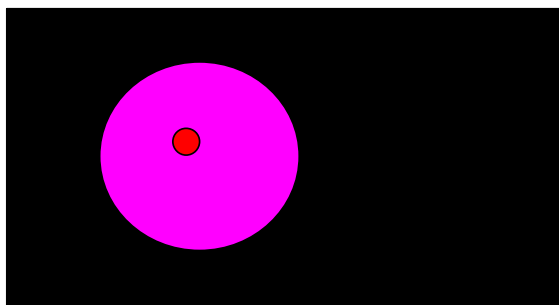
In a stressed power transmission system, some of the transmission lines are carrying power up to their limits. These transmission line constraints prevent power transferred from cheap generation area to expensive generation area through these constrained lines. Therefore, total system generation cost is increased. UPFC has the ability to insert a voltage vector in a transmission line



(a)



(b)



(c)

Figure 3.1: (a) Bad solution space; (b) bad solution space; (c) good solution space

to regulate the real power transfers, and can also independently control reactive power injections. Hence, it can redirect the power flows going through other unconstrained transmission lines to the expensive generation area and decrease the generation cost.

Installing UPFC in the congested areas has more effect to improve generation cost than installing UPFC in non-congested areas. Sensitivity analysis of power system before installing UPFC can provide a way to find congested areas, which are good candidates to install UPFC and potential good solutions described in section 3.2.1. The model of power system before installing UPFC can be described as:

$$\text{Min: } F(\mathbf{x}, \mathbf{u}) \quad (3.1)$$

$$\text{Subject to: } g_{i=1,2,3\dots m}(\mathbf{x}, \mathbf{u}) \leq 0 \quad (3.2)$$

$$h_{j=1,2,3\dots n}(\mathbf{x}, \mathbf{u}) = 0 \quad (3.3)$$

where $F(\mathbf{x}, \mathbf{u})$ is the objective function; $g_i(\mathbf{x}, \mathbf{u})$ is the inequality constraint; $h_j(\mathbf{x}, \mathbf{u})$ is the equality constraint. The Lagrangian function can be expressed:

$$L = F(\mathbf{x}, \mathbf{u}) + \sum_{i=1}^m \mu_i g_i(\mathbf{x}, \mathbf{u}) + \sum_{j=1}^n \lambda_j h_j(\mathbf{x}, \mathbf{u}) \quad (3.4)$$

where μ_i and λ_j are Lagrange multipliers for inequality and equality constraints respectively. μ_i is called marginal cost of the inequality constraint. It reflects the change of objective function by changing the constant of inequality constraint slightly. A large value of μ_i implies the corresponding inequality constraint is very binding while a zero μ_i means the corresponding inequality constraint is unbinding. By examining the marginal cost of transmission constraints, power flow congestions can be located.

The principle to optimally number branches is as follows: first, identify the congested branches by running base-case optimal power flow model without UPFC and examine high marginal cost branches; second, locate the branches adjacent to these congested branches. These selected branches

including high marginal cost branches and their adjacent branches are potentially optimal place to locate UPFC. The procedures of numbering the branches can be described as follows:

- (1) Run the base-case optimal power flow without installing UPFC and rank the marginal cost of branches;
- (2) Number the branch which has the largest marginal cost but not numbered yet;
- (3) Consecutively number the branches which are not numbered yet and adjacent to the numbered branch in step 2;
- (4) If the largest marginal cost of remaining unnumbered branches is less than a threshold value, number the all the remaining unnumbered branches consecutively based on their locations and the process is ended; otherwise go to step 2.

The flowchart of the procedures is shown in Fig. 3.2.

3.2.3 Configuration of the Algorithm

Genetic algorithm is being utilized and combined with linear programming to find the optimal placement and parameters for UPFC. The combined algorithm is designed and shown in Fig. 3.3. The genetic algorithm performs as the engine of the algorithm. It picks up locations for the linearized model, receives the fitness function values of picked locations, compares them and picks up new locations until the fitness function values converge.

3.2.3.1 Fitness Function

Normally, fitness function is formulated from objective function of the optimization problem. For a minimization problem, a popular way to construct fitness function, also known as penalty based fitness function, is to sum the objective function and the penalty of the violation of constraints. The performance of penalty based fitness function is highly dependent on the selection of penalty coefficients. An unsuitable penalty coefficients may result in the delay of convergence or even

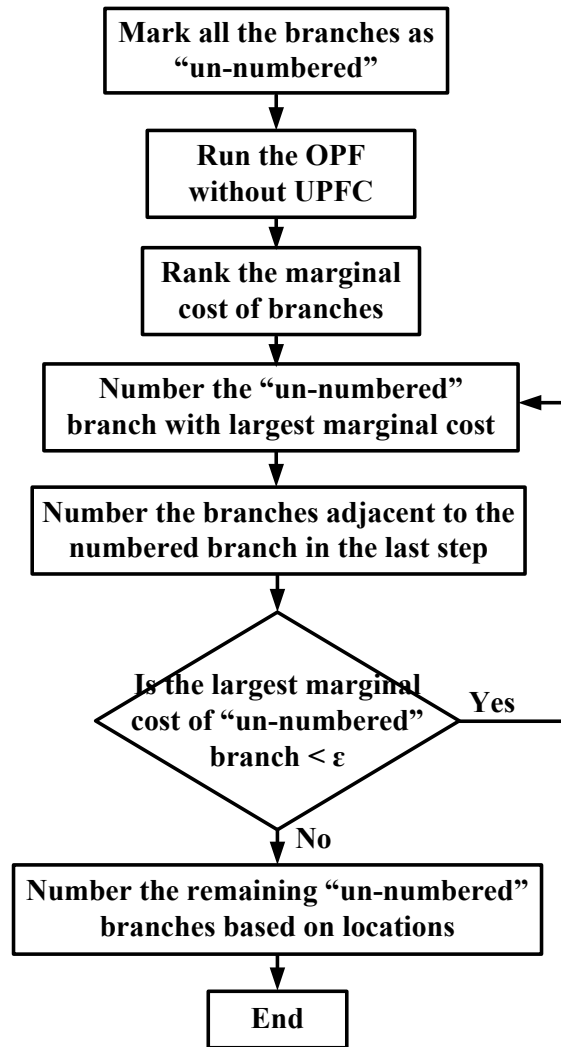


Figure 3.2: Flow chart of numbering branches

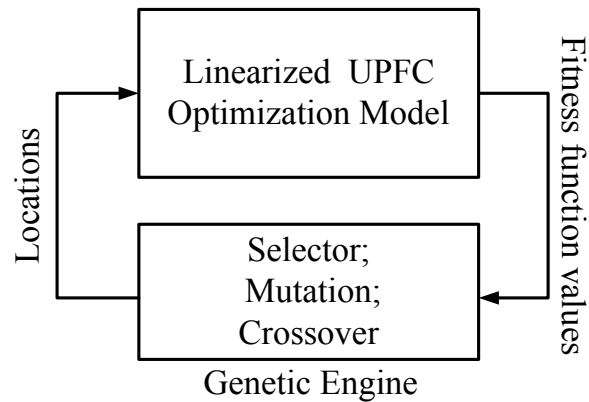


Figure 3.3: Configuration of the algorithm

making the the problem diverge. A penalty-parameter-less fitness function can be used to avoid the selection of penalty coefficients. It is described as:

$$f = \begin{cases} f_{min} & \text{for } 1 < l < l_{max} \\ F + c * (l - l_{max}) & \text{if } l > l_{max} \\ F & \text{if } l = 0 \end{cases} \quad (3.5)$$

where l_{max} is the number of locations to install UPFC; F is a large value, larger than the biggest value of the fitness function values when l is between 1 and l_{max} , so that once variable l is not selected in a valid position to install UPFC, the fitness function will get a large value and selector will not choose this point to survive; c is a coefficient penalizing the selection of l outside feasible positions.

3.2.3.2 Number of Genes

The number of genes to construct the chromosome is determined by:

$$\log_2^{l_{max}} - 1 < B \leq \log_2^{l_{max}} \quad (3.6)$$

where l_{max} is the number of locations to install UPFC.

3.2.3.3 Crossover

Crossover is to produce two new children by reorganizing the information from two parents. A single-point crossover is shown in Fig. 3.4. A random crossing site is chosen and two parents exchange the genes on the right side of the selected site to create two new children. If a suitable crossover place is selected, good genes can be combined from parents to form better children. On the other hand, if the selection place is not appropriate, the children can be worse than the parents. Children that inherit good genes from their parents will survive and reproduce in the next generation while those not inheriting good genes will die out after the selection operation.

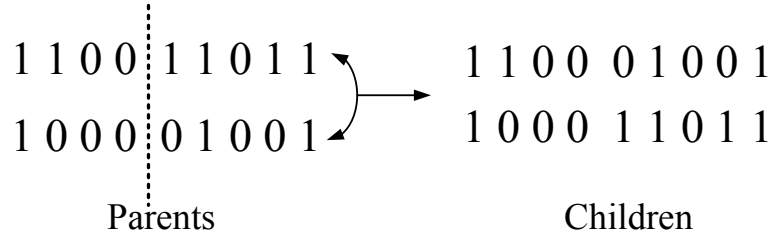


Figure 3.4: Crossover strategy

3.2.3.4 Mutation

Mutation operator, which changes 0 to 1 and vice versa with probability p_m , is applied to introduce diversity to the existing population. It can realize a local search by producing a point in the neighborhood of current point.

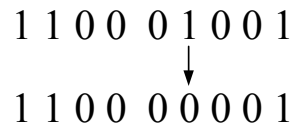


Figure 3.5: Mutation strategy

3.2.3.5 Selection

The selection operator selects good chromosomes in a population and forms a mating pool to reproduce children. This dissertation utilizes the strategy that sorts parents and children together based on the fitness function values and selects the half population with smaller values.

3.3 Case Study

To validate the effectiveness of the proposed genetic-linear combination algorithm for the optimal placement and parameter selection of UPFC, IEEE 300 test system [69] is studied. It has 411 transmission lines and 69 generators. In the original IEEE 300 bus system, the limits of transmission lines are too loose that none congestion exists. To stress the transmission system, the constraints of transmission lines are modified to $0.26/x$ p.u., where x are the reactance of transmission lines.

There are 411 transmission lines; therefore, the number of possible locations to install UPFC is 822. It can be calculated from Eq. (3.6) that the number of genes needed is 10. The crossover probability and mutation probability are taken as 0.9 and 0.2 respectively. The coefficients in the fitness function take values as follows: $M = 10^{12}$, $c=10^{11}$.

The simulation results of base case are shown in Table 3.1. It can be seen from Table 3.1 that the benefits brought by installing UPFC are very competitive. For example, the benefit investment ratio of half a year utilization of UPFC is about 5.71. This table also clearly presents that the series part of UPFC is more significant in reducing operating cost than the shunt part. If the longevity of UPFC is increased, the economic benefit of UPFC is also increased considerably.

Table 3.1: Simulation Optimal Placement and Parameter Selection of UPFC

No. of year	Location	Series(pu)	Shunt(pu)	Invest(M)	Benefit(M)
0.5 year	121–119	0.1749	0	0.70	3.99
1 year	191–225	1.6693	0	6.68	9.76
5 year	191–225	1.6749	0	6.70	70.56
10 year	191–225	1.6749	0	6.70	157.91

Table 3.2 shows the benefits of subsequent investments. It displays that the benefits of subsequent investment will decrease, since the congestion problem is relieved by the previous installation of UPFC.

Table 3.2: Simulation Results of Subsequent Investment in the Case of 5-Year Utilization of UPFC

Investment	Location	Series(pu)	Shunt(pu)	Invest(M)	Benefit(M)
1	191–225	1.6749	0	6.70	70.56
2	192–191	1.5070	0	6.03	67.35
3	121–119	0.1749	0	0.70	45.49

Fig. 3.6 compares two strategies of coding branch numbers. The utilization of UPFC is assumed to be five years. The program runs 200 generations each time and 100 times each strategy. The average of each generation of the 100 runs of each strategy are calculated and compared. The red curve represents the average fitness value of each generation when the branch numbers are

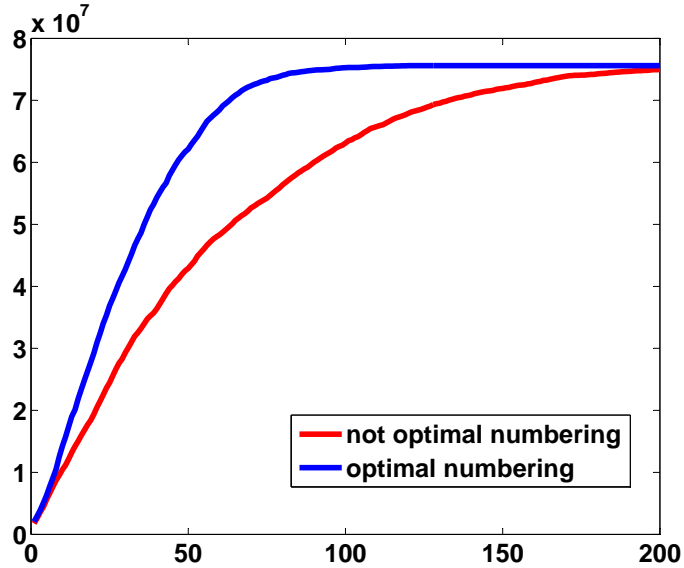


Figure 3.6: Average value of the population for the genetic algorithm with optimal branch numbering and not optimal branch numbering.

not optimized. The blue curve shows the average fitness function values of each generation when using optimal numbering strategy. It can be seen that good coding of branch number helps the program to converge to the optimal solution quicker. When using the optimal numbering strategy proposed in this section, the genetic algorithm converges in about 100 generations; however, for the one without optimal numbering strategy, the program converges after 200 generations.

3.4 Conclusion

This chapter develops an efficient approach combining genetic algorithm and the proposed linearized framework to find the optimal location and parameters of UPFC. It presents the benefits of installing UPFC versus investments by applying the proposed approach to the IEEE 300 bus system. The test results present the considerable benefits brought by installing UPFC. It also shows the diminishing returns when subsequent investments are made one after another. The contributions of this chapter is listed as follows:

1. Developed a combined algorithm using genetic algorithm and linearized optimal power flow framework for the optimal location and parameter selection of UPFC.

2. Developed an optimal branch numbering strategy to accelerate the convergence speed of the proposed UPFC location and parameter selection strategy.
3. The proposed location and parameter selection approach is a generalized approach and it can also be extended to other FACTS devices.

Part III

Distributed Methods for the Control in Microgrid

Chapter 4

Distributed Power Balance Control

4.1 Introduction

Normally, a microgrid can be operated in two modes: grid-connected mode and islanded mode. In grid-connected mode, all micro-sources are expected to supply power at their rated capacity to minimize power imported from the grid, and load can consume at its demand, since the power available in the grid is sufficient. While in islanded mode, micro-sources and load cannot generate or consume simply following their willing, since the grid is unavailable to consume or provide extra power for microgrids. It is required that the power provided by DGs must satisfy the total demand of load plus line loss. Otherwise, some load have to be shed in order to match power generation and power consumption. DGs and load need to be coordinated to keep the balance that at any instantaneous time, the power generation and consumption should be equal within the microgrid.

In large power system, system operators are employed to be responsible to dispatch generation or curtail load to keep power balance and maintain safe operation of the system. However, because of small size and large number of DGs, it is not feasible and economic to hire system operators to coordinate DGs and load to achieve power balance; While on the other hand, DGs with power electronic interfaces lack inertia and respond fast to the system disturbance which would easily

affect system transient and voltage stability; therefore, a fast reacting system operator is expected in microgrids.

For power balance control, a well-known method proposed previously to maintain power balance is P/f and Q/V droop control [34–38]. This method imitates intrinsic characters of synchronous generators. It obtains control signals locally and does not require communications with other components in the microgrid. It benefits from “plug and play”. However, it relies on the output-voltage settings of DGs; therefore, its performance may be compromised if a tight voltage regulation is expected [42]. Besides, droop control strategy affords no control of load, is therefore effective only when total generation capacity exceeds total load, which is not always the case in microgrids. MAS, one of the most popular distributed control entities, could behave as a system operator to manage power balance operation in microgrid [39–41]. Benefits from MAS include accomplishing “plug and play” attributes, avoiding single point failures, and realizing distributed control.

Refs. [43, 44] proposed an effective algorithm based on the Average Consensus Theorem to calculate system net power and maintain power balance of the microgrid. The algorithm in [43, 44] is implemented in a completely decentralized manner, but may take long to converge for large systems. In this chapter, we propose a novel MAS-based methods that accomplish exact power balance in three sweeps, regardless of system size. In the proposed, the information flows in parallel and the results are also obtained in a non-iterative way; therefore, this algorithm achieves superior performance in terms of speed without any convergence issues.

In order to maintain power balance, dispatch generation or demand within microgrids, the entire process contains three parts: determine information flow route, obtain net real and reactive power, and re-assign generation and load values. Since there is no central agent in the decentralized architecture of multi-agent system, no single agent unilaterally governs others to achieve a global goal. All agents are at the same hierarchical level to obey specific rules to communicate so that all those autonomous agents can coordinate to manage microgrids. Consider a system connected as Figure 4.1. It is a simple but typical structure and embodies a ring. It is easy to find

that a communication algorithm applied in this structure can be extended to a more complicated structure which may have multiple rings or radial lines. In this figure, each node represents an agent, and the position of the node shows topological position of the corresponding agent. An arc connecting two nodes implies that the agents represented by these two nodes are neighbors and they can communicate with each other to exchange information and data. Two agents without a line connecting them are not considered neighbors and can not communicate directly.

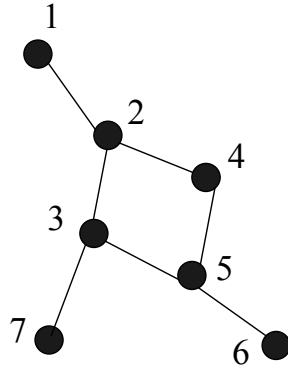


Figure 4.1: Multi-agent system structure.

To explain the following ideas, some definitions are provided first to clarify the process. The agent that is processing system information is called *current agent*. If agent A_1 transmits information to agent A_2 , then A_1 is called A_2 's *parent agent*, and A_2 is called A_1 's *child agent*. *View*, either local or global, is agent's knowledge of system information. This information consists of maximum real and reactive power generation capacity P_G , Q_G , dispatchable real and reactive power generation capacity P_{DG} , Q_{DG} , vital real and reactive load demand P_v , Q_v , and non-vital real and reactive load demand P_{nv} , Q_{nv} . Define *view* mathematically as vector \mathbf{u} .

$$\begin{aligned} \mathbf{u} &= [u_1, u_2, u_3, u_4, u_5, u_6, u_7, u_8]^T \\ &= [P_G, Q_G, P_{DG}, Q_{DG}, P_v, Q_v, P_{nv}, Q_{nv}]^T \end{aligned} \tag{4.1}$$

4.2 Parallel Method: Minimal Spanning Tree

4.2.1 Stage 1: Discovery of Minimal Spanning Tree

This process is intended to organize decentralized multi-agent system and facilitate to steer information flow. However, three major problems are encountered to discover power information of the microgrid. Firstly, a sophisticated communication protocol should be defined to conduct information flow so that all the nodes in the system can be spanned. Secondly, this protocol is able to route the information flow so that every node receives and processes information only once. Thirdly, real time control of multi-agent system requires this protocol to be able to discover system information in parallel, so that it can quickly react to the disturbance in the system. To overcome these problems, a minimal spanning tree can be constructed in MAS to direct the information flow.

The process can be summarized as follows:

- (a) A token is generated by a starting agent.
- (b) Every agent who receives the token, memorizes its *parent agent* ID, then it transmits the token to all its other neighbors, and stores its *child agent* IDs.
- (c) Any agent, who receives multiple tokens simultaneously, keeps one and discards others. At the same time, removes child-parent relationships with those whose tokens are discarded.

To demonstrate this algorithm, let us also consider the example shown in Fig. 4.1. Since all agents are identical, starting agent can be selected randomly. In this case, let us simply choose agent 1 as starting agent. Initially, agent 1 will generate a token and transmit it to agent 2. Then agent 2 receives the token and sends it to its neighbors, agent 3 and agent 4. After that, agent 3 will send the token to its neighbors, agent 5 and agent 7. In parallel, agent 4 will send the token to agent 5. Now for agent 5, it receives two tokens, so it discards one. Let us assume it discards the token coming from agent 3. Lastly, the token will flow from agent 5 to agent 6. Until now, all the agents in the system have been discovered. During this process, all agents will store their *parent*

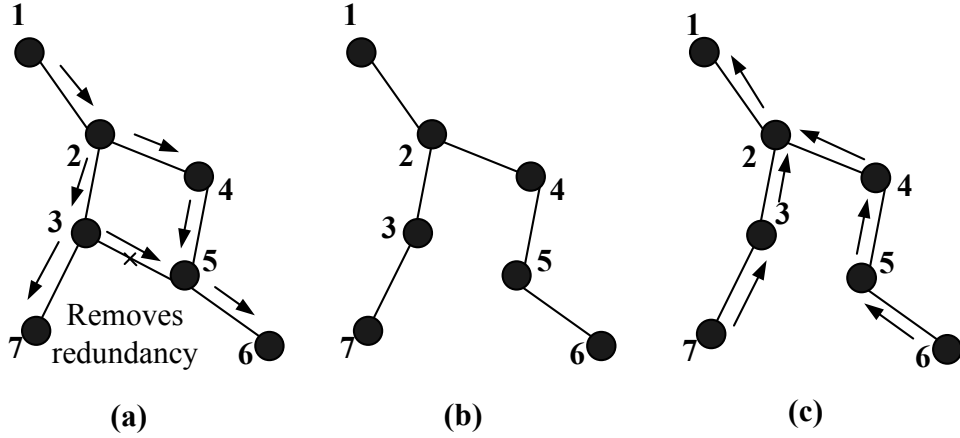


Figure 4.2: (a) Token transmission route. (b) Minimal spanning tree constructed. (c) Information flow path for Stage 2.

agent and *child agent* IDs. Their relationships are shown in Table 4.2.1. Fig. 4.2 (a) and (b) depict the transmission path of the token and the minimal spanning tree established by Stage 1.

Note that although removal of any one of the arcs 2-3, 2-4 or 4-5 instead of arc 3-5 has the same effect of establishing a minimal spanning tree, the sequence of discovery described above ensures the shortest communication time.

Table 4.1: Parent Child Relationship Diagram

Agent	1	2	3	4	5	6	7
Parent ID	-	1	2	2	4	5	3
Child ID	2	3,4	7	5	6	-	-

4.2.2 Stage 2: Information Feedback Process

Once the information flow path is established in Stage 1, the next step is intended to collect system generation and load data. This algorithm can be stated as follows:

- (a) When no new neighbors are discovered, each agent now responds its *parent agent* with local *view* of the system.

- (b) Every agent who receives system *view* information from all its *child agents*, processes this data as shown in (4.2) below and transmits updated *view* information to its *parent agent*.

$$\mathbf{u} = \mathbf{u}^{local} + \sum_{i \in \phi} \mathbf{u}^i \quad (4.2)$$

where \mathbf{u} is *current agent's* updated *view*; \mathbf{u}^{local} is *current agent's* local *view*; ϕ is the set of child IDs; \mathbf{u}^i is *child agent i's* updated *view*.

Stage 2 ensures that each local node *view* information flows back from *child agent* to its *parent agent*. Finally, the starting agent can obtain system global *view* and calculates net power based on (4.3). Fig. 4.2 (c) shows the information flow path of Stage 2.

$$\begin{bmatrix} P_{net} \\ Q_{net} \end{bmatrix} = \begin{bmatrix} 1 & 0 & 1 & 0 & -1 & 0 & -1 & 0 \\ 0 & 1 & 0 & 1 & 0 & -1 & 0 & -1 \end{bmatrix} \mathbf{u} \quad (4.3)$$

where P_{net} and Q_{net} are system net real and reactive power; \mathbf{u} is updated *view* of starting agent.

4.2.3 Stage 3: Generation and Load Dispatch

In Stage 2, starting agent obtains global *view* of system generation and load demand. Based on the information collected, decentralized agents can dispatch generation or curtail load from *parent agents* to *child agents*. This process is summarized as:

- (a) When receiving system net power values, each agent first adjusts local available generation or load to minimize the unbalanced power. Mathematically, it is described by (4.4)–(4.6).

Minimize:

$$|I_{net}^c| = |I_{net}^p - \tilde{I}_{DG} + \tilde{I}_{nv}|, \quad I \in \{P, Q\} \quad (4.4)$$

Subject to:

$$0 \leq \tilde{I}_{DG} \leq I_{DG} \quad (4.5)$$

$$0 \leq \tilde{I}_{nv} \leq I_{nv} \quad (4.6)$$

where I_{net}^c is system net P or Q after dispatch of *current agent*; I_{net}^p is system net P or Q obtained from *parent agent*; \tilde{I}_{DG} and \tilde{I}_{nv} are dispatched power values for *current agent*. Note that only dispatchable generators and non-vital load can be dispatched.

- (b) If local availability is not enough, each agent, based on the updated system *view* obtained in Stage 2, will split the net power values according to its *child agents*' dispatchable capability, and transmit new values to its *child agents*. Mathematically, it is stated as:

$$I_{net}^i = \begin{cases} \frac{I_{DG}^i}{\sum_{m \in \phi} I_{DG}^m} I_{net}^c & \text{if } I_{net}^c \geq 0 \\ \frac{I_{nv}^i}{\sum_{m \in \phi} I_{nv}^m} I_{net}^c & \text{if } I_{net}^c < 0 \end{cases}, I \in \{P, Q\} \quad (4.7)$$

where I_{net}^i is net P or Q for *child agent* i ; I_{DG}^i is u_3 or u_4 , updated dispatchable generation information that agent i obtained in Stage 2. ϕ is the set of *child agents*. I_{net}^c is the net P or Q obtained by *current agent*; I_{nv}^i is u_7 or u_8 , updated non-vital load information that *child agent* i obtained in Stage 2.

The information flow path in this step is in the opposite direction to that of Stage 2.

4.3 Multi-Agent System Implementation and Simulation

This subsection will describe the implementation of the MAS framework described above and compare its performance with other available methods proposed previously in the literature. In practice, the framework would comprise individual agents programmed to perform as described in

Sections 4.2.1, 4.2.2 and 4.2.3, and located at their respective positions in the actual network. Their interactions, as described in Sections 4.2.1, 4.2.2 and 4.2.3, would be conducted through parallel threads. However, in the laboratory, the entire system was simulated in a MATLAB environment, on a single computer with a single thread. This was implemented through “virtual agents” in the MATLAB code, using code representing agent functions at each node. In order to simulate multiple threads of multi-agent system in a single-thread program, this platform requires an extra variable for the time pointer. At a specific time t , the program holds t , and uses one thread to compute multiple threads sequentially. After computing all the threads, the program goes to $t + \Delta t$, where Δt is time step. Fig. 4.3 displays the time pointer in this process. The pointer at time t will not move to the next time $t + \Delta t$ until the processor computes all the necessary behaviors conducted by every agent at time t .

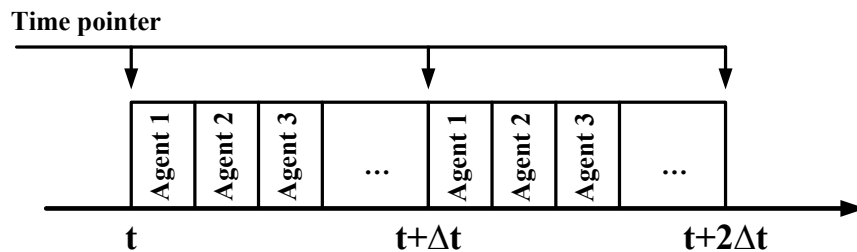


Figure 4.3: Simulation of multiple threads on a single-thread platform.

Power balance control is critical for stable operation of microgrids; therefore, it has the highest priority in the proposed multi-level control architecture.

To demonstrate the speed and effectiveness of the proposed power balance control strategy for MAS, IEEE 14-bus, 30-bus, 57-bus and 118-bus systems are tested. The system configurations and data can be obtained from [69].

If two nodes are adjacent to each other through direct electrical connection, their agents are neighbors and they can communicate directly with each other. The simulations are conducted by selecting agent 1 (corresponding to bus 1) as starting agent. Simulation results are shown in Table 4.3. A hop represents the path between two neighbor nodes. Note that this lists the maximum number of hops required for the power balance control; because for the last sweep, once the net

power reaches zero, power balance is achieved and net power information does not need to be transmitted further. However, in this simulation, power balance is obtained when the dispatch information has reached all the agents.

Table 4.2: Simulation Results for Power Balance Control

Period	IEEE 14 bus	IEEE 30 bus	IEEE 57 bus	IEEE 118 bus
Hops	12	18	30	42

The time to achieve power balance control can be estimated from the number of hops shown in Table 4.3. The actual execution time of the algorithm depends on the specific implementation, in terms of hardware and software. Ref. [43] uses equation (4.8) to estimate the communication time.

$$T = \frac{n_i \times n_d \times n_b}{R} \quad (4.8)$$

where n_i is the number of hops for the algorithm; n_d is the number of data points required to be transmitted; n_b is the number of bits used to represent each data point; R is the communication speed in bits/second. For instance, for IEEE 118 bus system, the total number of hops is 42, with 14 hops per sweep. If the token in the first sweep is represented by 8 bits, and each data point in the second and third sweeps is represented by 16 bits, then for a network speed of 10Mbit/s, the execution time can be estimated as $(14 \times 1 \times 8 + 14 \times 8 \times 16 + 14 \times 2 \times 16) / 10\,000\,000 = 0.000235$ s.

Ref. [43] used the IEEE 162-bus system [69]. We compare here the performance of the proposed algorithm with that in [43] for the same system. The agent at bus 1 is chosen as starting agent. It takes 9 hops for each sweep, requiring 27 hops in all to reach power balance. Assuming the same number of bits and communication rate as those in [43], the estimated time can be computed as $(9 \times 1 \times 8 + 9 \times 8 \times 16 + 9 \times 2 \times 16) / 10\,000\,000 = 0.0001512$ s. However, [43] reports that it took their algorithm 0.1283 s to converge. Note that the times calculated here and in [43] do not consider time delays or other factors. They vary for different implementations of hardware and software. However, this approximation clearly shows the speed advantage for the proposed

algorithm, which results from the parallel nature of information flow in this algorithm.

Further discussion: the speed of the proposed algorithm depends highly on the coupling of the agents. For example, for the two 7-node MAS structures shown in Fig. 4.4, if the starting agent is chosen as agent 1, the first requires only 1 hop for each sweep, while the second requires 6 hops for each sweep. Therefore, for the same scale MAS, the tighter coupling (higher number of branches) the MAS has, the faster the solution can be reached. Most MAS systems will comprise a combination of the two, and the execution time will depend on how tightly coupled the agents are.

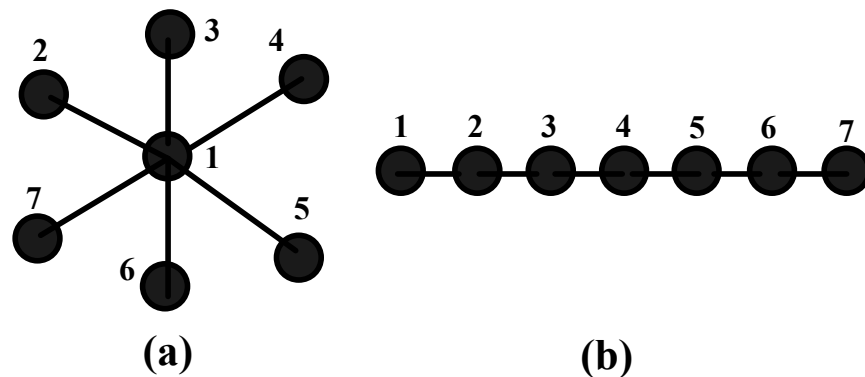


Figure 4.4: Two MAS structures: (a) completely parallel resulting in tightest coupling; (b) completely sequential resulting in loosest coupling.

4.4 Summary

This chapter proposed a distributed power balance control algorithm based on a decentralized multi-agent system. The contributions of this chapter are listed as follows:

1. The information flows in parallel by this algorithm; therefore, it achieves superior speed performance and is applicable for on-line power balance control;
2. The proposed algorithm implements power balance control in a non-iterative way; therefore, it does not have any convergence problem.

Chapter 5

Distributed Power Balance Control

Considering Voltage Regulation and Losses

5.1 Introduction

Chapter 4 proposes a fast and reliable distributed power balance control strategy. It can achieve superior performance in terms of speed without any convergence problems, due to the characteristics that its information flows in parallel and the results are obtained in a non-iterative way. However, it does not consider losses in the transmission lines; therefore, it may introduce considerable power balance error in the resistance-dominant network, such as distribution system or microgrids. Furthermore, this algorithm does not consider the effect of voltage regulation by generators, which is commonly used in most power systems. Ref. [43, 44] shares the same shortcomings as chapter 4. To overcome the mentioned drawbacks, this chapter proposes a distributed multi-agent based power flow algorithm, in which each agent has its local power flow equation and updates state information simultaneously with limited data from their immediate neighbors. Ref. [75] proposed a distributed power flow algorithm for multi-agent platform; however, its algorithm updates state information sequentially from one agent to another, which limits its speed, especially in multi-agent framework, where communication speed rather than computation speed is the bottleneck that re-

stricts the speed of algorithm. The distributed power flow algorithm proposed in this chapter fully makes use of communication time, and updates state information synchronously among agents, which offers considerable speed advantage. Based on the proposed power flow algorithm, this chapter also shows that real and reactive unbalanced power can be calculated at slack node. This net power acquisition is implemented fully distributed; therefore, it provides a possible solution for distributed load shedding or restoration.

5.2 Net Power Acquisition by Gauss Method

Assume in each bus of the microgrid, there is a Node Agent. It has information about local generation, such as real power capacity, reactive power capacity, voltage magnitude that is going to be maintained; meanwhile, it also has local load information, such as real and reactive power demands by the load. If two nodes are connected electrically, then the corresponding agents are marked as neighbors. Agents with neighborhood can communicate with each other; those without neighborhood relationship cannot communicate.

Assume N nodes in the system, with net power input P_n, Q_n . If it is a load node, then P_n and Q_n are negative; if it is a generator node, then P_n and Q_n are positive.

5.2.1 Distributed Construction of Y_{bus}

Conventionally, to perform power flow, we need to first build the bus admittance matrix, Y_{bus} , which contains system structure and admittance information. In multi-agent based power flow, we still need system information for power flow calculation. However, this approach differs from traditional centrally computational method, in this distributed based framework, Y_{bus} is constructed locally. Each agent only obtain part of Y_{bus} information. The construction principle is shown below:

For agent i , it constructs i^{th} row of Y_{bus} matrix:

$$Y_i = [Y_{i1} Y_{i2} \dots Y_{iN}] \quad (5.1)$$

$$Y_{ii} = \sum_{n=1}^N y_{in} \quad (5.2)$$

$$Y_{in} = -y_{in} \quad \text{when } (n \neq i) \quad (5.3)$$

where, Y_i is the system parameters constructed by agent i for power flow calculation; Y_{ii} is the i^{th} element of Y_i ; Y_{in} is the n^{th} element of Y_i , when $n \neq i$. y_{ii} represents equivalent admittance between bus i and ground. y_{in} when $n \neq i$, is equivalent admittance between bus i and bus n .

Recall that in Y_{bus} matrix, if bus i and bus n are not connected, $Y_{in} = -y_{in} = 0$. Since neighborhood is determined by electrical connection, it also means if agent i and agent n are not neighbors, then $Y_{in} = 0$, expressed in (5.4).

$$Y_{in} = 0 \quad \text{if } (n \notin N(i)) \quad (5.4)$$

where, $N(i)$ is a set of agents that are neighbors of agent i .

Construction principles based on equation (5.1)-(5.4) shows that all the information required to build system parameters by agent i are y_{in} , where $n = 1, 2, \dots, N$. Agent i can obtain these parameters locally without global information.

5.2.2 Agent Based Power Flow

Let us select node 1 as slack node. When calculating the power flow, its voltage magnitude and angle are maintained constant. Other nodes use their original real and reactive power inputs (PQ node) or real power input and voltage magnitude requirement (PV node) to calculate voltage magnitude (PQ node), voltage angle (PQ or PV node) or reactive power demand (PV node).

Local power flow equation for agent m is (5.5)

$$S_m = V_m I_m^* = V_m \left[\sum_{n=1}^N Y_{mn} V_n \right]^* \quad (5.5)$$

where S_m is the complex power input to node m; V_m is the voltage vector at node m; I_m is the current input into node m. Y_{mn} is built following principles of section 5.2.1. Rewrite this equation:

$$V_m = \frac{1}{Y_{mm}} \left[\frac{S_m^*}{V_m^*} - \sum_{\substack{n=1 \\ n \neq m}}^N Y_{mn} V_n \right] \quad (5.6)$$

where, $m = 2, 3, \dots, N$

From (5.4), $Y_{mn} = 0$, if agent n is not a neighbor of agent m. Then we obtain:

$$V_m = \frac{1}{Y_{mm}} \left[\frac{S_m^*}{V_m^*} - \sum_{n \in N(m)} Y_{mn} V_n \right] \quad (5.7)$$

where, $N(m)$ is a set of agents that are neighbors of agent m.

To solve power flow, Gauss method is adopted. Differs from traditional Gauss-based power flow, in this multiagent framework, each agent solves its own nodal power flow locally by exchanging the required data with its neighbors. Writing the local power flow equation using the iterative form of Gauss method, we get:

$$V_m^{(k+1)} = \frac{1}{Y_{mm}} \left[\frac{S_m^{*(k)}}{V_m^{*(k)}} - \sum_{n \in N(m)} Y_{mn} V_n^{(k)} \right] \quad (5.8)$$

where, k is the iteration number.

The local power flow equation (5.8) shows that each agent only needs to exchange with its neighbors the voltage values from the last iteration in order to update voltage data in its local calculation. It does not need system global information or information beyond its neighbors to

calculate its local power flow.

Now, if node m is a PV node, then it first has to estimate Q_m :

$$Q_m^{(k+1)} = \text{Im} \left[V_m^{(k)} \sum_{n \in N(m)} \left(Y_{mn} V_n^{(k)} \right)^* + V_m^{(k)} \left(Y_{mm} V_m^{(k)} \right)^* \right] \quad (5.9)$$

where $Q_m^{(k+1)}$ is the reactive power needed to maintain pre-specific voltage magnitude in the $(k+1)^{th}$ iteration. Then it updates the voltage:

$$V_m^{(k+1)'} = \frac{1}{Y_{mm}} \left[\frac{P_m - jQ_m^{(k+1)}}{V_m^{*(k)}} - \sum_{n \in N(m)} Y_{mn} V_n^{(k)} \right] \quad (5.10)$$

$$V_m^{(k+1)} = V_m^{(k+1)'} \left[\frac{V_m}{|V_m^{(k+1)'}|} \right] \quad (5.11)$$

If $Q_m^{(k+1)} \geq Q_m^{max}$, then $Q_m^{(k+1)} = Q_m^{max}$. If $Q_m^{(k+1)} \leq Q_m^{min}$, then $Q_m^{(k+1)} = Q_m^{min}$.

This means the generator does not have enough reactive power capacity to further maintain voltage magnitude. So the node changes to a PQ node, and voltage magnitude will vary. Voltage update is now updated by (5.12).

$$V_m^{(k+1)} = \frac{1}{Y_{mm}} \left[\frac{P_m - jQ_m^{(k+1)}}{V_m^{*(k)}} - \sum_{n \in N(m)} Y_{mn} V_n^{(k)} \right] \quad (5.12)$$

5.2.3 Net Power Acquisition

After agent-based Gauss power flow calculation method, each agent could obtain local voltage magnitude and angle, and they satisfy the following equation:

$$\bar{P}_m + j\bar{Q}_m = P_m + jQ_m = V_m \left[\sum_{n=1}^N Y_{mn} V_n \right]^* \quad (5.13)$$

where \bar{P}_m and \bar{Q}_m are calculated real and reactive power; P_m and Q_m are original planned real and reactive power input.

Also we could calculate real and reactive power input at node 1:

$$\bar{P}_1 + j\bar{Q}_1 = V_1 \left[\sum_{n=1}^N Y_{1n} V_n \right]^* \quad (5.14)$$

where \bar{P}_1 and \bar{Q}_1 are calculated real and reactive power at node 1.

Losses of lines are categorized by relationship with nodes. If a line connects both node m and node n, then we define half of that line loss is contributed to node m, the other half of that line loss is contributed to node n. If a line connects node m and ground, then we say that all of the line loss is contributed to node m. Then local losses related to node m can be calculated by equation (5.15).

$$P_m^{loss} + jQ_m^{loss} = y_{mm}V_mV_m^* + \frac{1}{2} \sum_{\substack{n=1 \\ n \neq m}}^N y_{mn}[V_mV_m^* + V_nV_n^* - V_mV_n^* - V_nV_m^*] \quad (5.15)$$

where P_m^{loss} and Q_m^{loss} stand for real and reactive power losses related to node m respectively.

So the total losses in the system can be expressed as:

$$\begin{aligned}
P^{loss} + jQ^{loss} &= \sum_{m=1}^N (P_m^{loss} + jQ_m^{loss}) \\
&= \sum_{m=1}^N \left[y_{mm}V_mV_m^* + \frac{1}{2} \sum_{\substack{n=1 \\ n \neq m}}^N y_{mn}[V_mV_m^* + V_nV_n^* - V_mV_n^* - V_nV_m^*] \right] \\
&= \sum_{m=1}^N \left[y_{mm}V_mV_m^* + \sum_{\substack{n=1 \\ n \neq m}}^N y_{mn}[V_mV_m^* - V_mV_n^*] \right] \\
&= \sum_{m=1}^N \left[V_mV_m^* \sum_{n=1}^N y_{mn} + \sum_{\substack{n=1 \\ n \neq m}}^N y_{mn}[-V_mV_n^*] \right] \\
&= \sum_{m=1}^N \left[Y_{mm}V_mV_m^* + \sum_{\substack{n=1 \\ n \neq m}}^N Y_{mn}V_mV_n^* \right] \\
&= \sum_{m=1}^N \left[\sum_{n=1}^N Y_{mn}V_mV_n^* \right]
\end{aligned} \tag{5.16}$$

where P^{loss} and Q^{loss} are total system real and reactive power losses.

Therefore, total system generation deficiency or surplus can be calculated:

$$\begin{aligned}
\Delta P + j\Delta Q &= \sum_{m=1}^N (P_m + jQ_m) - (P^{loss} + jQ^{loss}) \\
&= P_1 - \bar{P}_1 + jQ_1 - j\bar{Q}_1 + \sum_{m=1}^N (\bar{P}_m + \bar{Q}_m) - (P^{loss} + jQ^{loss}) \\
&= P_1 - \bar{P}_1 + jQ_1 - j\bar{Q}_1 + \sum_{m=1}^N V_m \left[\sum_{n=1}^N Y_{mn}V_n \right]^* \\
&\quad - \sum_{m=1}^N \left[\sum_{n=1}^N Y_{mn}V_mV_n^* \right] \\
&= P_1 - \bar{P}_1 + jQ_1 - j\bar{Q}_1
\end{aligned} \tag{5.17}$$

where ΔP and ΔQ are generation deficiency or surplus for the system, compared with load demands taking line losses into consideration. Note that if $\Delta Q \geq 0$, the reactive power is automatically balanced, because voltage regulator at slack bus will control the reactive power output of the generator to balance reactive power. However, if $\Delta Q \leq 0$, load dispatch is required to maintain reactive power balance.

From equation (5.17), it shows that the power deficiency considering line losses in the system can be calculated at slack node. Agent at node 1 knows generator capacity or load demand P_1 and Q_1 , also it can calculate \bar{P}_1 and \bar{Q}_1 from voltage and angle data in power flow calculation. Then it can obtain power shortage in the system.

5.3 Multi-Agent Implementation Algorithm

Normally, multi-agent system is formed by two or more agents. Each agent in multi-agent system can perceive environments, communicate with their immediate neighbors and perform locally to realize their functions, and therefore system overall function can be realized. Based on the mathematical foundations stated in section 5.2.2 and 5.2.3, microgrid generation deficiency or surplus can be computed in multi-agent environment by the following algorithms:

Generation Surplus or Deficiency Algorithm

//Initialization:

forall Agent A_i **do**

//set up neighborhood:

set up $N(A_i)$

//Input system data:

gather system admittance data y_{in}

//obtain local Y row:

Compute Y_i by (5.1), (5.2) and (5.3)

//Input node information:

$A_i \leftarrow V_i$, for A_i is responsible for a slack bus

$A_i \leftarrow P_i, Q_i$, for A_i is responsible for a PQ bus
 $A_i \leftarrow P_i, |V_i|, Q_i^{max}$, for A_i is responsible for a PV bus
repeat
 //Update voltage for PQ agents:
forall $A_i \in$ PQ Agents **do**
 ask for V from neighbors
 compute V_i by (5.8)
 //Update voltage for PV agents:
forall $A_i \in$ PV Agents **do**
 ask for V from neighbors
if $Q_i \leq Q_i^{max}$, **then** compute V_i by (5.9), (5.10) and (5.12)
else compute V_i by (5.11)
until $\Delta V < \epsilon V$
 //Compute real and reactive power difference at slack agent
for slack agent A_1 **do**
 compute calculated real and reactive power by (5.14)
 compute real and reactive power deficiency or surplus by (5.17).

5.4 Load and Generation Dispatch

In the dispatch process, initially, all the agents are marked as “unprocessed”. Once the slack bus agent obtains net power ΔP and ΔQ of the system, MAS system can dispatch generation or load following a sequential three-step algorithm:

1. Process. Modify local control variables to minimize ΔP and ΔQ and mark current agent as “processed”;
2. Next. Transmit net power values to the neighbor who is marked “unprocessed”.

3. Return. If the current agent has no neighbors or all the neighbors are marked as “processed”, the return net power values to its parent agent.

The proposed three-step algorithm is capable to route the information flow to span all the agents in MAS in a sequential way and coordinate them for power balance control. Figure 5.1 displays one of the information flow paths of the load and generation dispatch for the system structure shown in Figure 4.1. It can be computed that the maximum number of hops required for load and generation dispatch process is $2 \times (N - 1)$, where N is the number of agents in the system.

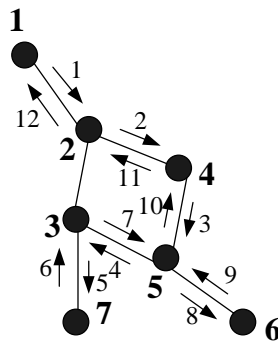


Figure 5.1: Information flow path for multi-agent system

Discussions: Since load and generation dispatch process does not consider losses, it is recommended that after a certain number of agents finishing their dispatch process, MAS can select a current agent with generators as new slack agent and implement distributed power flow again and obtains updated net power; then it continues load and generation dispatch process among those agents which are still marked “unprocessed”.

5.5 Simulation Result

To demonstrate the proposed multi-agent based load shedding algorithms, a five bus system from [74] is tested.

5.5.1 Five-Bus System

Original system configuration is shown in Fig. 5.2. Bus input data and Line input data are modified and displayed in Table 5.5.1 and 5.5.1. All the data have be transformed into per unit.

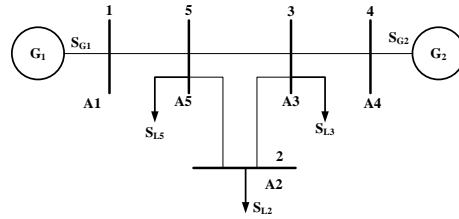


Figure 5.2: Tested five-bus system

Table 5.1: Bus Input Data for Five-Bus System

Bus	Type	V	δ	(P_G, Q_G)	(P_L, Q_L)	Q_+^G	Q_-^G
1	slack	1.0	0	(2, 1)	(0, 0)	-	-
2	PQ	-	-	(0, 0)	(5, 2.8)	-	-
3	PV	1.05	0	(5.4, -)	(3, 0.4)	4.0	-2.8
4	PQ	-	-	(0, 0)	(3, 1)	-	-
5	PQ	-	-	(0, 0)	(1.8, 1.0)	-	-

Table 5.2: Line Input Data for Five-Bus System

Bus to Bus	R'	X'	G'	B'
1 - 5	0.0015	0.02	0	0
2 - 4	0.009	0.1	0	1.72
2 - 5	0.0045	0.05	0	0.88
3 - 4	0.00075	0.01	0	0
4 - 5	0.00225	0.025	0	0

5.5.1.1 Multi-agent Based Construction of Y_{bus}

Based on the construction principles expressed as (5.1)-(5.4), 1st row of Y_{bus} built by Agent A_1 is:

$$Y_{12} = Y_{13} = Y_{14} = 0$$

$$Y_{15} = -\frac{1}{0.0015 + j0.02} = -3.73 + j49.72$$

$$Y_{11} = 3.73 - j49.72$$

All the data needed to compute local Y_1 can be obtained locally by Agent A_1 . Other agents can establish their own local Y_i vectors in the same manner. Results of Y_{bus} matrix is shown in Table 5.5.1.1.

Table 5.3: Local Y_i Vectors

	Y_i
A_1	$[3.73 - j49.72 \ 0 \ 0 \ 0 \ -3.73 + j49.72]$
A_2	$[0 \ 2.68 - j28.46 \ 0 \ -0.89 + j9.92 \ -1.79 + j19.84]$
A_3	$[0 \ 0 \ 7.46 - j99.44 \ -7.46 + j99.74 \ 0]$
A_4	$[0 \ -0.89 + j9.92 \ -7.46 + j99.44 \ 11.92 - j147.96 \ -3.57 + j39.68]$
A_5	$[-3.73 + j49.72 \ -1.79 + j19.84 \ 0 \ -3.57 + j39.68 \ 9.09 - j108.58]$

5.5.1.2 Multi-Agent Based Power Flow Calculation

Assume flat start, $V_2^{(0)} = 1.0$, $V_3^{(0)} = 1.05$, $V_4^{(0)} = 1.0$, $V_5^{(0)} = 1.0$. The first iteration of Gauss method for multiagent system is as follows:

Agent 2:

$$V_2^{(1)} = \frac{1}{Y_{22}} \left[\frac{S_2^{*(0)}}{V_2^{*(0)}} - \sum_{n \in N(2)} Y_{2n} V_n^{(0)} \right] = 0.947 \angle -10.30^\circ$$

Agent 3:

$$Q_3^{(1)} = \text{Im} \left[V_3^{(0)} \sum_{n \in N(3)} \left(Y_{3n} V_n^{(0)} \right)^* + V_3^{(0)} \left(Y_{33} V_3^{(0)} \right)^* \right] = 4.91$$

$$Q_3^{(1)} > Q_3^{max} - Q_{3L} = 4.0 - 0.4 = 3.6$$

Therefore:

$$Q_3^{(1)} = 3.6$$

$$V_3^{(1)} = \frac{1}{Y_{33}} \left[\frac{P_3 - jQ_3^{(1)}}{V_3^{*(0)}} - \sum_{n \in N(3)} Y_{3n} V_n^{(0)} \right] = 1.039 \angle 1.11^\circ$$

Agent 4:

$$V_4^{(1)} = \frac{1}{Y_{44}} \left[\frac{S_4^{*(0)}}{V_4^{*(0)}} - \sum_{n \in N(4)} Y_{4n} V_n^{(0)} \right] = 1.033 \angle -1.13^\circ$$

Agent 5:

$$V_5^{(1)} = \frac{1}{Y_{55}} \left[\frac{S_5^{*(0)}}{V_5^{*(0)}} - \sum_{n \in N(5)} Y_{5n} V_n^{(0)} \right] = 0.996 \angle -0.93^\circ$$

If we define convergence criterion as a voltage tolerance of 0.001 pu shown in (5.18), it needs 39 iterations to converge. The first five iteration results are given at Table 5.5.1.2.

$$\left| V_i^{(k)} - V_i^{(k+1)} \right| \leq 0.001 \quad \forall i \quad (5.18)$$

5.5.1.3 Netpower Acquisition

After system node voltages are obtained, total netpower can be computed at slack agent:

Table 5.4: Results for the First Five Iteration

No.	Agent 2: V_2	Agent 3: V_3	Agent 4: V_4	Agent 5: V_5
1	$0.947\angle -10.30^\circ$	$1.039\angle 1.11^\circ$	$1.033\angle -1.13^\circ$	$0.996\angle -0.93^\circ$
2	$0.920\angle -10.81^\circ$	$1.05\angle 0.13^\circ$	$1.019\angle -1.22^\circ$	$0.996\angle -3.14^\circ$
3	$0.916\angle -12.79^\circ$	$1.05\angle -0.06^\circ$	$1.026\angle -2.48^\circ$	$0.986\angle -3.21^\circ$
4	$0.905\angle -13.18^\circ$	$1.05\angle -1.28^\circ$	$1.022\angle -2.74^\circ$	$0.987\angle -4.02^\circ$
5	$0.904\angle -13.97^\circ$	$1.05\angle -1.56^\circ$	$1.022\angle -3.81^\circ$	$0.983\angle -4.16^\circ$

Agent 1:

$$\bar{P}_1 + j\bar{Q}_1 = V_1 \left[\sum_{n=1}^N Y_{1n} V_n \right]^* = 7.34 + j1.36$$

$$P_s + jQ_s = P_1 - \bar{P}_1 + Q_1 - \bar{Q}_1 = -5.34 - j0.36$$

Therefore, considering generators and transmission network characteristics (PV, PQ, power flow), line losses, the deficiency of generation in the system is $-5.34-j0.36$. If simply neglecting these factors, netpower is calculated as:

$$P_s + jQ_s = \sum (P_G - P_L) + j(\sum Q_G - Q_L) = -5.4 - j0.2$$

Because of the voltage magnitude requirements at node 3, generators at node 3 will not simply provide maximum reactive power, even though reactive power in the system is deficient. Therefore, neglecting system operation principles and generation characters, the net reactive power estimation are not accurate. In this case, its error is above 44%. Real power difference between this two methods mainly resulted from system losses. In microgrids, with low voltage level and mainly resistant network, this loss sometimes could not be omitted.

5.5.2 14-Bus System, 30-Bus System and 57-Bus System

To test feasibility of the proposed algorithm, 3 different systems with 14 buses, 30 buses and 57 buses obtained from university of washington [69] are studied individually. Time expense for

multi-agent system's convergence to the result are calculated.

5.5.2.1 14-Bus System

It costs multi-agent system 175 iterations to converge to the result if the voltage acceptable error is set to be 10^{-7} . If the communication rate is still 10 Mbit/s and each data is represented by 16 bits and each iteration is required to transmit two data, voltage magnitude and angle, then the time used for convergence is $175 \times 16 \times 2/10\,000\,000 = 0.56 \times 10^{-3}$ s. Total generation capacity is $272.4 + j138$ MVar, total complex load is $259 + j73.5$ MVar, total generation is $272.4 + j103.74$. Net power obtained at by slack node agent is $0.008 - j0.114$ MVar. The number of hops required for load and generation dispatch is 26; therefore, the dispatch takes $26 \times 2 \times 16/10\,000\,000 = 0.832 \times 10^{-4}$ s.

5.5.2.2 30-Bus System

In this case, multi-agent system needs 411 iterations to converge to the result if the voltage acceptable error is set to be 10^{-7} . If the communication rate is still 10 Mbit/s and each data is represented by 16 bits, the time used for convergence is $411 \times 16 \times 2/10\,000\,000 = 1.3152 \times 10^{-3}$ s. Total generation capacity is $300.2 + j178$ MVar, total complex load is $238.4 + j126.2$ MVar, total generation $300.2 + j135$. Net power obtained at by slack node agent is $0.76 - j0.61$ MVar. The number of hops required for load and generation dispatch is 58; therefore, the dispatch takes $58 \times 2 \times 16/10\,000\,000 = 1.856 \times 10^{-4}$ s.

5.5.2.3 57-Bus System

In this case, multi-agent system needs 499 iterations to converge to the result if the voltage acceptable error is set to be 10^{-7} . If the communication rate is still 10 Mbit/s and each data is represented by 16 bits, the time used for convergence is $499 \times 16 \times 2/10\,000\,000 = 1.5968 \times 10^{-3}$ s. Total generation capacity is $928.9 + j499$ MVar, total complex load is $1250 + j336.4$ MVar, total generation is $1278.97 + j198.44$. Net power obtained at by slack node agent is $-350.07 - j147.18$ MVar.

The number of hops required for load and generation dispatch is 112; therefore, the dispatch takes $112 \times 2 \times 16/10\,000\,000 = 3.584 \times 10^{-4}$ s.

The comparison with the algorithm proposed in chapter 4 is shown in Table 5.5.2.3.

Table 5.5: Comparisons Between Power Balance Control Algorithms

Algorithms	Name	Unit	14 bus	30 bus	57 bus
No loss	Net power	Hops	8	12	20
	Dispatch	Hops	4	6	10
	Total Time	Second	0.672×10^{-4}	1.008×10^{-4}	1.68×10^{-4}
With loss	Net power	Iteration	175	411	499
	Dispatch	Hops	26	58	112
	Total Time	Second	6.432×10^{-4}	1.5008×10^{-3}	1.9552×10^{-3}

5.6 Summary

This chapter proposes a multi-agent based distributed power flow algorithm, in which each agent is only required to get access to the local data without any knowledge of global information. By communicating local control data with its immediate neighbors, each agent can obtain its state information. The contributions of this chapter includes:

1. It offers an innovative way to obtain state information of power system in a complete distributed way, in which each node in the system is only required to get access to the local information without any awareness of global information.
2. In this algorithm, real and reactive net power can be calculated at slack bus, which can be used as a theoretical foundation for distributed load shedding or restoration process.
3. This algorithm is also applicable for real-time power balance control of microgrids.

Chapter 6

Distributed Economic Dispatch

6.1 Introduction

The algorithms in Chapter 4 ensure stable steady state operation, and are adequate for most microgrids. However, if a microgrid is amenable to optimal dispatch, i.e., if its generating capacity exceeds its load and has some DGs that are dispatchable, then the framework proposed in this chapter can also perform economic dispatch. This can be achieved by applying the following algorithms, which modify the dispatched power values obtained in Chapter 4 to realize minimum generation cost.

In traditional bulk power system, economic dispatch is usually conducted in a central controller, which has access to global system information. However, characterized as flexible and “plug and play”, microgrids are preferable to be controlled in a distributed manner. Ref. [64, 65] presented, respectively, a two-level incremental cost consensus algorithm, and an evolutionary programming method for economic dispatch based on MAS environment. These are both dedicated algorithms for solving economic dispatch problems, but are complex and slow to converge. This chapter presents a robust and fast algorithm for on-line economic dispatch of distributed generators in microgrids based on a decentralized architecture of multi-agent system. In this architecture, all DGs are equipped with identical agents, which could only perceive local information or obtain neces-

sary information from their neighbors. By competition and corporation with each other, agents intend to maximize their own profit, therefore an optimal global solution could be obtained. In this algorithm, total generation cost always changes in a non-increasing direction. This decentralized algorithm also allows the system to continue operation in the presence of single point failure. If any agent in the system fails, only the cost in that node is not optimized; while the cost for the remaining system can still be minimized.

This chapter will first deduce necessary conditions for minimal cost operation of microgrids. Then it proposes an innovative multi-agent communication algorithm to implement the minimal principle in multi-agent environment. A proof of convergence is also presented. In the end, a five-agent, IEEE-118 systems are investigated to validate the proposed multi-agent system.

6.2 Economic Dispatch Model

Assume there are n generators in a microgrid. Each generator has a convex cost function $F_i(P_i)$ in terms of real power output P_i . If system losses are not considered, the economic dispatch problem can be stated as follows: given total system load, schedule real power output of each generator so that the total generation cost is minimized while satisfying upper and lower output constraints of generators, as well as real power balance requirement. Mathematically, this optimization problem can be stated as follows:

Minimize:

$$F = \sum_{i=1}^n F_i(P_i) \quad (6.1)$$

Subject to:

$$P_D = \sum_{i=1}^n P_i \quad (6.2)$$

$$P_i^{min} \leq P_i \leq P_i^{max} \quad (6.3)$$

where

- F_i = cost function of generation unit i
 P_i = real power output of generation unit i
 P_D = total load in microgrid
 P_{loss} = total loss in microgrid
 P_i^{min} = lower limit of generation unit i
 P_i^{max} = upper limit of generation unit i

The Lagrange function can be constructed as (6.4):

$$\begin{aligned}
 L = \sum_{i=1}^n F_i + \lambda(P_D - \sum_{i=1}^n P_i) + \sum_{i=1}^n \lambda^i (P_i^{min} \\
 + s_i^2 - P_i) + \sum_{i=1}^n \lambda_i (P_i^{max} - t_i^2 - P_i)
 \end{aligned} \tag{6.4}$$

where

$\lambda, \lambda_i, \lambda^i$ = Lagrange multipliers

s_i, t_i = real variables that convert inequality constraints to equality (i.e., slack and surplus variables)

Based on the necessary condition, at the minimum cost point, the partial derivatives of the Lagrange function should be zero. Therefore:

$$\frac{\partial L}{\partial P_i} = \frac{\partial F_i}{\partial P_i} - \lambda - \lambda^i - \lambda_i = 0 \tag{6.5}$$

$$\frac{\partial L}{\partial s_i} = 2\lambda^i s_i = 0 \tag{6.6}$$

$$\frac{\partial L}{\partial t_i} = 2\lambda_i t_i = 0 \tag{6.7}$$

When $P_i^{min} < P_i < P_i^{max}$, then $s_i \neq 0, t_i \neq 0$. Based on (6.5)–(6.7), it is easy to obtain

$$\lambda^i = 0, \lambda_i = 0, \frac{\partial F_i}{\partial P_i} = \lambda \quad (6.8)$$

Alternatively, when $P_i = P_i^{min}$ or $P_i = P_i^{max}$, according to (6.5)–(6.7):

$$s_i = 0, \lambda_i = 0, \frac{\partial F_i}{\partial P_i} - \lambda - \lambda^i = 0 \text{ when } P_i = P_i^{min} \quad (6.9)$$

$$t_i = 0, \lambda^i = 0, \frac{\partial F_i}{\partial P_i} - \lambda - \lambda_i = 0 \text{ when } P_i = P_i^{max} \quad (6.10)$$

Equations (6.8)–(6.10) describe necessary conditions to obtain minimum generation cost. This just implies that at the optimal operating point, generators in the system are dispatched at equal incremental cost, except those units that have already reached upper or lower limits.

Now the power balance requirement in the microgrid can be satisfied by multi-agent control as described in Chapter 4. Each agent obtains an assignment that satisfies power balance described by equation (6.11), but it is not the optimal value that minimizes generation cost.

$$\sum_{i=1}^n P_i^{(0)} = P_D \quad (6.11)$$

where $P_i^{(0)}$ = initial generation assignment from power balance control for generation agent i . Realize that this initial value is within generation limits of generation agent i .

Two neighbor agents m and n can meet optimal conditions (6.8)–(6.10) by implementing the behavior described by (6.12) (6.13):

$$F'_m(P_m^{(k+1)}) = F'_n(P_n^{(k+1)}) \quad (6.12)$$

$$P_m^{(k+1)} + P_n^{(k+1)} = P_m^{(k)} + P_n^{(k)} \quad (6.13)$$

where $F'_m = dF_m/dP_m$. Agent behavior as in (6.12) and (6.13) provides a means of achieving

minimum generation cost.

However, if agent m reaches its limit before it satisfies (6.12), then (6.12) does not need to be satisfied. Agent m chooses its limit as new assignment, and agent n calculates its assignment by (6.14). A similar logic applies to agent n .

$$P_n^{(k+1)} = P_m^{(k)} + P_n^{(k)} - P_m^{(k+1)} \quad (6.14)$$

where $P_m^{(k+1)} = P_m^{limit}$, the limit can be the upper bound or lower bound of agent m , depending on which one prevents agent m from having the same incremental cost as agent n . This behavior prevents generation output from violating generation limits, thus equation (6.17) is always valid.

6.3 Proof of Convergence

To establish the stability of this algorithm, a convergence analysis is performed, based on a Lyapunov function. Note that a convex and differentiable cost function $F_i: \chi \rightarrow \mathbb{R}$ satisfies the first-order convexity condition:

$$F_i(y) \geq F_i(x) + F_i'(x)(y - x), \forall x, y \in \chi, \quad (6.15)$$

Define a Lyapunov function $V: \chi^N \subset \mathbb{R}^N \rightarrow \mathbb{R}$ of the form shown in (6.16):

$$V(\mathbf{P}^{(k)}) = \sum_{i \in \nu} F_i(P_i^{(k)}) \quad (6.16)$$

where $\mathbf{P}^{(k)}$ is a vector consisting of nodal generation values in iteration k ; $P_i^{(k)}$ is the i^{th} element of $\mathbf{P}^{(k)}$ representing generation value for agent i ; ν is the set of agents in the system.

Note that F_i is the cost function for generator unit i , so it is non-negative if P_i is within generation limits. Therefore, we have:

$$V(\mathbf{P}^{(k)}) \geq 0 \quad (6.17)$$

Assume in iteration $k + 1$, agent m and agent n accomplish behaviors described by (6.12), (6.13). Then the change of the lyapunov function would be:

$$\begin{aligned}
& V(\mathbf{P}^{(k+1)}) - V(\mathbf{P}^{(k)}) \\
&= F_m(P_m^{(k+1)}) + F_n(P_n^{(k+1)}) - F_m(P_m^{(k)}) - F_n(P_n^{(k)}) \\
&\leq F_m(P_m^{(k+1)}) + F_n(P_n^{(k+1)}) \\
&\quad - \left[F_m(P_m^{(k+1)}) + F'_m(P_m^{(k+1)}) \left(P_m^{(k)} - P_m^{(k+1)} \right) \right] \\
&\quad - \left[F_n(P_n^{(k+1)}) + F'_n(P_n^{(k+1)}) \left(P_n^{(k)} - P_n^{(k+1)} \right) \right] \\
&= -F'_m(P_m^{(k+1)}) \left(P_m^{(k)} - P_m^{(k+1)} \right) - F'_n(P_n^{(k+1)}) \left(P_n^{(k)} - P_n^{(k+1)} \right) \\
&= 0
\end{aligned} \tag{6.18}$$

If in iteration $k + 1$, agent m reaches its limit before it satisfies (6.12), then agent m will choose its limit and agent n will implement behavior (6.14). To proof the convergence of this behavior, let us study the case that the marginal cost of agent m is smaller than that of agent n at iteration k , described by equation (6.19). A similar proof can apply in the case that the marginal cost of agent m is larger than that of agent n at iteration k .

$$F'_m(P_m^{(k)}) < F'_n(P_n^{(k)}) \tag{6.19}$$

If F_m and F_n are convex cost functions, generator m will increase its generation to increase its marginal cost; while generator n will decrease its generation to decrease its marginal cost. The relationships between P_m^k and P_m^{k+1} , P_n^k and P_n^{k+1} are shown in equations (6.20) and (6.21) respectively. Figure 6.1 shows the relationships between them.

$$P_m^{(k)} < P_m^{(k+1)} \tag{6.20}$$

$$P_n^{(k)} > P_n^{(k+1)} \quad (6.21)$$

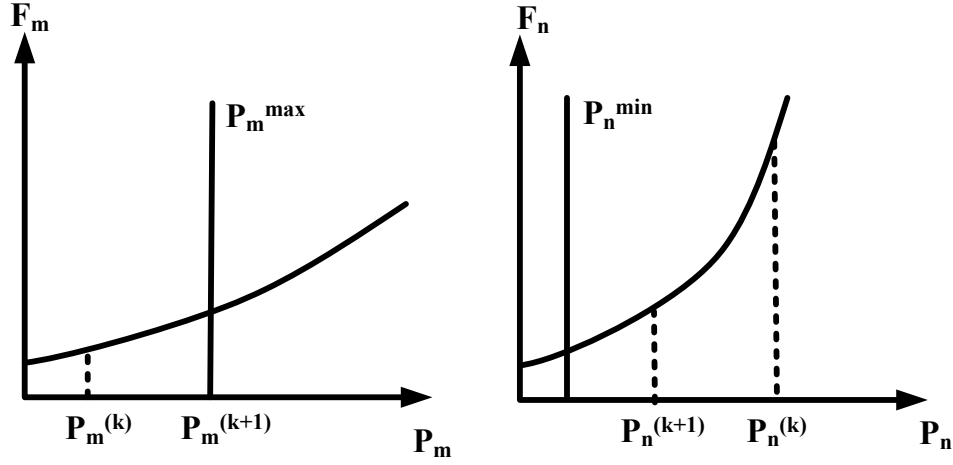


Figure 6.1: Cost curve for agent m and agent n

Since agent m reaches its maximum limit before reaching identical marginal cost as agent n , its marginal cost at iteration $k + 1$ will be still smaller than the marginal cost of agent n , expressed in equation (6.22).

$$F'_m(P_m^{(k+1)}) < F'_n(P_n^{(k+1)}) \quad (6.22)$$

Hence, the change of lyapunov function is

$$\begin{aligned}
& V(\mathbf{P}^{(k+1)}) - V(\mathbf{P}^{(k)}) \\
&= F_m(P_m^{(k+1)}) + F_n(P_n^{(k+1)}) - F_m(P_m^{(k)}) - F_n(P_n^{(k)}) \\
&\leq F_m(P_m^{(k+1)}) + F_n(P_n^{(k+1)}) \\
&\quad - \left[F_m(P_m^{(k+1)}) + F'_m(P_m^{(k+1)}) \left(P_m^{(k)} - P_m^{(k+1)} \right) \right] \\
&\quad - \left[F_n(P_n^{(k+1)}) + F'_n(P_n^{(k+1)}) \left(P_n^{(k)} - P_n^{(k+1)} \right) \right] \tag{6.23} \\
&= -F'_m(P_m^{(k+1)}) \left(P_m^{(k)} - P_m^{(k+1)} \right) - F'_n(P_n^{(k+1)}) \left(P_n^{(k)} - P_n^{(k+1)} \right) \\
&= F'_m(P_m^{(k+1)}) \left(P_n^{(k)} - P_n^{(k+1)} \right) - F'_n(P_n^{(k+1)}) \left(P_n^{(k)} - P_n^{(k+1)} \right) \\
&= \left(F'_m(P_m^{(k+1)}) - F'_n(P_n^{(k+1)}) \right) \left(P_n^{(k)} - P_n^{(k+1)} \right) \\
&< 0
\end{aligned}$$

Therefore, the convergence of the designed algorithm is guaranteed.

It is easy to verify that the final result $\mathbf{P}(P_1, P_2, \dots, P_N)$ satisfies Karush-Kuhn-Tucker Conditions shown in equations (6.24-6.29).

$$\nabla F(P) - \sum_{j=1}^{2N} u_j \nabla g_j(P) - v \nabla h(P) = 0 \tag{6.24}$$

where,

$$\nabla g_j(P) = P_j^{max} - P_j \geq 0, \quad j = 1, 2, \dots, N \tag{6.25}$$

$$\nabla g_j(P) = P_{j-N} - P_{j-N}^{min} \geq 0, \quad j = N + 1, N + 2, \dots, 2N \tag{6.26}$$

$$h(P) = \sum_{i=1}^N P_i - P_D \tag{6.27}$$

$$u_j g_j(P) = 0, \quad j = 1, 2, \dots, 2N \quad (6.28)$$

$$u_j \leq 0, \quad j = 1, 2, \dots, 2N \quad (6.29)$$

Therefore, the final result is a KKT point. According to KKT Sufficiency Theorem [67], since $F(P)$ is convex, every $g_j(P)$ is concave, and $h(P)$ is linear, the KKT point is the global optimal point.

The procedure for decentralized agents to achieve optimal economic dispatch is as follows:

- (a) Agent m selects its neighbor agent n .
- (b) Both agents implement behaviors (6.12) and (6.13), if one agent encounters a limit, then it uses this limit as its new assignment, meanwhile, the other agent implements behavior (6.14).
- (c) If the assignments of all agents converge within the accepted tolerance, optimization process is terminated. Otherwise, steps (a) through (c) are repeated.

Figure 6.2 displays the flow chart for economic dispatch in multi-agent platform.

Generation agents can implement behaviors described above simultaneously; hence, the convergence time for this algorithm is more competitive than single-thread optimization. However, to implement this algorithm, generation agents may be required to discover extra neighbors, apart from topological neighbors. Because this algorithm is based on communications between generation agents, topologically, it is possible that one generation agent may not have any generation agent as a neighbor; then its cost can not be optimized. Also note that not all microgrids permit economic dispatch; the algorithm presented in this section enhances the general framework for the control of microgrids, and remains available should a microgrid evolve to where it does permit economic dispatch.

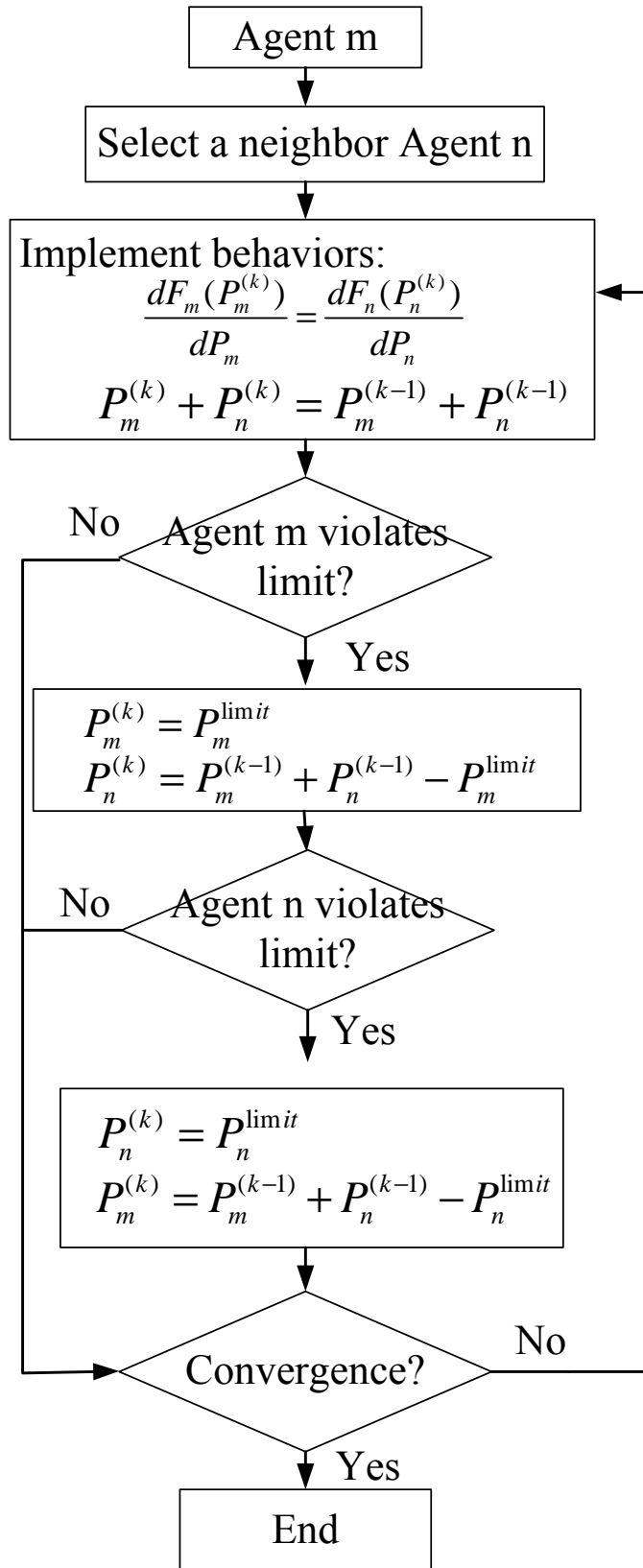


Figure 6.2: Flow chart for economic dispatch

6.4 Simulation Results

Economic dispatch is an additional service provided by MAS where the capability exists. It can help to optimize total generation cost, but it cannot change total generation amounts determined by power balance control.

To validate the proposed agent-based economic dispatch algorithm, a small prototype microgrid with five DGs are studied. Assume the cost function satisfy polynomial equation expressed in (8.7). Other forms of cost functions also can be optimized by the proposed algorithm, as long as they are convex. The microgrid cost data are shown in Table 6.4. Generation 4 is a renewable source, so it is operated in maximum power point. If not equipped with storage device, its output power is preferable not to be regulated. The neighbor relationships for this small microgrid is shown in Fig. 6.3. A line connecting two agents indicate neighbor relationship between them.

$$F = a_0 + a_1P + a_2P^2 \quad (6.30)$$

Table 6.1: Generation Data for the Microgrid

Gen. No.	P_{max} (kW)	P_{min} (kW)	a_0	a_1	a_2
1	400	200	8	0.096	0.00012
2	1000	300	12	0.072	0.00008
3	800	100	9	0.064	0.00001
4	600	600	-	-	-
5	900	150	10	0.084	0.00014

Initially, let us assume total load and line losses are 2600 kW. Initial values for Generation 1 to Generation 5 are 300 kW, 500 kW, 400 kW, 600 kW and 800 kW respectively. Fig. 6.4 shows the dispatched results for each generation. Only 4 iterations are needed to achieve optimal solution. It is seen in Fig. 6.5 that marginal costs are converged to an identical value in the end to achieve minimal operation cost except the one of the undispatchable source, Generation 4. Fig. 6.6 displays total cost in microgrid for the same amount of generation is reduced from \$339 to \$304.

The proposed economic dispatch algorithm is also applied to IEEE 118-bus test system. This

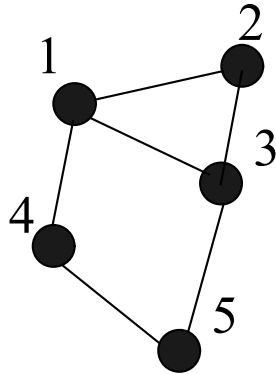


Figure 6.3: Neighborhood relationship diagram

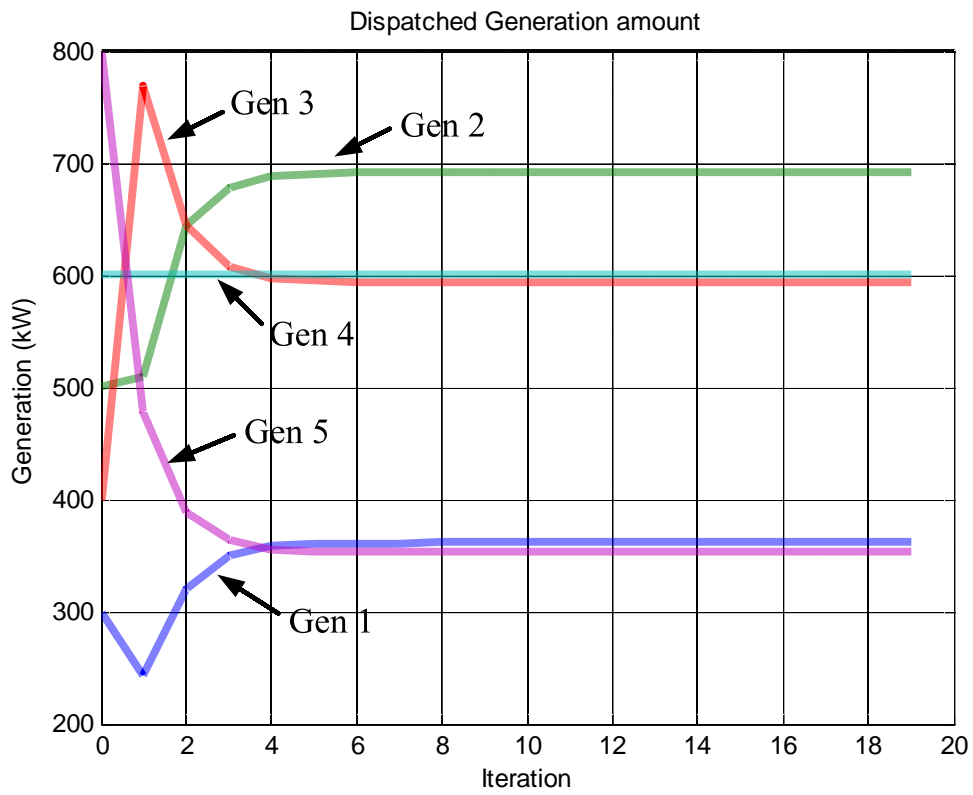


Figure 6.4: Generation dispatch result for five-agent system

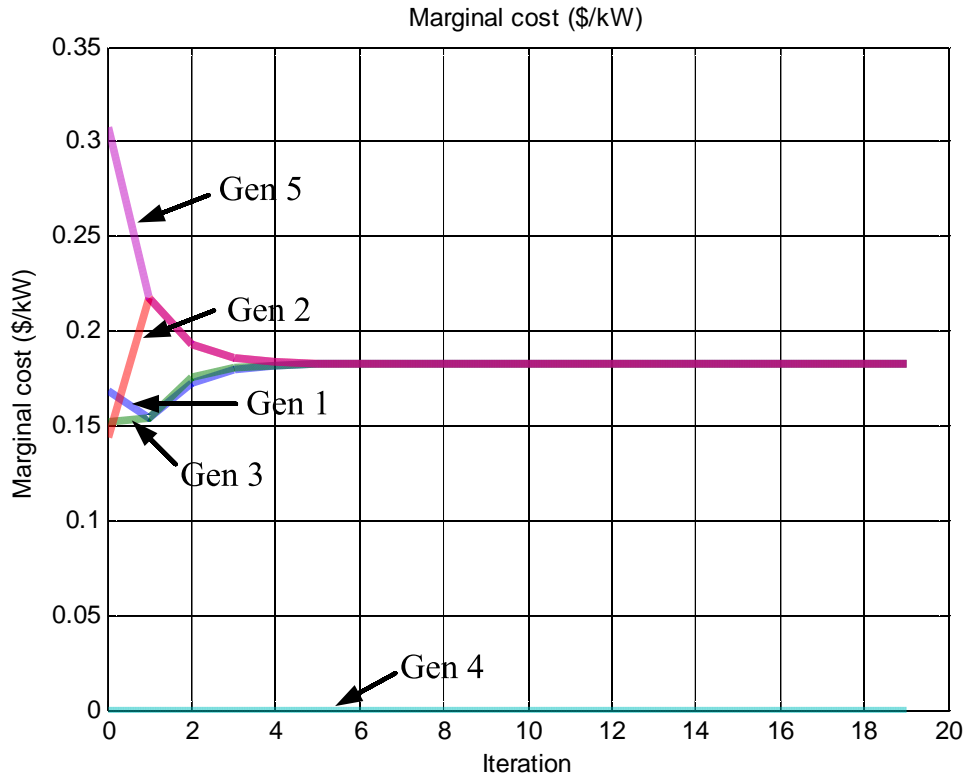


Figure 6.5: Marginal cost for five-agent system

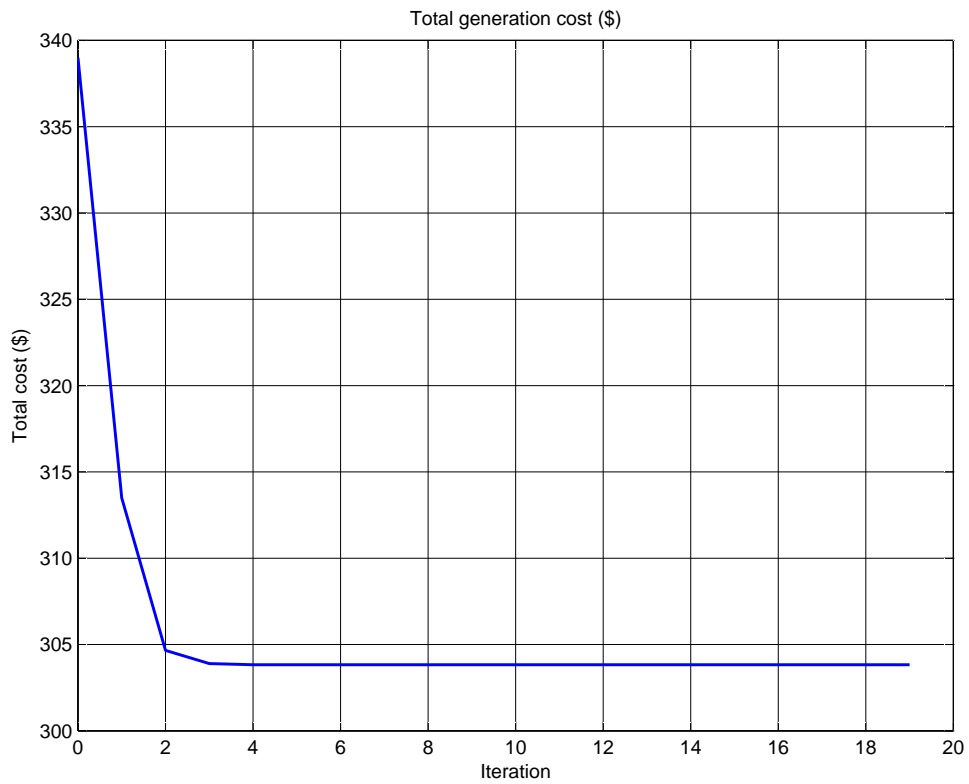


Figure 6.6: Generation cost for five-agent system

system has 54 generators; therefore, 54 agents are involved in this control. Total load demand is 4.377×10^3 MW. Assume that each agent has six direct neighbors. (The number of neighbors in this case is not initially known, as explained in the last paragraph of Section 6.3.) Generation cost and limit data are obtained from [70]. Initially, assume that the 54 generators share the load in proportion to their capacities. If the convergence tolerance is set to 1×10^{-4} pu, it takes 46 iterations to converge. Simulation results are shown in Fig. 6.7. If each agent stores cost coefficients and generation upper and lower limits of its neighboring generators, then the only data required to be communicated is the generation value. Therefore, an estimated time can be computed as $46 \times 1 \times 16/10\,000\,000 = 0.0000736$ s. This time does not include the computational time; however, considering the computation required in this algorithm is not complex and the computation time is usually much smaller than communication time, the total computation time will not be significant.

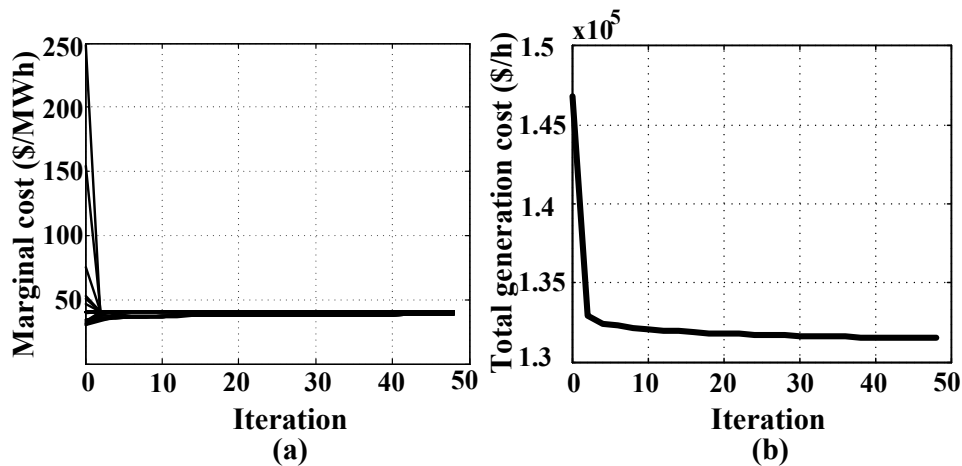


Figure 6.7: Simulation results for economic dispatch

Further discussion: Fig. 6.7(b) shows that the cost decreases rapidly in the first few iterations, while in subsequent iterations the improvements diminish. In this example, the saving is about $\$1.5 \times 10^4$ /h in the first 12 iterations; however, in the last 34 iterations, the saving is only about $\$5 \times 10^2$ /h. Therefore, if the tolerance is set appropriately larger, the time required for the algorithm can be reduced tremendously, while the saving is not compromised too much. In this case, if the tolerance is set to 1×10^{-3} , it takes 12 iterations to converge. So the time is reduced by 73.91%

while the saving in cost is only reduced by about 3.34%.

6.5 Summary

This chapter proposes a potential solution for distributed economic dispatch realization in a decentralized multi-agent platform. A decent communication algorithm based on the consensus theorem is proposed. In this algorithm, all agents are completely identical and autonomous. They do not have access to system global information; however, by making use of their local information and limited communications with their immediate neighbors, these agents are able to compete and cooperate with each other to achieve a global minimum operation cost. The contributions of this chapter are listed below:

1. It proposes a potential distributed solution for economic dispatch by a decentralized multi-agent system.
2. Proof of convergence and proof of global optimization are presented in this chapter.
3. Because of the synchronous characters, this algorithm is capable to satisfy speed requirement of on-line economic dispatch.
4. This algorithm also allows the system to continue operation in the presence of single point failure. If any agent in the system fails, only the cost in that node is not optimized; while the cost for the remaining system can still be minimized.

Chapter 7

Distributed Economic Dispatch Considering Network Constraints

7.1 Introduction

In chapter 6, it proposed a distributed synchronous algorithm to optimize generation cost without considering network constraints. It is realized in a decentralized multi-agent platform, in which each agent can only get access to local information. By collaborating and competing with its neighbors, each agent is trying to minimize its own generation cost while satisfying total demand requirement; therefore, total generation cost is minimized. It is shown that this algorithm is guaranteed to converge to the global optimal point. The speed of the algorithm is demonstrated to be capable for on-line economic dispatch. However, this algorithm does not consider network constraints, such as voltage magnitude requirements of buses or capacity limits of transmission lines. In a stressful power system, these constraints can have considerable influences on generation dispatch, which can not be overlooked. In this chapter, it proposes an innovative distributed economic dispatch algorithm considering network constraints for a decentralized multi-agent system, in which each agent is responsible for local control variables and can observe partial or full system states. The proposed algorithm can also optimize total generation cost in a non-increasing

direction. Simulation results show that if each agent can observe full system states, the multi-agent system can achieve global optimum; if each agent can only observe local system states, multi-agent system can still optimize generation cost, but it may be trapped by a local optimum.

7.2 Problem Formulation

Conventional economic dispatch is implemented in a central controller, which has global information of the system. The problem can be formulated as:

$$\text{Min: } F(\mathbf{x}, \mathbf{u}) \quad (7.1)$$

$$\text{Subject to: } g(\mathbf{x}, \mathbf{u}) \leq 0 \quad (7.2)$$

$$h(\mathbf{x}, \mathbf{u}) = 0 \quad (7.3)$$

However, in the decentralized multi-agent platform, there is no central unit that has global information of the system. Each agent is only limited to access its local information and necessary information from its immediate neighbors. Consider a system of N agents, where each agent i , $i \in \mathbb{A} = [1, 2, \dots, N]$ is responsible for an area A_i of the system. In each area, the agent has a set of control variables, $\mathbf{u}_i \in \mathbb{R}^{n_i}$, which can be real and reactive power output of generators. It also has information of local states, $\mathbf{x}_i = [x_{i1}, x_{i2}, \dots, x_{im}]$, which can be bus voltage magnitudes, bus angles. Based on its available state information and state information from its neighbors, each agent can compute real and reactive power flow through transmission lines in its area. Two agents are allowed to have the observability over the same bus or the same transmission line, but each control variable is only belonged to one local agent. To clarify the decentralized algorithm, some notations are defined first. $\mathcal{N}(i)$ is the set of agents that are neighbors of agent i ; \mathbf{x}_i^B is a vector of the states for the boundary buses that agent i can observe; \mathbf{f}_i^B is the real and reactive power flowing through the boundary of agent i ;

In order to optimize generation cost, each agent i and its immediate neighbors are required to implement the following optimization for their control variables:

$$\text{Min:} \quad \sum_{m \in \{i, \mathbf{N}(i)\}} F_m(\{\mathbf{u}_m\}) \quad (7.4)$$

$$\text{Subject to:} \quad g_{A_m}(\{\mathbf{x}_{A_m}\}, \{\mathbf{u}_{A_m}\} | \{\mathbf{x}_{A_m}^B\}, \mathbf{f}_{A_m}^B) \leq 0 \quad A_m = A_i + A_{\mathbf{N}(i)} \quad (7.5)$$

$$h_{A_m}(\{\mathbf{x}_{A_m}\}, \{\mathbf{u}_{A_m}\} | \{\mathbf{x}_{A_m}^B\}, \mathbf{f}_{A_m}^B) = 0 \quad A_m = A_i + A_{\mathbf{N}(i)} \quad (7.6)$$

where, m is the set of agent i and its immediate neighbors; F_m is the cost function for the control variables in the area of agent m ; A_m is the area that combines the areas that agent i and its immediate neighbors are responsible for; \mathbf{x}_{A_m} and \mathbf{u}_{A_m} are the states and control variables inside area A_m ; g_{A_m} and h_{A_m} are lists of inequality and equality constraints on \mathbf{x}_{A_m} and \mathbf{u}_{A_m} , given that the states $\mathbf{x}_{A_m}^B$ and real and reactive power flows $\mathbf{f}_{A_m}^B$ of the boundary of A_m are held constant.

Equations (7.4)–(7.6) can be understood intuitively in this way, each time agent i and its immediate neighbors form an area, and optimize the cost inside this area while maintaining the states and power flows through transmission lines on the boundary constant; therefore, it does not interfere the states and control variables in other areas. This algorithm is also applicable to be implemented in parallel, as long as the parallel formed areas do not have overlap with each other.

7.3 Proof of Convergence

To analyze the stability of the proposed algorithm, this Section performed a convergence analysis based on a Lyapunov function.

Define a Lyapunov function $V: \chi^N \subset \mathbb{R}^N \rightarrow \mathbb{R}$ of the form shown in (7.7):

$$V(\mathbf{u}^k) = \sum_{i \in \nu} F_i(\mathbf{u}_i^{(k)}) \quad (7.7)$$

where $\mathbf{u}^{(k)}$ is a vector consisting of system control values in iteration k ; $\mathbf{u}_i^{(k)}$ is control variable values in iteration k for agent i ; ν is the set of agents in the system.

Since F_i is the cost function of generator units, $F_i \geq 0$. Then, we have

$$V(\mathbf{u}^k) \geq 0 \quad (7.8)$$

If in iteration k , agent i and its immediate neighbors $N(i)$ implement the behaviors in described by equations (7.4)–(7.6). Then we have:

$$V(\mathbf{u}^{(k+1)}) - V(\mathbf{u}^{(k)}) = \sum_{i \in \nu} F_i(\mathbf{u}_i^{(k+1)}) - \sum_{i \in \nu} F_i(\mathbf{u}_i^{(k)}) \quad (7.9)$$

Since equations (7.4)–(7.6) maintain the states and power flows on the boundary of A_m ; therefore, it does not interfere the states and control variables in the area other than A_m , hence we have:

$$\sum_{i \in \nu, i \notin A_m} F_i(\mathbf{u}_i^{(k+1)}) = \sum_{i \in \nu, i \notin A_m} F_i(\mathbf{u}_i^{(k)}) \quad (7.10)$$

Therefore,

$$V(\mathbf{u}^{(k+1)}) - V(\mathbf{u}^{(k)}) = \sum_{i \in A_m} F_i(\mathbf{u}_i^{(k+1)}) - \sum_{i \in A_m} F_i(\mathbf{u}_i^{(k)}) \quad (7.11)$$

Since the behaviors (7.4)–(7.6) optimize the generation cost inside area A_m , we have

$$\sum_{i \in A_m} F_i(\mathbf{u}_i^{(k+1)}) \leq \sum_{i \in A_m} F_i(\mathbf{u}_i^{(k)}) \quad (7.12)$$

Therefore,

$$V(\mathbf{u}^{(k+1)}) - V(\mathbf{u}^{(k)}) \leq 0 \quad (7.13)$$

Therefore, the convergence of the proposed algorithm is guaranteed.

7.4 Simulation Results

7.4.1 Linearized Economic Dispatch Considering Network Constraints

To testify the proposed decentralized economic dispatch algorithm, IEEE 14-bus test system is studied [69]. The simulation conducted in this subsection utilizes linearized optimal power flow model described in Chapter 2. In this system, it has 5 generators located at bus 1, bus 2, bus 3, bus 6 and bus 8 respectively.

The simulation will test two cases: in the first one, each agent can observe all the system states; while in the second one, only local states can be observed by the agent. IEEE 14 bus system has very large capacity limit on transmission lines, therefore, the constraints of transmission line do not limit the power flow. Only bus limit is active. To examine the effect of constraints of transmission lines, each simulation case will test two scenarios. The first one is the original system with transmission lines of large capacities. In the second scenario, the capacity limit of transmission line connecting bus 1 and bus 2, and the capacity limit of transmission line connecting bus 1 and bus 5 are changed to 19.99 p.u. and 29.99 p.u. respectively.

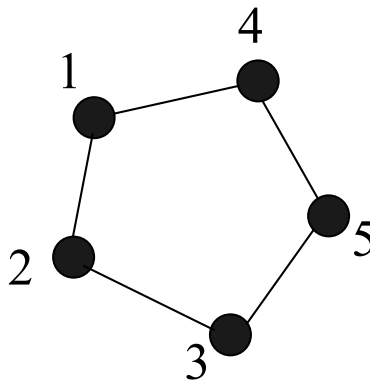


Figure 7.1: Neighborhood relationship for IEEE 14 bus system

Case 1: each agent is responsible to control one generator, but can observe all the states of the system. The neighborhood relationship is shown in Figure 7.1. A straight line connecting two nodes indicate these two nodes are neighbors. In scenario 1, the generation cost curve is shown in Figure 7.2. The final optimal generation result is 8.5559×10^3 \$/hr. In scenario 2, the generation cost curve is shown in Figure 7.3. The final optimal generation result is 9.3737×10^3 \$/hr, which is larger than the result obtained in scenario 1. Because scenario 2 is more constrained than scenario 1, its optimal value is larger.

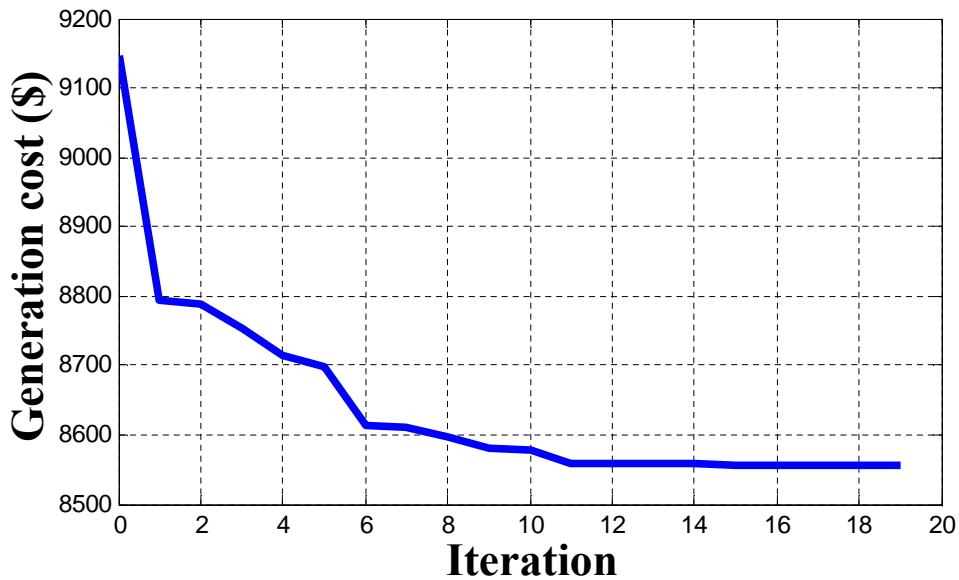


Figure 7.2: Generation cost curve for the first scenario of case 1

Table 7.1: Observed Area for Each Bus

Agent No.	Bus No. in the observed area
1	1, 5, 6
2	1, 2, 3, 4
3	3, 4, 5, 6, 7, 8
4	5, 6, 10, 11, 12, 13, 14
5	7, 8, 9

Case 2: in this case, each agent is also responsible to control one generator, but it is limited to observe local states. The neighborhood relationship is also shown in Figure 7.1. The local area that each agent can observe is shown in Table 7.1. In scenario 1, the optimal generation cost is

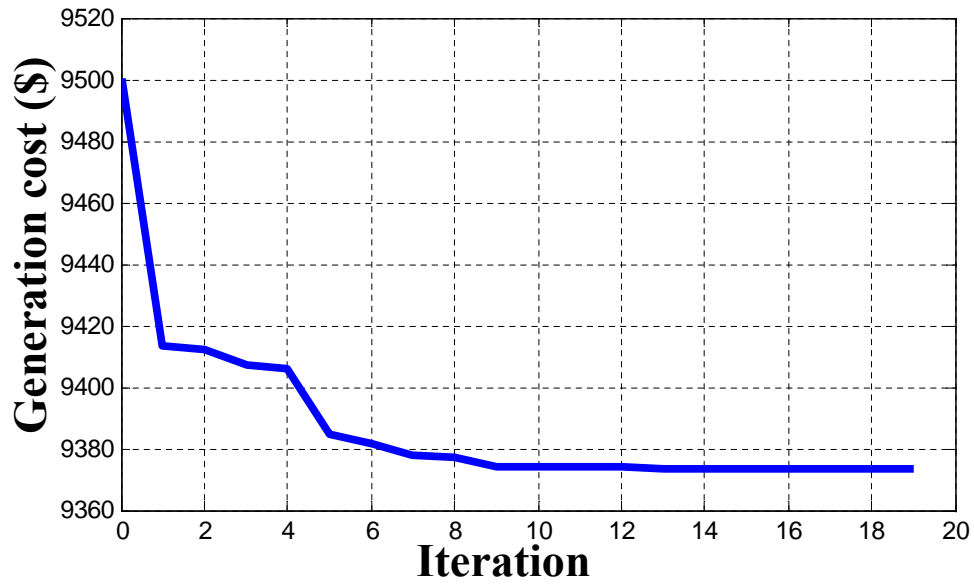


Figure 7.3: Generation cost curve for the second scenario of case 1

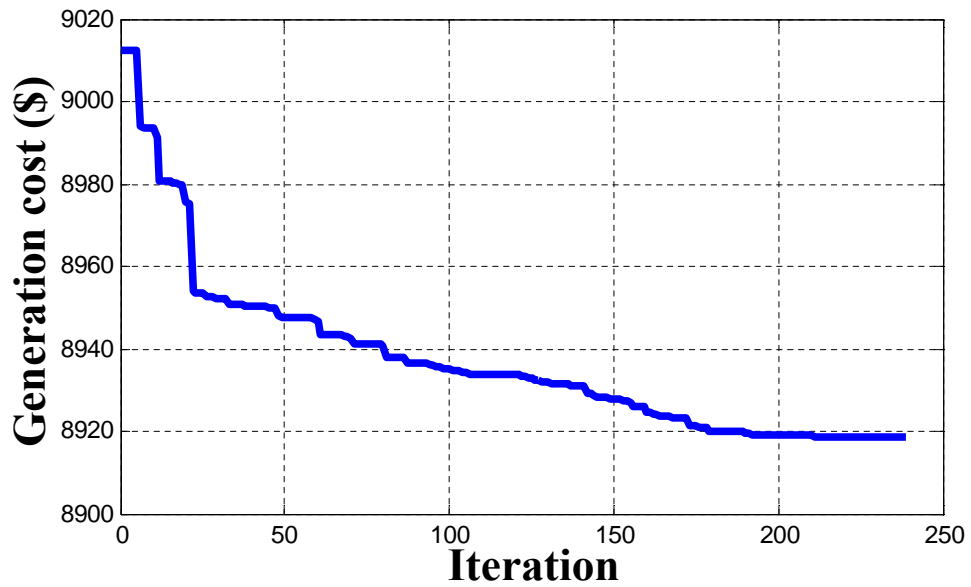


Figure 7.4: Generation cost curve for the first scenario of case 2

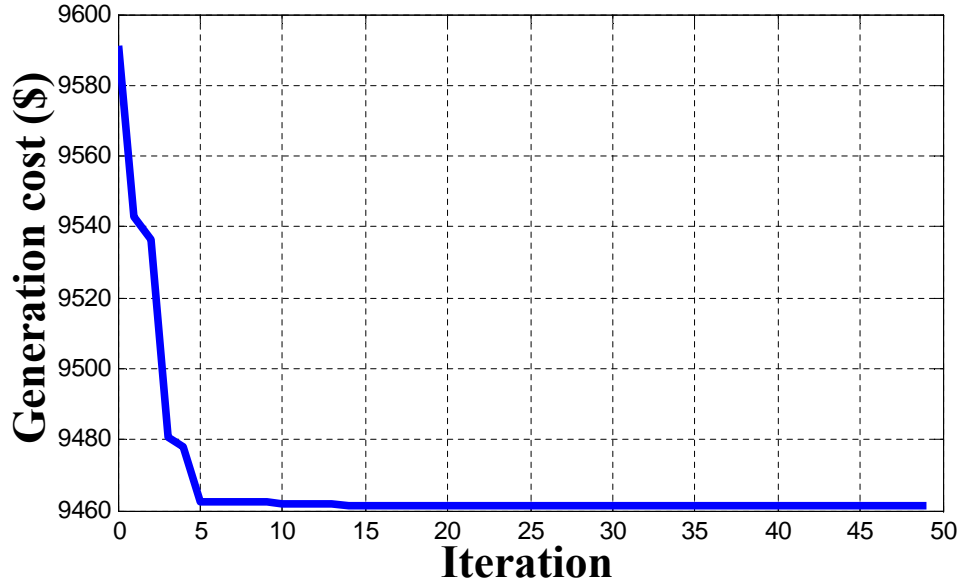


Figure 7.5: Generation cost curve for the second scenario of case 2

8.9187×10^3 \$/hr. The generation cost curve is shown in Figure 7.4. In scenario 2, the optimal generation cost is 9.4614×10^3 \$/hr. The generation cost curve is shown in Figure 7.5. It can be seen that multi-agent system can reduce generation cost in a non-increasing way. However, because each agent lacks observability over some of states, the optimal solution is easily got trapped by the local optimum. The optimal value obtained by multi-agent system in this case highly depends on the initial point and how large area each agent can observe.

If we implement the algorithm with no network constraints described in Chapter 6, the optimal generation cost is 7.6426×10^3 \$/hr; The centralized linearized economic dispatch obtains the optimal generation cost of 8.5559×10^3 \$/hr for scenario 1 and 9.3717×10^3 \$/hr for scenario 2. The reason that the algorithm in Chapter 6 achieves less generation cost than the centralized linearized economic dispatch is that it does not consider network constraints. The fewer constraints it considers, the less value it obtains. But the value is also more inaccurate. The results are summarized and analyzed in Table 7.2. It can be seen that multi-agent system with full observability of system states can achieve global optimum. Multi-agent system with partial observability can optimize generation cost, however, because each agent does not get access to full states, the optimal generation cost is sacrificed and highly depends on the initial point and the observability of each

agent.

Table 7.2: Result Summary

Architecture	Scenarios	Scenario 1		Scenario 2	
	Type	Gen cost(\$/hr)	Error	Gen cost (\$/hr)	Error
Centralized	Network Constraint	8.5559×10^3	0	9.3717×10^3	0
Distributed	No Network Constraint	7.6426×10^3	10.67%	7.6426×10^3	18.45%
	Full Observability	8.5559×10^3	0	9.3737×10^3	0.02%
	Partial Observability	8.9187×10^3	4.24%	9.4614×10^3	0.96%

7.4.2 Nonlinear Economic Dispatch Considering Network Constraints

The proposed decentralized algorithm of economic dispatch can also be implemented in the nonlinear optimization models of power system. IEEE 9-bus system is tested to verify the proposed algorithm. It has three generators located at bus 1, bus 2 and bus 3 respectively. In this simulation, we assigned three agents, each of which is responsible for one generator. Since there are only three agents in the system, each time only two agents are communicating and optimize their local area together.

The simulation will also test two cases: in the first one, each agent can observe full system states; in the second one, only partial system states can be observed by the agent. Each case will also have two scenarios: the first one will use the original system; the second will change the capacity of transmission line connecting bus 1 and bus 4 to 1.5 p.u.

Case 1: each agent is responsible to control one generator, but can observe full states of the system. In scenario 1, the generation cost curve is shown in Figure 7.6. The optimal generation cost obtained by these distributed fully observable agents is 5.2967×10^3 . In scenario 2, the generation cost curve is shown in Figure 7.7. The optimal generation cost obtained is 5.4995×10^3 . Because the network constraints are more stressful in the second scenario than they are in the first scenario, the optimal value obtained in the scenario 2 is larger than it is obtained in scenario 1.

Case 2: each agent is responsible to control one generator, but can only observe partial of the

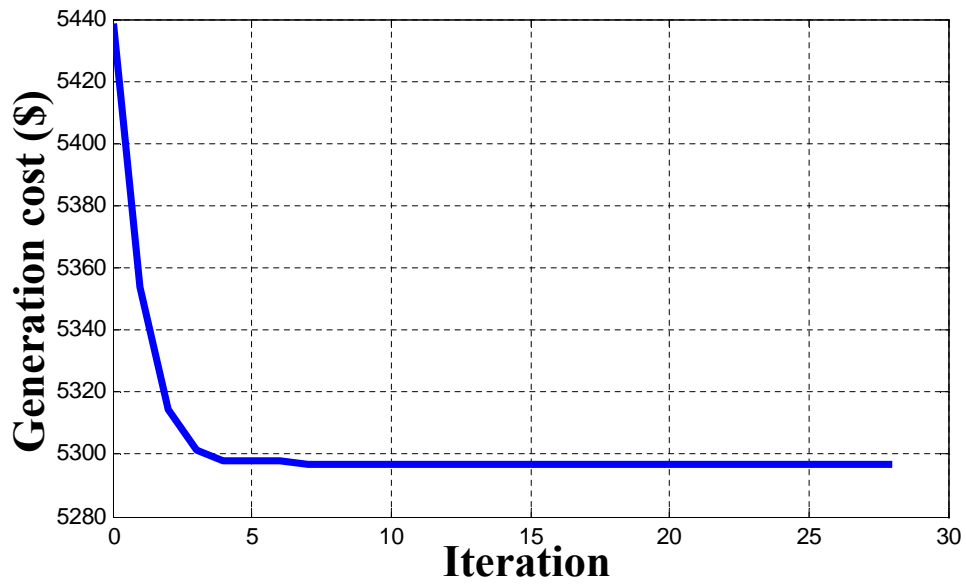


Figure 7.6: Generation cost curve for the first scenario of case 1 for AC models

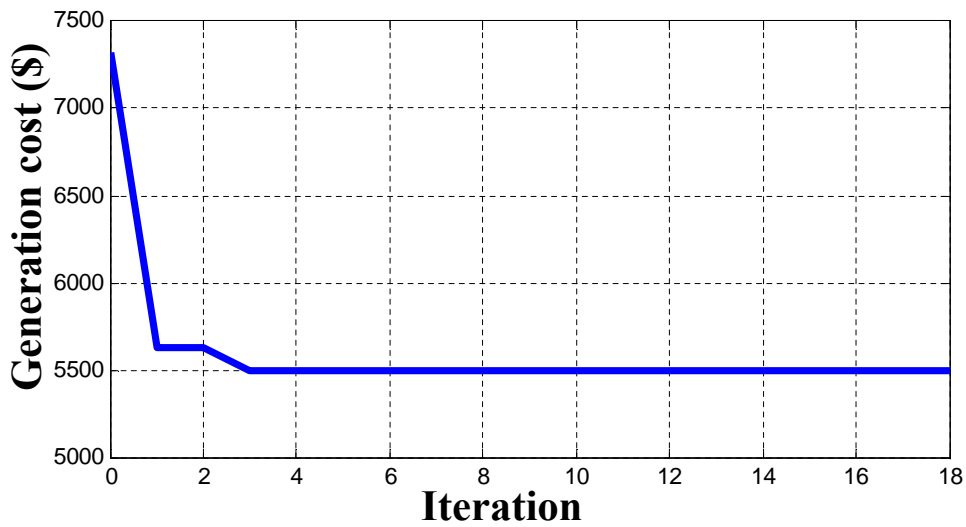


Figure 7.7: Generation cost curve for the second scenario of case 1 for AC models

states in the system. The local area that each agent can observe is shown in Table 7.3. In scenario 1, the optimal generation cost is 5.3423×10^3 . The generation cost curve is shown in Figure 7.8. In scenario 2, the optimal generation cost is 5.6187×10^3 . The generation cost curve is shown in Figure 7.9. Multi-agent system with partial observability can minimize generation cost; however, it is not guaranteed to achieve global optimal. The optimal value obtained in the end depends on the initial solution and the size of the area each agent can observe.

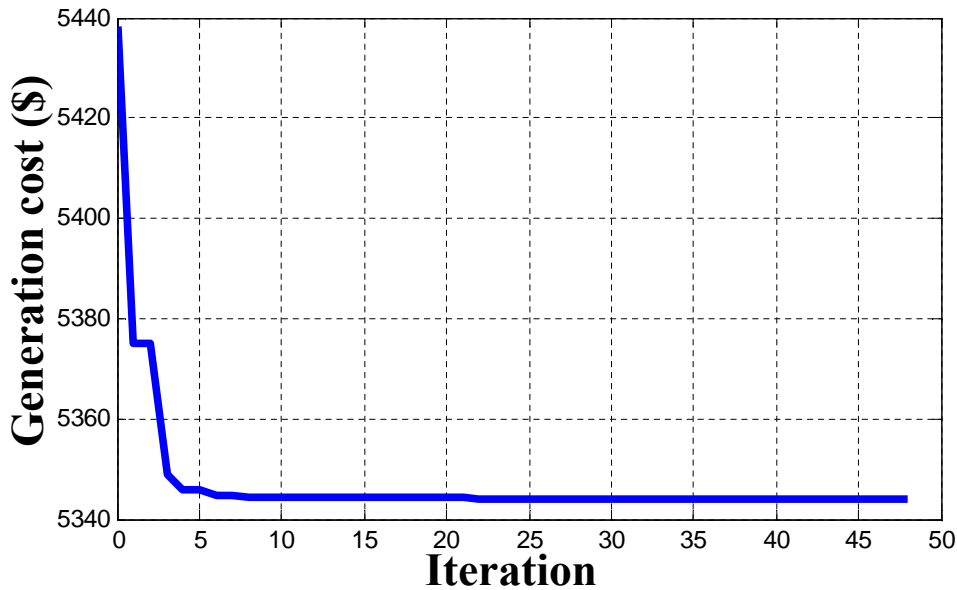


Figure 7.8: Generation cost curve for the first scenario of case 2 for AC models

Table 7.3: Observed Area for Each Bus for IEEE 9-Bus System

Agent No.	Bus No. in the observed area
1	1, 4, 5, 7, 8
2	2, 4, 6, 7, 9
3	3, 5, 6, 8, 9

If we implement the algorithm with no network constraints described in Chapter 6, the optimal generation cost is 5.216×10^3 \$/hr; The centralized linearized economic dispatch obtains the optimal generation cost of 5.2967×10^3 \$/hr for scenario 1 and 5.4995×10^3 \$/hr for scenario 2. The results are summarized and analyzed in Table 7.4. It can be seen that multi-agent system with full observability of system states can achieve global optimum. Multi-agent system with partial

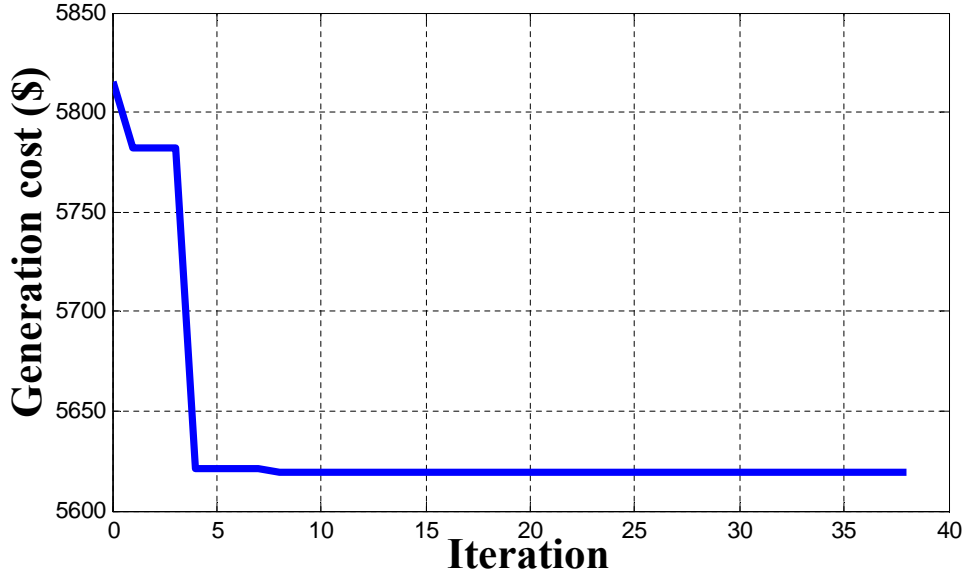


Figure 7.9: Generation cost curve for the second scenario of case 2 for AC models

observability can optimize generation cost, however, because each agent does not get access to full states, the optimal generation cost is sacrificed and highly depends on the initial point and the observability of each agent.

Table 7.4: Result Summary

Architecture	Scenarios	Scenario 1		Scenario 2	
	Type	Gen cost(\$/hr)	Error	Gen cost (\$/hr)	Error
Centralized	Network Constraint	5.2967×10^3	0	5.4995×10^3	0
Distributed	No Network Constraint	5.216×10^3	1.53%	5.216×10^3	5.16%
	Full Observability	5.2967×10^3	0	5.4995×10^3	0%
	Partial Observability	5.3423×10^3	0.86%	5.6187×10^3	2.17%

7.5 Summary

This chapter proposes a distributed algorithm for economic dispatch considering network constraints based on a decentralized multi-agent platform. Convergence of the proposed algorithm is presented to ensure its stability. By implementing the proposed algorithm, total generation cost is always changing in a non-increasing direction. The simulation shows that if each agent in the

multi-agent system can observe system states globally, the proposed algorithm can help multi-agent system achieve global optimum as a centralized controller; if each agent can only observe local system states, this algorithm can help multi-agent system minimize generation cost, but it may get trapped by local optimum. In the second case, it is highly suggested that multi-agent system can make use of available information from the system and start with an initial point as better as possible. The contributions of this chapter are listed below:

1. It proposes a general distributed solution for economic dispatch by a decentralized multi-agent system taking network constraints into account. The proposed algorithm can be used for DC model, linearized AC model or full AC model.
2. Proof of convergence is presented in this chapter.
3. The proposed algorithm is applicable to be implemented in a parallel manner, which potentially provides speed advantage.
4. This algorithm also allows the system to continue operation in the presence of single point failure. If any agent in the system fails, only the cost for the control variables of that agent is not optimized; while the cost for the remaining system can still be minimized.

Chapter 8

Multi-Agent Implementation and Multi-Level Control Architecture

8.1 Multi-Level Control Structure

This dissertation proposes a hierarchical control structure displayed in Fig. 8.1 for the control of microgrids. The upper decentralized multi-agent layer, acting as a quick-responding system operator, is responsible for power balance and economic dispatch control. The lower local control layer, in response to the power commands required by MAS, regulates real and reactive power output of local DGs.

For the MAS power balance control, the fast three-sweep algorithm proposed in chapter 4 can be used to react to power unbalance in real time, so as to maintain stable operation of microgrids. The functions of the three sweeps are to determine information flow route, obtain net real and reactive power, and dispatch generation and load. All the information in these three sweeps is designed to flow in parallel, so that the required communication can be achieved rapidly in the proposed MAS architecture. MAS power balance control is critical for stable operation; therefore, it has the highest priority in MAS computation and control.

Economic dispatch is conducted on-line among agents that are responsible for generation nodes

(also called generation agents). Since real power balance is maintained in MAS power balance control layer, economic dispatch will optimize total generation cost while maintaining total real power generation.

As shown in Fig. 8.1, each local controller will receive real and reactive power settings from the MAS layer and implement local control for DGs. However, because only load information is transmitted and losses are not calculated, the MAS power balance control achieves an approximate allocation of generation. The losses, which equal the difference in actual generation and load, can be compensated by local controller with reserved generation capacity.

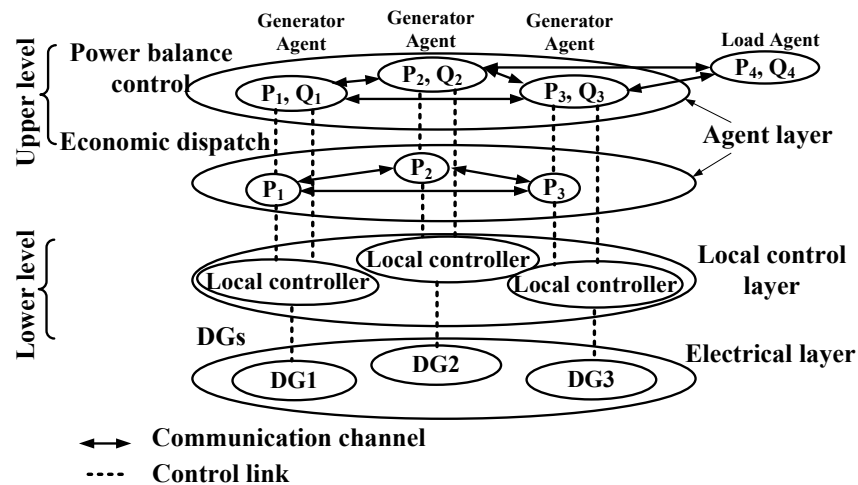


Figure 8.1: Proposed hierarchical control architecture.

8.2 Multi-Agent Implementation

Multi-agent system is implemented here in Java Agent DEvelopment (JADE) [71, 72] framework, which complies with the Foundation of Intelligent Physical Agents (FIPA) [73]. FIPA Semantic Language (FIPA-SL) is adopted in this work for agent communication.

The action of an agent is realized by implementing behaviors. Each behavior is an object of a class that extends *Behaviour* class in the *jade.core.behaviours* package. There are two main behaviors for the proposed agents: Power Balance and Economic Dispatch.

1. **Power Balance:** This behavior implements the algorithm described in Chapter 4. It contains

three sub-behaviors:

- (a) **Token Transfer:** This sub-behavior implements the algorithm in Section 4.2.1 and builds parent-child relationships among agents, based on a minimal spanning tree. In summary, this behavior waits for the first token, rejects all other tokens which come later, and removes neighborhood relationships with those agents whose tokens are rejected. Then this behavior sends the token to all its other *child agents*.
 - (b) **Information Feedback:** This sub-behavior implements the algorithm in Section 4.2.2 and helps collect *view* information from *child agents* to *parent agents*. When each agent receives *view* from all its *child agents*, this sub-behavior processes the *view* and sends the updated *view* to the *parent agent*.
 - (c) **Generation or Load Dispatch:** This sub-behavior implements the algorithm in Section 4.2.3. It receives net power values from *parent agent*, adjusts local dispatchable generation or non-vital load to minimize net power, and splits net power values for its *child agents* based on (4.7). When net real and reactive power values are both zeros after local adjustment, this sub-behavior informs neighbors of power balance completion. If an agent receives information of power balance completion from all its *child agents*, this sub-behavior informs *parent agent* of power balance completion. If an agent receives information of power balance completion from *parent agent*, this sub-behavior informs *child agents* of power balance completion.
2. **Economic Dispatch:** This behavior, as the name suggests, realizes economic dispatch function by implementing the algorithm proposed in Chapter 6. There are two states of this behavior:
- (a) **Inquiry state:** The agent sends inquiring and local generation value to one of its neighbors to ask for economic dispatch implementation. If it receives *accept* and *local generation* values from its neighbor, it updates its generation value by computing (6.12)

and (6.13) and goes to the *reply state*. If it receives refuse from the neighbor, it goes to the *reply state*. During *inquiry state*, whenever the agent receives other agents' inquiry for economic dispatch implementation, it refuses.

- (b) **Reply state:** This state waits for *inquiry* from other agents. If it receives *inquiry*, it replies with *accept* and *local generation* values; then it updates *local generation* by computing (6.12) and (6.13). There is also a time interval set for *reply state*. When the time expires, the behavior goes to *inquiry state*.

8.3 Simulation Platform of Lower Level

Lower-level simulation platform consists of local control layer and electrical layer. In this simulation, electrical layer is constructed by master-slave organized DGs with PE interfaces. The configuration of a generic PE interface is shown in Fig. 8.2. L and C are, respectively, the inductance and capacitance of the output stage inductors and capacitors. In master-slave organization, PE-based DGs in an islanded microgrid can be classified into two types: a master inverter operates in voltage source mode, providing voltage support for the microgrid; all other (slave) inverters operate as current sources, supplying specific real and reactive power into the microgrid.

8.3.1 Master Power Electronic Interfaces

The objective of the control strategy for voltage-source PE interface is to output required voltage at the sending point, which will be used as the reference voltage level for the microgrid. Normally, sources which are employed to offer voltage support in microgrids have large reserve capacity, so that it is able to provide or absorb extra power when any disturbance occurs in the microgrids, thereby maintaining the voltage.

A multi-loop control strategy with an inner current control loop and an outer voltage control loop is adopted for the voltage-source PE interface shown in Fig. 8.3. The transfer function of the inner current control loop is described by

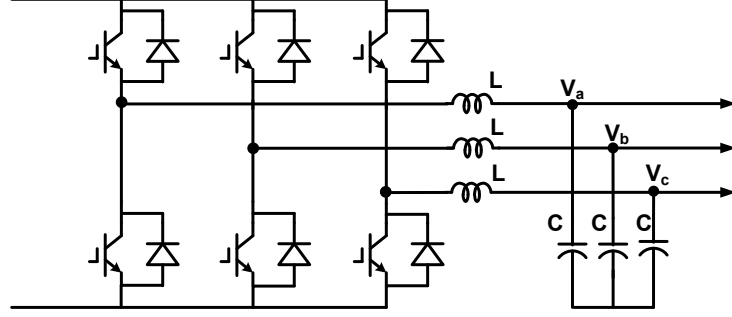


Figure 8.2: Configuration of PE interface.

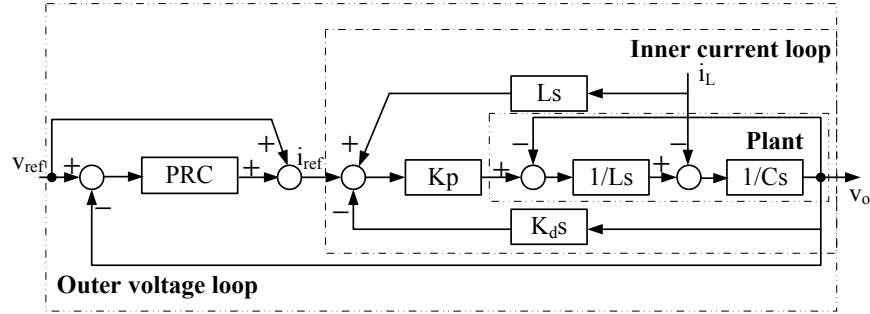


Figure 8.3: Control block for voltage-source power electronic interface.

$$V_o = \frac{K_p}{LCs^2 + K_p K_d s + 1} I_{ref} - \frac{(1 - K_p)L_s}{LCs^2 + K_p K_d s + 1} I_L \quad (8.1)$$

To improve the response to load variation, a feedforward loop is adopted for the load current. If $K_p = 1$, from the transfer function, the coefficient of I_L is zero; therefore, the effect of load current on the output voltage is compensated. The damping ratio of the inner loop is derived as

$$\xi = \frac{K_d K_p}{2\sqrt{LC}} \quad (8.2)$$

The differential feedback from the capacitor voltage introduces damping into the system, avoiding high resonant peak from a pure LC filter. The damping ratio can be adjusted by adjusting K_d . Theoretically, the optimal performance can be obtained when $\xi = 0.707$, from which K_d can be computed.

In order to smooth the transition from grid-connected mode to islanded mode when the grid fails, a reference voltage feed-forward loop is utilized to accelerate the response of the control sys-

tem. Traditional stationary PI controllers suffer from steady state error when tracking sinusoidal waveforms. High gain can decrease the error, but it will also decrease magnitude and phase margin, potentially introducing instability. A popular method of minimizing the steady state error is to use a PI controller in DQ space. However, it requires computations for the frame transformation. Moreover, sources in microgrids can be single-phase or three-phase. The implementations of single-phase and three-phase DQ controls are different. This platform utilizes a low-pass to band-pass technique expressed in (8.3) that can transform a dc compensation network in rotating frame into an equivalent ac compensation network in stationary frame to achieve identical response feature in the frequency area of interest [68] (it should be noted that the terms in the parentheses on the right comprise the argument of the gain function):

$$G_{AC}(s) = G_{DC} \left(\frac{s^2 + \omega_0^2}{2s} \right) \quad (8.3)$$

Hence the equivalent PI controller in rotational frame can be expressed in the stationary frame as:

$$G_{PRC}(s) = K_{p1} + \frac{2K_i s}{s^2 + \omega_0^2} \quad (8.4)$$

This controller, which is also called Proportional Resonant (PR) controller, can vastly boost the gain at resonant frequency. It does not require frame transformation and can be uniformly implemented for both single-phase and three-phase sources. Theoretically, at resonant frequency, infinite gain can be obtained to remove steady state error. Since PR controller can affect the phase within the band of resonant frequency, a careful selection of K_{p1} and K_i is required to decrease the bandwidth of PR controller while maintaining sufficient phase margin around resonant frequency.

8.3.2 Slave Power Electronic Interfaces

Slave PE interfaces work in current control mode and supply specific real and reactive power assigned by multi-agent system into the microgrid. In this simulation platform, voltage level is set

up by a master PE interface source, and slave PE interfaces do not directly participate in voltage control. Instead, they regulate their output current to provide specified real and reactive power output. Since voltage is maintained by the voltage source, in order to produce required real and reactive power output using multi-agent system, current-source PE interfaces can adjust their current to regulate power.

The controller shown in Fig. 8.4 is utilized for a slave inverter. A proportional resonant controller is also employed to decrease steady state error. However, the classic PR controller as expressed in equation (8.4) can not be applied here, because current control inverter is a first order system. The plant originally has a -90° phase shift, while the classic PR controller will introduce another -90° phase shift at resonant frequency, which will cause the system to be unstable. To overcome this instability problem, a modified form of PR controller as expressed in (8.5) is utilized, where ω_c is the breakpoint frequency of dc transfer function [68]. The new controller can boost gain considerably at resonant frequency while its phase shift can be adjusted by changing K_i .

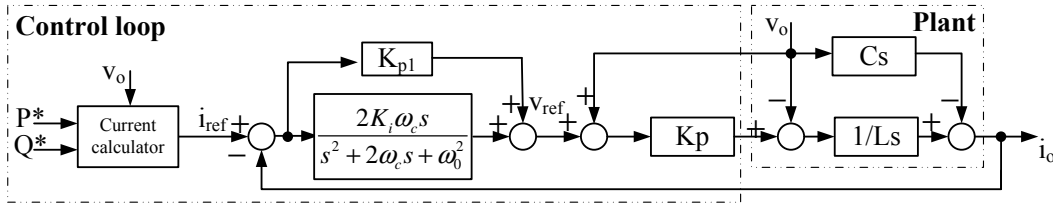


Figure 8.4: Control block for current-source power electronic interface.

$$G_{MPRC}(s) = K_{p1} + \frac{2K_i\omega_c s}{s^2 + 2\omega_c s + \omega_0^2} \quad (8.5)$$

A feedforward loop of output voltage achieves acceleration of the controller's dynamic response to the commands from the multi-agent system, and diminishes the influence of the load's effect on the output current. If $K_p = 1$, the open loop transfer function for the reference current is described by (8.6). K_{p1} , K_i and ω_c can be designed to obtain sufficient phase margin, while the gain at fundamental frequency is still boosted sufficiently so that steady state error can

be minimized.

$$G_o(s) = \frac{K_{p1}s^2 + 2(K_i + K_{p1})\omega_c s + K_{p1}\omega_0^2}{Ls^3 + 2L\omega_c s^2 + L\omega_0^2 s} \quad (8.6)$$

8.4 Multi-Level Control Architecture

To demonstrate the effectiveness of the proposed multi-level control architecture, a prototype microgrid shown in Fig. 8.5 is simulated in MATLAB/SIMULINK. MAS is implemented using JADE described in section 8.2. This study system is connected to a utility through a breaker at point of common coupling (PCC). The breaker in this simulation is open; therefore the microgrid is operated in islanded mode. (Note that in grid-connected mode, the grid at the PCC would provide the voltage reference, and all inverters in the microgrid operate in current control mode.) Agents A1–A7 are responsible for bus 1–bus 7 respectively. The structure of the multi-agent system is the same as that of Fig. 4.1. Since buses 1, 3, 5 and 7 are equipped with DGs, their agents are called generation agents. To enable economic dispatch between these four agents, assume that they establish neighborhood relationships among themselves, and are able to communicate with each other. All the other neighborhood relationships are established based on electrical connections.

The generator data for this microgrid are shown in Table 8.1. The system consists of four DGs, among which DG3 is a solar panel. It is controlled at maximum power point, consequently, its real power output is not dispatchable. DG1 is partially dispatchable, while DG2, DG4 are both fully dispatchable. Their power outputs can be adjusted through commands from the multi-agent system. The generator cost function of a micro-source is expressed as:

$$F = a_0 + b_0 P + c_0 P^2 \quad (8.7)$$

Detailed data for the PE interfaces and local controllers are displayed in Table 8.2. The studied load profile is shown in Table 8.3. The message traces of token transfer to build minimal spanning tree structure among MAS are shown in Fig. 8.6. The sequence of agents that receive the token

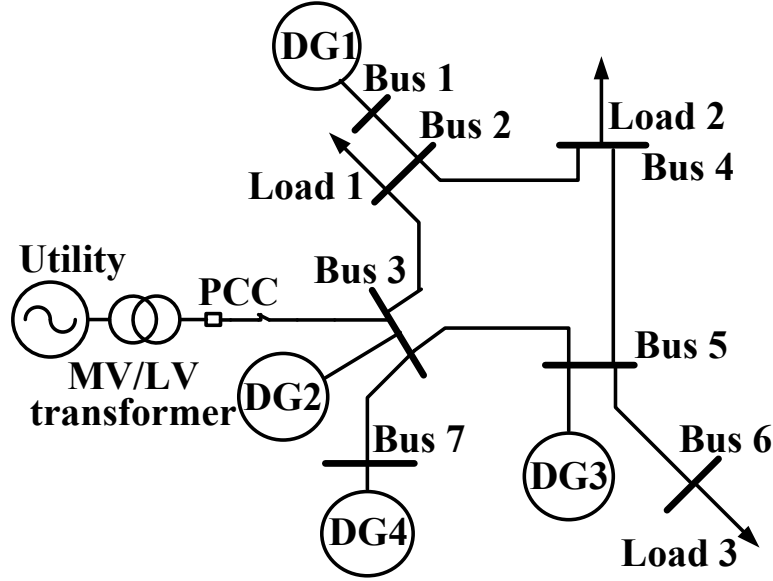


Figure 8.5: Microgrid configuration under study.

Table 8.1: Generation Data

Node	Max Gen		Min Gen		Coefficient		
	kW	kvar	kW	kvar	a_0 (\$)	b_0 (\$/kWh)	c_0 (\$/kW ² h)
DG1	20	10	10	0	8	0.012	0.008
DG2	10	6	0	0	12	0.016	0.01
DG3	15	0	15	0	4	0	0
DG4	10	4	0	0	6	0.014	0.013

verifies the description in Section 4.2.1. It should be pointed that after receiving the token from A3, agent A5 refuses the token which comes later from A4 and breaks the neighborhood relationship with A4. This rule helps remove the communication redundancy and construct minimal spanning tree structure. After building the minimal spanning tree, the *view* information is transmitted from *child agent* to *parent agent* shown in Fig. 8.7. Agents A7, A6 and A4 stay at leaves of the minimal spanning tree; therefore, they initialize the Information Feedback Process described in Section 4.2.2.

The message traces of Generation or Load Dispatch Process during 0 s – 0.05 s are shown in Fig. 8.8. Total power demand is $40 + j16$ kvar, less than total generation capacity, which is $55 + j20$ kvar. Therefore, the starting agent A1 will cut off its dispatchable generation $10 + j4$

Table 8.2: Data for PE Interfaces and Local Controllers

	DG1	DG2	DG3	DG4
L	1 mH	0.56 mH	0.4 mH	0.56 mH
C	6.34 μF	11.6 μF	13 μF	11.6 μF
K_p	1	1	1	1
K_d	0.000316	0.000114	0.000102	0.000114
K_{p1}	3	4	4	4
K_i	20	80	80	80

Table 8.3: Load Profile

Period	Load 1 (kVA)	Load 2 (kVA)	Load 3 (kVA)
0s – 0.05s	10 + $j3$	20 + $j10$	10 + $j3$
0.05s – 0.1s	5 + $j3$	18 + $j5$	10 + $j5$
0.1s – 0.15s	25 + $j8$	20 + $j6$	13 + $j4$
0.15s – 0.2s	20 + $j5$	15 + $j6$	13 + $j4$

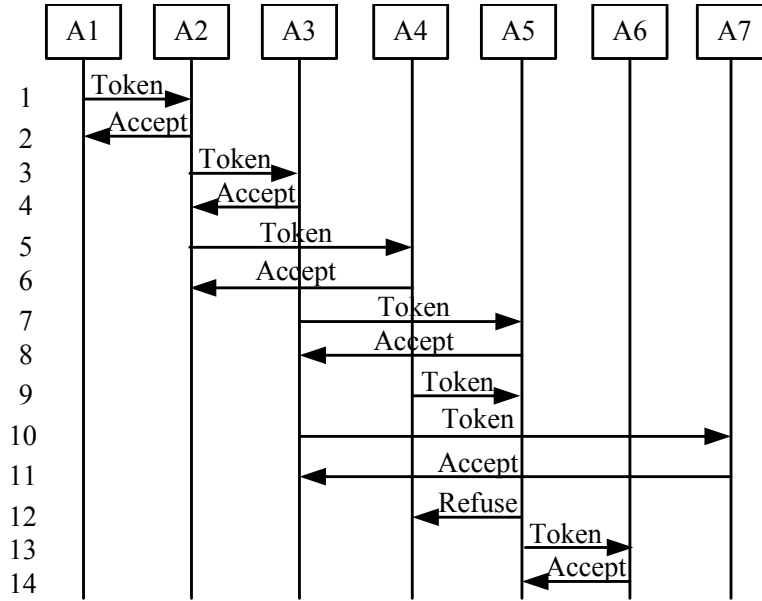


Figure 8.6: Traces of messages for token transfer.

and send net power value $5 + j0$ kW to A2. Since bus 2 does not have generation connected to it, A2 can not reduce net power. It splits the net power values according to its *child agents*' updated view expressed by (4.7). A4 is the leaf agent and it does not have generation connected to it. From (4.7), the split net power values it receives are $P_{net4} = 0, Q_{net4} = 0$. The net power for A3 is $5 + j0$ kvar. A3's local dispatchable generation can reduce 5 kW to make net power zero, which initializes A3 to inform its neighbors of power balance completion. At the same time, A4 detects

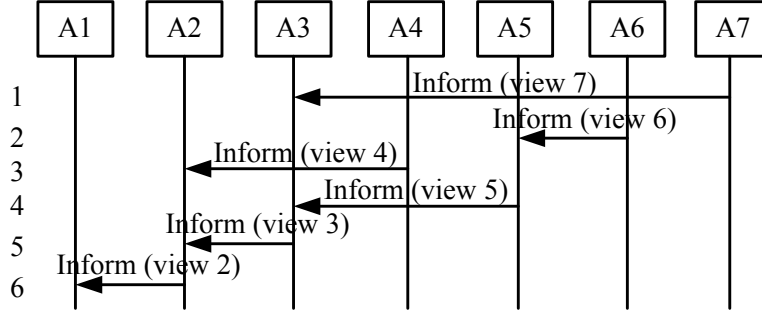


Figure 8.7: Traces of messages for Information Feedback Process.

that the net power it receives is also zero. Then A4 will inform A2 of power balance completion. When A2 receives power balance completion from both A3 and A4, it will inform its *parent agent* A1 of power balance completion. After power balance, MAS can also conduct economic dispatch. The optimal generation values are obtained as follows: $P_{DG1} = 10.465$ kW, $P_{DG2} = 8.172$ kW, $P_{DG3} = 15$ kW, $P_{DG4} = 6.3631$ kW. Convergence of the proposed economic dispatch is shown in Fig. 8.9(a). For this small system, only three iterations are needed for convergence. The global marginal cost is around \$0.18/kWh. DG3 is a solar panel. Its output power cannot be dispatched and so its marginal cost does not change. Fig. 8.9(b) shows the iterations to obtain the optimal generation values. None of dispatchable generators reaches its real power limit in this case. Total reactive power demand during this period is 16 kvar; hence, after MAS power balance control, reactive power generation values for the DGs are: $Q_{DG1} = 10$ kvar, $Q_{DG2} = 2$ kvar, $Q_{DG3} = 0$ kvar, $Q_{DG4} = 4$ kvar.

At time $t = 0.5$ s, load changes. The total real power demand is 33 kW, which is still less than the total generation capacity. The economic dispatch is displayed in Fig. 8.11. The global marginal cost converges to \$0.106/kWh. DG1 is constrained by its lower limit of real power output; therefore, its marginal cost converges to \$0.172/kWh, larger than global marginal cost. From Fig. 8.10(b), new optimal generation values for this load profile are: $P_{DG1} = 10$ kW, $P_{DG2} = 4.4783$ kW, $P_{DG3} = 15$ kW, $P_{DG4} = 3.5217$ kW. The total reactive power demand is 13 kvar. Reactive power generation dispatch values are: $Q_{DG1} = 10$ kvar, $Q_{DG2} = 0$ kvar, $Q_{DG3} = 0$ kvar, $Q_{DG4} = 3$ kvar.

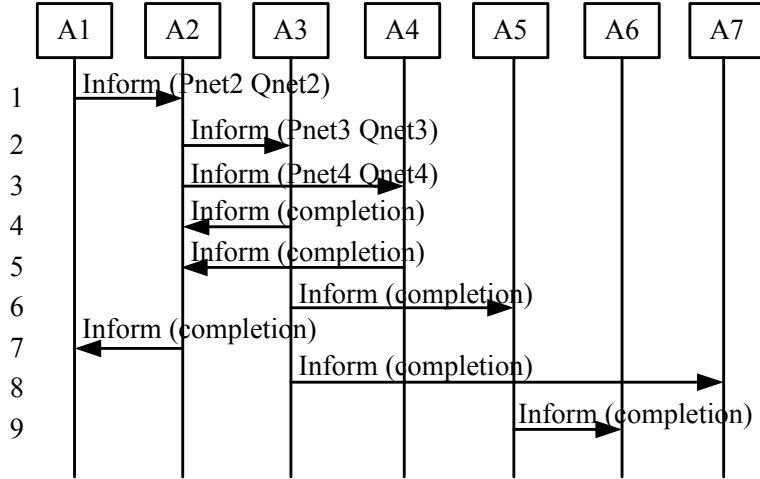


Figure 8.8: Traces of messages for Generation or Load Dispatch.

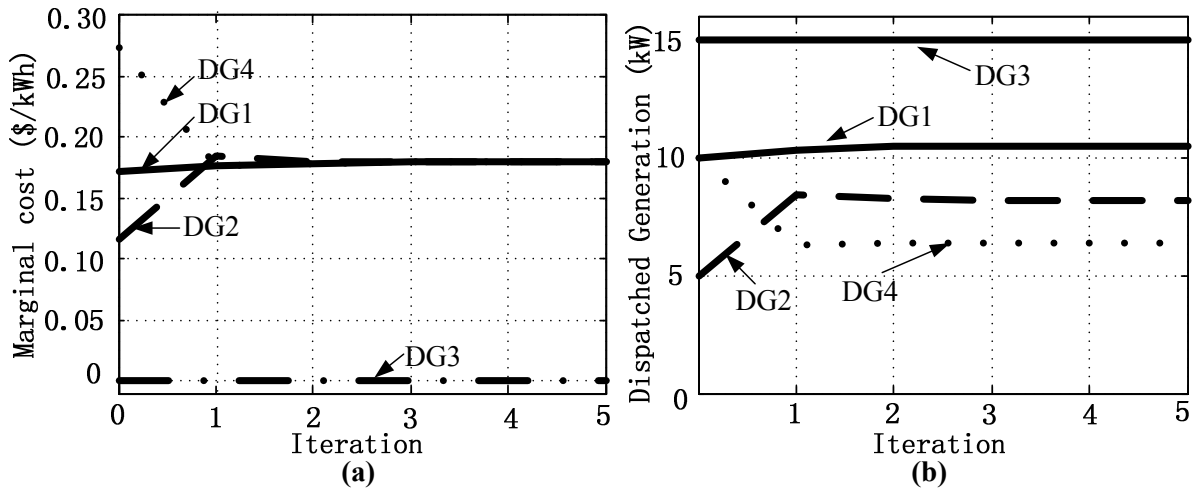


Figure 8.9: (a) Convergence of marginal cost. (b) Dispatched values for the DGs.

At time $t = 1.0$ s, total real power demand increases to 58 kW, but total real power generation capacity is 55 kW. Therefore, MAS power balance control will shed 3 kW load. In this simulation, load 3 will be curtailed by 3 kW. Since load demand is larger than generation capacity. MAS will not conduct economic dispatch and all DGs are required to output maximum real power to reduce load shedding. Total reactive power demand is 18 kvar, still less than total reactive power capacity. The resulting reactive power dispatch values in this stage are: $Q_{DG1} = 8$ kvar, $Q_{DG2} = 6$ kvar, $Q_{DG3} = 0$ kvar, $Q_{DG4} = 4$ kvar.

At time $t = 1.5$ s, total real demand decreases to 48 kW shown in Table 8.3. Fig. 8.11 displays

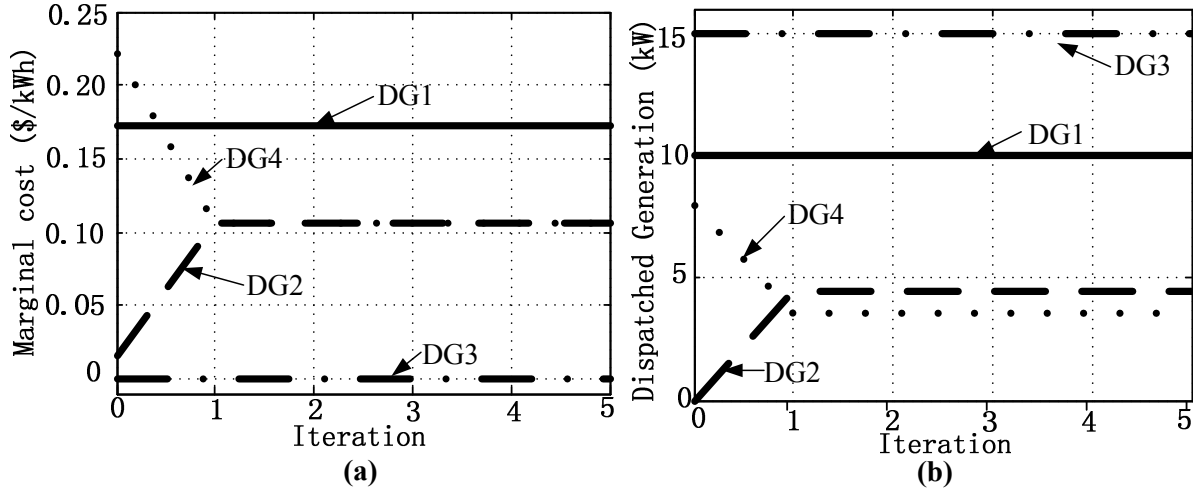


Figure 8.10: (a) Convergence of marginal cost. (b) Dispatched values for the DGs.

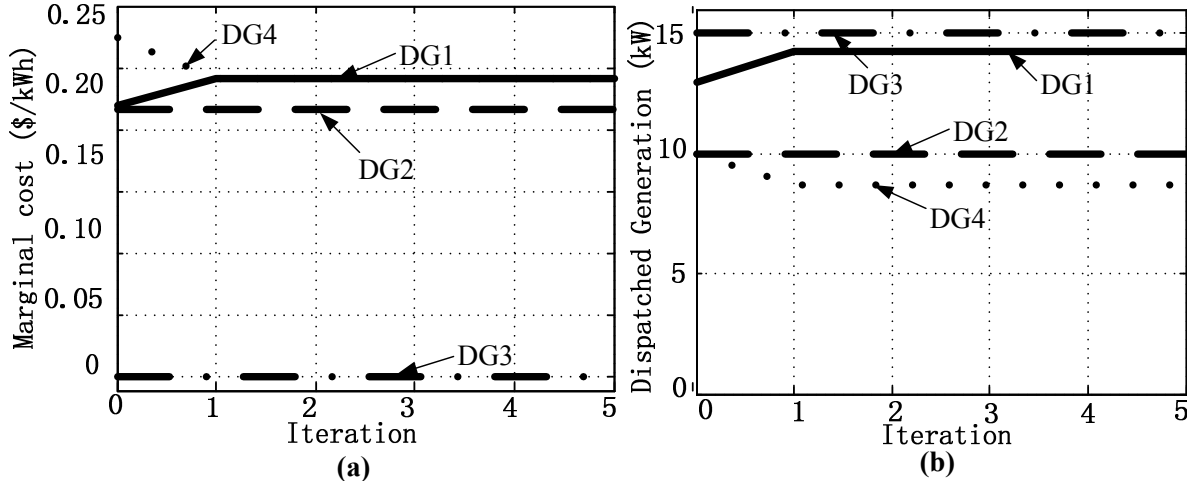


Figure 8.11: (a) Convergence of marginal cost. (b) Dispatched values for the DGs.

economic dispatch process. From the figure, it can be seen that real power output of DG2 reaches its upper limit, therefore its marginal cost is lower than the global value; while for DG1 and DG4, their output does not reach the limit, so their marginal cost converges. The optimal dispatch values are: $P_{DG1} = 14.29$ kW, $P_{DG2} = 10$ kW, $P_{DG3} = 15$ kW, $P_{DG4} = 8.71$ kW. Total reactive power demand decreases by 3 kvar; therefore Q_{DG1} drops to 5 kvar.

Fig. 8.12 displays simulation results for the DGs and loads. Fig. 8.13 shows output current transitions of DGs at the times of load changes.

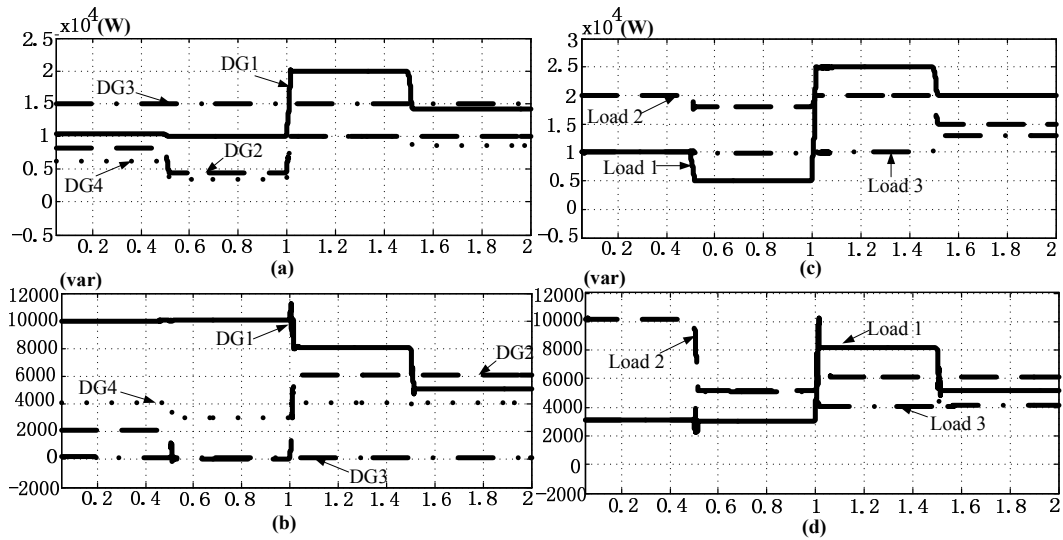


Figure 8.12: (a) Real power output of DGs. (b) Reactive power output of DGs. (c) Real power consumed by Load. (d) Reactive power consumed by Load.

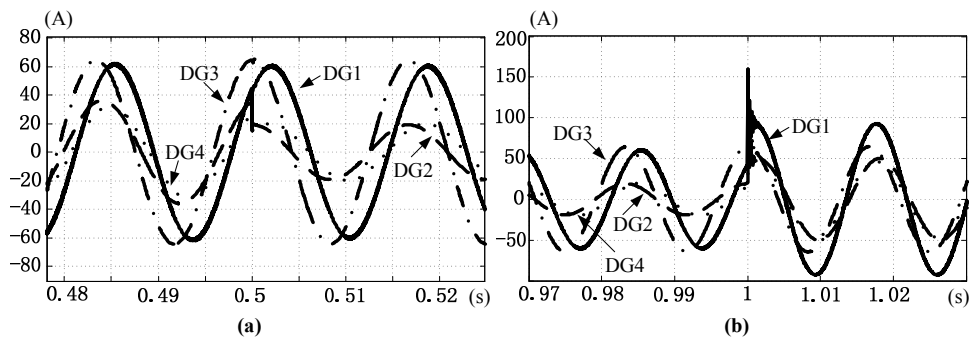


Figure 8.13: (a) Output current transitions of DGs at 0.5s. (b) Output current transitions of DGs at 1.0s.

8.5 Summary

In this chapter, multi-agent system is implemented using JADE platform. A comprehensive multi-level control architecture was presented for master-slave organized microgrids with PE interfaced DGs. The MAS power balance control strategy that can accomplish exact power balance in three sweeps, regardless of system size, was used as the upper control layer. The lower MAS based economic dispatch layer, utilizing limited communications between neighboring agents, is able to conduct economic dispatch on-line. Local control layer complies with the instructions from multi-agent system and implement controls locally. These three layers collaborate and interact with each

other to act as a united control system, which can operate microgrids in a safe, economic and stable way. In the presence of markets, the quadratic generation cost function can be replaced by bids, and the associated objective function, such as social welfare function, can also be optimized by the proposed MAS. The performance of the proposed strategy was demonstrated on a test system. Its benefits, both in terms of speed as well as robustness in tracking time-varying loads, were demonstrated.

Part IV

Conclusions

Chapter 9

Contributions and Future Work

9.1 Contributions

This dissertation presents linearization and distributed methods for optimization and control of smart grid and microgrid. The contributions include:

1. This dissertation presents linearization method to linearize optimal power flow problem with FACTS devices. The linearized model can achieve fast and reliable advantage as traditional DC model; furthermore, it does not sacrifice accuracy and can obtain full state information.
2. This dissertation presents a combined algorithm using genetic algorithm and linearized optimal power flow framework for the optimal location and parameter selection of UPFC. An optimal branch numbering strategy is proposed to accelerate the convergence speed of the algorithm.
3. This dissertation presents a distributed method for the power balance control of microgrids. The information flows in parallel and results are obtained in non-iterative way; therefore, the algorithm can achieve superior performance in terms of speed without any convergence issues.
4. In the context that requires to consider losses and voltage regulation, this dissertation presents

a distributed power balance algorithm based on Guess method. The distributed power flow algorithm fully makes use of communication time, and updates state information synchronously among agents, which offers potential speed advantage.

5. In the microgrid that is amenable to economic dispatch, this dissertation proposes a distributed economic dispatch algorithm based on the consensus theorem. Convergence of the proposed algorithm and proof of achieving global optimum are also presented. This algorithm is also capable for on-line economic dispatch.
6. In a stressful power system network, this dissertation proposes a distributed economic dispatch algorithm considering network constraints. Convergence of the proposed algorithm is demonstrated. The distributed power flow algorithm fully makes use of communication time, and updates state information synchronously among agents, which offers potential speed advantage.
7. This dissertation presents the implementation of the proposed multi-agent system in JADE environment. A comprehensive multi-level control system is proposed in this dissertation for safe and economic operation of microgrids.

9.2 Future Work

1. Develop an algorithm that examines all the load scenarios within acceptable size of memory. This will cover two possible solutions, 1) combining nonlinear techniques and the algorithm developed in this chapter to reduce the size of memory. 2) decoupling coefficients matrix of equality and inequality constraints to divide the memory size into small pieces and examines these pieces one by one.
2. Simulate nonlinear model and DC model for comparisons in terms of calculation time and accuracy.
3. Extend the developed algorithm to other FACTS devices.

4. Simulation the distributed economic dispatch algorithm considering network constraints on a larger system.
5. Complete the distributed control framework by developing distributed state estimator.

BIBLIOGRAPHY

BIBLIOGRAPHY

- [1] “Smart Grid,” available at http://en.wikipedia.org/wiki/Smart_grid.
- [2] A. J. Wood and B. F. Wollenberg, *Power Generation Operation and Control*. New York: Wiley, 1996.
- [3] B. Stott and E. Hobson, “Power system security control calculations using linear programming, part I,” *IEEE Trans. Power App. Syst.*, vol. PAS-97, no. 5, pp. 1713–1720, Sep./Oct. 1978.
- [4] B. Stott and E. Hobson, “Power system security control calculations using linear programming, part II,” *IEEE Trans. Power App. Syst.*, vol. PAS-97, no. 5, pp. 1721–1731, Sep./Oct. 1978.
- [5] O. Alsac, J. Bright, M. Prais and B. Stott, “Further development in LP-based optimal power flow,” *IEEE Trans. Power Syst.*, vol. 5, no. 3, pp. 697–711, Aug. 1990.
- [6] R. Fletcher and E. S. de al Maza, “Nonlinear programming and nonsmooth optimization by successive linear programming,” *Math. Program.*, vol. 43, no. 3, pp. 235–256, Jan. 1989.
- [7] J. A. Momoh, *Electric Power System Applications of Optimization*. New York: Marcel Dekker, Inc., 2001.
- [8] H. Ambriz-Perez, E. Acha, C. R. Fuerte-Esquivel and A. de la Torre, “Incorporation of a UPFC model in an optimal power flow using Newton’s method,” *IET Gen. Transm. Distrib.*, vol. 145, no. 3, pp. 336–344, May 1998.
- [9] H. Ambriz-Perez, E. Acha, and C. R. Fuerte-Esquivel, “Advanced SVC models for Newton-Raphson load flow and Newton optimal power flow studies,” *IEEE Trans. Power Syst.*, vol. 15, no. 1, pp. 129–136, Feb. 2000.
- [10] S. Sivasubramani and K. S. Swarup, “Sequential quadratic programming based differential evolution algorithm for optimal power flow problem,” *IET Gen. Transm. Distrib.*, vol. 5, no. 11, pp. 1149–1154, Nov. 2011.
- [11] I. M. Nejdawi, K. A. Clements and P. W. Davis, “An efficient interior point method for sequential quadratic programming based optimal power flow,” *IEEE Trans. Power Syst.*, vol. 15, no. 4, pp. 1179–1183, Nov. 2000.
- [12] R. Salgado, A. Brameller, and P. Aitchison, “Optimal power flow solutions using the gradient projection method. Part 1: Theoretical basis,” *IET Gen. Transm. Distrib.*, vol. 137, no. 6, pp. 424–428, Nov. 1990.
- [13] R. Salgado, A. Brameller, and P. Aitchison, “Optimal power flow solutions using the gradient projection method. Part 2: Modelling of the power system equations,” *IET Gen. Transm. Distrib.*, vol. 137, no. 6, pp. 429–435, Nov. 1990.

- [14] H. Wang, C. E. Murillo-Sánchez, R. D. Zimmerman, and R. J. Thomas, “On computational issues of market-based optimal power flow,” *IEEE Trans. Power Syst.*, vol. 22, no. 3, pp. 1185–1193, Aug. 2007.
- [15] Y. Fu, M. Shahidehpour, Z. Li, “Security-constrained unit commitment with AC constraints,” *IEEE Trans. Power Syst.*, vol. 20, no. 2, pp. 1001–1013, May 2005.
- [16] G. Geng and Q. Jiang, “A two-level parallel decomposition approach for transient stability constrained optimal power flow,” *IEEE Trans. Power Syst.*, vol. 27, no. 4, pp. 2063–2073, Nov. 2012.
- [17] A. A. Sousa, G. L. Torres, and C. A. Cañizares, “Robust optimal power flow solution using trust region and interior-point methods,” *IEEE Trans. Power Syst.*, vol. 26, no. 2, pp. 487–499, May 2011.
- [18] C. Y. Chung, W. Yan, and F. Liu, “Decomposed predictor-corrector interior point method for dynamic optimal power flow,” *IEEE Trans. Power Syst.*, vol. 26, no. 3, pp. 1030–1039, Aug. 2011.
- [19] A. A. A. Esmin, G. Lambert-Torres, and A. C. Zambroni de Souza, “A hybrid particle swarm optimization applied to loss power minimization,” *IEEE Trans. Power Syst.*, vol. 20, no. 2, pp. 859–866, May 2005.
- [20] A. G. Bakirtzis, P. N. Biskas, C. E. Zoumas, and V. Petridis, “Optimal power flow by enhanced genetic algorithm,” *IEEE Trans. Power Syst.*, vol. 17, no. 2, pp. 229–236, May 2002.
- [21] J. G. Vlachogiannis, N. D. Hatziargyriou, and K. Y. Lee, “Ant colony system-based algorithm for constrained load flow problem,” *IEEE Trans. Power Syst.*, vol. 20, no. 3, pp. 1241–1249, Aug. 2005.
- [22] Qin Lei, “High performance control of inverter interfaced distributed generation,” Master Thesis, Michigan State University, 2012.
- [23] T. Otani and H. Kobayashi, “A SCADA system using mobile agents for a next-generation distribution system,” *IEEE Trans. Power Del.*, vol. 28, no. 1, pp. 47–57, Jan. 2013.
- [24] C. W. Gellings, “Innovation and Smart Grids,” EPRI, available at: http://www.egr.msu.edu/mitraj/misc/Gellings_Innovation_Smart_Grids.pdf, Jan. 2012.
- [25] Shaoyun Ge, “Optimal power system operation and control incorporating FACTS Devices,” Ph.D. Dissertation, The Hong Kong Polytechnic University, Aug. 1998.
- [26] Edison Electric Institute, “Transmission projects: at a glance,” Washington, D. C., Feb. 2010.
- [27] “IEEE reliability test system,” *IEEE Trans. Power App. Syst.*, vol. PAS-98, no. 6, pp. 2047–2054, Nov./Dec. 1979.
- [28] Klaus Habur and Donal O’Leary, “Flexible Alternating Current Transmission Systems. For Cost Effective and Reliable Transmission of Electrical Energy,” Siemens Co.

- [29] R. N. Allan, R. Billinton, N. M. K. Abdel-Gawad, "The IEEE reliability test system—extension to and evaluation of the generating system," *IEEE Trans. Power Syst.*, vol. 1, no. 4, pp. 1–7, Nov. 1986.
- [30] J. Hao, L. B. Shi and Ch. Chen, "Optimizing location of unified power flow controllers by means of improved evolutionary programming," *IEE Proceedings–Generation, Transmission and Distribution*, vol. 151, Issue 6, pp. 705–712, Nov. 2004.
- [31] E. Ghahremani and I. Kamwa, "Optimal placement of multiple-type FACTS devices to maximize power system loadability using a generic graphical user interface," *IEEE Trans. Power Syst.*, vol. 28, Issue 2, pp. 764–778, May 2013.
- [32] P. K. Tiwari and Y. R. Sood, "Efficient and optimal approach for location and parameter setting of multiple unified power flow controllers for a deregulated power sector," *IET Generation, Transmission and Distribution*, doi:10.1049, , pp. 958–967, June 2012.
- [33] S. An, J. Condren and T. W. Gedra, "An ideal transformer UPFC model, OPF first-order sensitivities, and applications to screening for optimal UPFC locations," *IEEE Trans. Power Syst.*, vol. 22, No. 1, pp. 68–75, Feb. 2007.
- [34] M. C. Chandorkar, D. M. Divan, and R. Adapa, "Control of parallel connected inverters in standalone AC supply systems," *IEEE Trans. Ind. Appl.*, vol. 29, pp. 136–143, Jan./Feb. 1993.
- [35] Peng, F.Z., YunWei Li, L.M. Tolbert, "Control and Protection of Power Electronics Interfaced Distributed Generation System in a Customer-Driven Microgrid," *Power & Energy Society General Meeting*, Calgary, AB, July, 2009, pp. 1-8.
- [36] R. Majumder *et al.*, "Improvement of stability and load sharing in an autonomous microgrid using supplementary droop control loop," *IEEE Trans. Power Syst.*, vol. 25, no. 2, pp. 796–808, May 2010.
- [37] S. J. Ahn *et al.*, "Power-sharing method of multiple distributed generators considering control modes and configurations of a microgrid," *IEEE Trans. Power Del.*, vol. 25, no. 3, pp. 2007–2016, Jul. 2010.
- [38] F. Katiraei and M. R. Iravani, "Power management strategies for a microgrid with multiple distributed generation units", *IEEE Trans. Power Syst.*, vol. 21, no. 4, pp. 1821–1831, Nov. 2006.
- [39] A. L. Dimeas and N. D. Hatziargyriou, "Operation of a multi-agent system for microgrid control", *IEEE Trans. Power Syst.*, vol. 20, no. 3, pp. 1447–1455, Aug. 2005.
- [40] Niannian Cai and Joydeep Mitra, "A decentralized control architecture for a microgrid with power electronic interfaces" *Power Symposium, Proc. of the 42th Annual North American*, Alinton, TX, Sep. 2010.
- [41] J. Mitra *et al.*, "Intelligent methods for smart microgrids," in *Proc. IEEE Power & Energy Soc. General Meeting*, Detroit, MI, Jul. 2011.

- [42] S. K. Mazumder, M. Tahir, and K. Acharya, "Master-slave current-sharing control of a parallel dc-dc over a RF communication interface", *IEEE Trans. Ind. Electron.*, vol. 55, no. 1, pp. 59–66, Jan. 2008.
- [43] Y. Xu and W. Liu, "Novel multiagent based load restoration algorithms for microgrids," *IEEE Trans. Smart Grid*, vol. 2, no. 1, pp. 152–161, Mar. 2011.
- [44] Y. Xu and W. Liu, "Stable multi-agent-based load shedding algorithm for power systems," *IEEE Trans. Power Syst.*, vol. 26, no. 4, pp. 2006–2014, Mar. 2011.
- [45] S. Suryanarayanan and J. Mitra, "Enabling Technologies for the Customer-driven Microgrid," *IEEE Power & Energy Society General Meeting*, Calgary, AB, July 2009, pp. 1-3.
- [46] S. D. J. McArthur *et al.*, "Multi-agent systems for power engineering applications — Part I: concepts, approaches, and technical challenges," *IEEE Trans. Power Syst.*, vol. 22, no. 4, pp. 1743–1752, Nov. 2007.
- [47] S. D. J. McArthur *et al.*, "Multi-agent systems for power engineering applications — Part II: technologies, standards, and tools for building multi-agent systems," *IEEE Trans. Power Syst.*, vol. 22, no. 4, pp. 1753–1759, Nov. 2007.
- [48] S. Talukdar and V. C. Ramesh, "A multi-agent technique for contingency constrained optimal power flows," *IEEE Trans. Power Syst.*, vol. 9, no. 2, pp. 855–861, May 1994.
- [49] N. P. Yu, C. C. Liu, and J. Price, "Evaluation of market rules using multi-agent system method," *IEEE Trans. Power Syst.*, vol. 25, no. 1, pp. 470–479, Feb. 2010.
- [50] P. Wei, Y. Yan, Y. Ni, J. Yen, and F. E. Wu, "A decentralized approach for optimal wholesale cross-border trade planning using multi-agent technology," *IEEE Trans. Power Syst.*, vol. 16, no. 4, pp. 833–838, Nov. 2001.
- [51] J. Jung, C. C. Liu, S. L. Tanimoto, and V. Vittal, "Adaptation in load shedding under vulnerable operating conditions," *IEEE Trans. Power Syst.*, vol. 17, no. 4, pp. 1199–1205, Nov. 2002.
- [52] N. Cai and J. Mitra, "A decentralized control architecture for a microgrid with power electronic interfaces" in *Proc. 42th Annual North American Power Symposium*, Alington, TX, Sep. 2010.
- [53] S. D. J. McArthur and S. M. Strachan, "The design of a multi-agent transformer condition monitoring system," *IEEE Trans. Power Syst.*, vol. 19, no. 4, pp. 1845–1852, Nov. 2004.
- [54] E. E. Mangina, S. D. J. McArthur, J. R. McDonald, and A. Moyes, "A multi-agent system for monitoring industrial gas turbine start-up sequences," *IEEE Trans. Power Syst.*, vol. 16, no. 3, pp. 396–401, Aug. 2001.
- [55] S. D. J. McArthur, C. D. Booth, and J. R. McDonald, and I. T. McFadyen, "An agent-based anomaly detection architecture for condition monitoring," *IEEE Trans. Power Syst.*, vol. 20, no. 4, pp. 1675–1682, Nov. 2005.

- [56] H. Wan, K. K. Li, and K. P. Wong “A multi-agent approach to protection relay coordination with distributed generators in industrial power distribution system,” in *Proc. 40th IAS Annual Meeting Ind. Appl.*, vol. 2, pp. 830–836, Oct. 2005.
- [57] F. Daneshfar and H. Bevrani, “Load-frequency control: a GA-based multi-agent reinforcement learning,” *IET Gen. Transm. Distrib.*, vol. 4, no. 1, pp. 13–26, Jan. 2010.
- [58] T. Nagta and H. Sasaki, “A multi-agent approach to power system restoration,” *IEEE Trans. Power Syst.*, vol. 17, no. 2, pp. 457–462, May 2002.
- [59] J. M. Solanki, S. Khushalani, and N. N. Schulz, “A multi-agent solution to distribution systems restoration,” *IEEE Trans. Power Syst.*, vol. 22, no. 3, pp. 1026–1034, Aug. 2007.
- [60] N. Cai, X. Xu, and J. Mitra, “A hierarchical multi-agent control scheme for a black start-capable microgrid,” in *Proc. IEEE Power & Energy Soc. General Meeting*, Detroit, MI, Jul. 2011.
- [61] M. E. Baran and I. M. Markabi, “A multi-agent-based dispatching scheme for distributed generators for voltage support on distribution feeders,” *IEEE Trans. Power Syst.*, vol. 22, no. 1, pp. 52–59, 2007.
- [62] M. E. Elkhatab, R. El-Shatshat, and M. M. A. Salama, “Novel coordinated voltage control for smart distribution networks with DG,” *IEEE Trans. Smart Grid*, vol. 2, no. 4, pp. 598–605, Dec. 2011.
- [63] H. Ni, G. T. Heydt, and L. Mili, “Power system stability agents using robust wide area control,” *IEEE Trans. Power Syst.*, vol. 17, no. 4, pp. 1123–1131, Nov. 2002.
- [64] Z. Zhang, X. Ying, and M. Y. Chow, “Decentralizing the economic dispatch problem using a two-level incremental cost consensus algorithm in a smart grid environment,” in *IEEE Power Eng. Soc. Gen. Meeting*, Tampa, FL, Jul. 2007.
- [65] A. Abbasy and S. H. Hosseini, “A novel multi-agent evolutionary programming algorithm for economic dispatch problems with non-smooth cost functions,” in *Proc. 43th Annual North American Power Symposium*, Boston, MA, Aug. 2011.
- [66] S. K. Mazumder, K. Acharya, and M. Tahir, “Joint optimization of control performance and network resource utilization in homogeneous power networks,” *IEEE Trans. Ind. Electron.*, vol. 56, no. 5, pp. 1736–1745, May 2009.
- [67] K. Deb, *Optimization for Engineering Design—Algorithms and Examples*, PHI Learning Private Limited, New Delhi, 2012.
- [68] D. N. Zmood and D. G. Holmes, “Stationary frame current regulation of PWM inverters with zero steady-state error,” *IEEE Trans. Power Electron.*, vol. 18, no. 3, pp. 814–822, May 2003.
- [69] *Power Systems Test Case Archive*. [Online]. Available at: <http://www.ee.washington.edu/research/pstca>.

- [70] R. D. Zimmerman and C. Murillo-Sánchez, MATPOWER User's Manual. [Online]. Available at: <http://www.pserc.cornell.edu/matpower/>.
- [71] JADE, Java agent development framework, available at: <http://jade.tilab.com/>.
- [72] F. Bellifemine, G. Caire, D. Greenwood, Developing multi-agent systems with JADE, New York: Wiley, 2007.
- [73] FIPA, Foundation of intelligent physical agents, available at: <http://www.fipa.org/>.
- [74] J. Duncan Glover, Mulukutla S. Sarma and Thomas J. Overbye, Power System Analysis and Design, Fourth Edition: Thompson, 2007.
- [75] M. Wolter, H. Guercke and T. Isermann et al, "Multi-agent Based Distributed Power Flow Calculation," *Power & Energy Society General Meeting, 2010 IEEE*, Minneapolis, MN, July, 2010, pp. 1-6.